The ESO Council Visits Chile

H. VAN DER LAAN, Director General, ESO

Far from the dreary winter clouds of Europe and in a less formal attire than usual, the members of the ESO Council have just paid a working visit to the ESO installations in Chile, the first since 1972. Under a deep blue sky they climbed the site of the future VLT Observatory at Paranal, and another day and night was spent at La Silla, providing Council delegates with an opportunity to experience life in the remote desert and also to visit the astronomers at the telescopes at night.

This visit of Council was arranged at a particularly appropriate time, one year after the historic decision to choose Paranal for the VLT. It began officially on December 2 with the inauguration of the ESO Exhibition "Explorando el Universo" at the Casa Central of the Universidad de Chile in downtown Santiago. A large number of illustrious guests responded to the joint invitation by the Rector of the Universidad de Chile, Prof. Jaime Lavados Montes and myself. The Chilean Minister of Education, Don Ricardo Lagos Escobar, delivered the official opening speech, and many members of the diplomatic corps in Santiago, including the ambassadors and chargés d'affaires of the ESO member countries and numerous representatives of the local authorities honoured the ceremony by their presence.

The Minister of Education praised the role of astronomy in Chile and extended a special welcome to the members of the ESO Council whom he wished a happy and fruitful stay in his country. He talked about the virtues of astronomy as a science with an apparently unlimited potential for new, exciting discoveries and an indivisible part of culture. He valued the international efforts to support Chilean astronomers in various ways and he looked forward to an even closer collaboration in the future.

Council at Paranal on December 3, 1991. From left to right in back row: Mrs. A. Hansen (Germany), Messrs. J.-P. Swings (Belgium), W.N. Brouw (Netherlands), C. de Loore (Belgium), J. Bezemer (Netherlands), H. E. Jørgensen (Denmark), P. Léna (France), C. Chiuderi (Italy), F. Bello (Portugal) and P.-O. Lindblad (Sweden); from left to right in front row: Messrs. M. Grewing (Germany), J. Damagnez (France), P. Creola (Switzerland), F. Pacini (Italy; President), H. van der Laan (Director General of ESO), H. Grage (Denmark; Vice-President), G. Carante (Italy), M.O. Ottoson (Sweden) and M. Golay (Switzerland).

The Chilean Minister of Education, Don Ricardo Lagos Escobar (second from right); Prof. F. Pacini, President of the ESO Council (left); Prof. Jaime Lavados Montes, Rector of the Universidad de Chile (second from left); and Prof. H. van der Laan, Director General of ESO, at the inauguration of the ESO Exhibition at the Universidad de Chile in Santiago on December 2. The display will remain open to the public until the end of January 1992, whereafter it will be transferred to La Serena for display during the annual summer fair in that city. From there it later travels to Antofagasta.

In my discourse I emphasized that the vitality of any research enterprise depends first and foremost on its human resources. The most important condition for the successful elaboration of ESO's partnership with Chile's astronomy community is that community's ability to attract more talents from the body of students with interest in science, to astronomy. This point was also discussed with care in two separate audiences with two of Chile's ministers, Don Ricardo Lagos and Don Edgardo Boeninger, in the week before.

The next day, Council travelled by air to Antofagasta and onwards to Paranal by bus. The stark desert landscape was admired by the delgates, some of whom visited Atacama for the first time. On the top of the mountain, they were received by various members of the ESO staff, including those who have been responsible for the long-term site testing that finally led to the acceptance of Paranal as the VLT site. There was ample opportunity to inspect the progress of the levelling of the top (including a big blast that day!) and to get a feeling for the unusual working and living conditions at this remote site. In the evening, Council returned to Antofagasta and spent the night there. A visit was arranged to the site in the outskirts of the town where ESO is acquiring a small property for its future installations in that city.

Council left Antofagasta in the early afternoon of December 4, flew to La Serena (Ladeco, the internal Chilean airline, had been convinced to make an unscheduled stop there) and on to La Silla by ESO bus. Here the Council members were met by the La Silla staff and spent the rest of the day informing themselves about the state of affairs at ESO's main installation, and also about the preparations for the move to Santiago of part of the staff, in particular the Administration, to begin in the course of 1992.

In the evening, visits were arranged to the various telescopes. The sky was clear and there was a beautiful view of the sunset over the Pacific, at the present time with a particularly strong red hue due to the dust in the high atmosphere from the eruption earlier this year of the Pinatubo volcano on the Philippines (cf. the photo on page 66). Then the marvellous southern sky came into view, adding this grandest of all inspirations in astronomy to the delegates' many impressions.

The actual Council meeting took place on December 4 (in Antofagasta), 5 (at La Silla) and 6 (in the UN CEPAL building in Santiago) and dealt with a number of important matters. Council was pleased to learn that the VLT project is proceeding according to the foreseen time schedule and, in particular, within the agreed budget frame. The recent successful production of the first 8-metre blank at Schott for the VLT (which still has to be ceramized into the zero-expansion Zerodur material) was noted with enthusiasm. The planning of the VLT instrumentation is progressing at a good pace (cf. the overview article in *Messenger* **65**, p.10; September 1991).

Another important agenda item was a thorough discussion about the relations with the host state of our observatories, summing up more than 25 years of excellent collaboration between ESO and Chile, and considering how in the future these bonds can be made more effective still to both partners' benefit, now that ESO is building the VLT Observatory.

On Monday, December 9, the President of the Republic of Chile, Don Patricio Aylwin Azocar, granted an audience to a small ESO delegation, headed by Prof. Franco Pacini, President of the ESO Council. President Aylwin was informed about the state of development of our Organization, in which he expressed a keen, appreciative interest. The ESO delegation expressed its gratitude for the hospitality and support from the Republic's authorities during the past 28 years and looks forward to continued collaboration in the decades to come.

Most of the Council members returned to Europe at the end of the week. Before departure, many of them expressed satisfaction about the visit, having found it very useful and contributing to the work of Council. They came away with a better understanding of the conditions at the remote sites and were visibly impressed by the ESO operations. This working visit had certainly fulfilled expectations.

A reception was held at the ESO Guesthouse in Santiago, in the evening of December 2.

VLT Contracts

M. TARENGHI and R.M. WEST, ESO

The 8.2-metre Mirrors

Last year, ESO awarded the contracts for manufacture of the 8.2-metre blanks to Schott Glaswerke AG in Mainz and for their polishing to R.E.O.S.C. in Paris, respectively (cf. *Messenger* 53, p. 2 and 57, p. 34.)

At Schott, each of the three annealing/ceramizing ovens was filled with a meniscus blank. On November 12 one blank came out after completion of the annealing and was transported onto a CNC machine for machining to the desired meniscus shape. This activity was followed immediately by the next cast.

At REOSC the new building reached the roofing stage in October (Fig. 1). In December the installation of the INNSE turntable and SOCOFRAM computer-controlled polisher will start. It is expected that the new 8-m polishing factory will be ready for the first tests on the 8-m dummy in April 1992.

The Main Structure

On September 24, another major VLT contract was signed with the "AES Consortium" of three Italian companies during a small ceremony at the ESO Headquarters in Garching. It concerns the construction of the main mechanical structures of the four 8-m VLT unit telescopes, each of which will weigh more than 440 tons and yet must be machined with sub-micron precision in order to allow astronomical observations of the highest quality.

The Consortium partners are: *Ansaldo Componenti* (of the IRI Finmeccanica Group, leader of the Consortium and active in the field of energy generation components, located in Genova), *EIE* (European Industrial Engineering, in the field of engineering design, in Mestre) and *SOIMI* (Società Impianti Industriali, member of the Asea-Brown Boveri (ABB) Group, an integrated multi-service organization specialized in construction and maintenance of industrial plants, in Milan).

The contract was signed by Messrs. Ferruccio Bressani (Director General of Ansaldo Componenti), Gianpietro Marchiori (Member of the Board of EIE) and Luigi Giuffrida (Managing Director of SOIMI) on behalf of the Consortium, and by Professor Harry van der Laan, Director General of ESO.

It includes the design, manufacture, pre-erection and thorough testing in Europe of the four VLT unit telescope structures, as well as the subsequent dismantling, packing and transport to the VLT Observatory at Paranal. The contract also covers the erection and final testing at Paranal.

The items to be supplied by the contractors include all of the steel structures which will carry the optical mirror cells and astronomical instruments; advanced hydrostatic bearings on which these heavy structures will rest; direct drive motors with 9-metre diameter which will move the telescopes (the design of these motors is based on an axial, dual air-gap configuration and they will be some of the biggest ever built), and high-precision encoders that will measure the exact position of the telescopes, so that they can be correctly and accurately pointed. A schematic drawing of one of the four VLT unit telescopes with all of these components is shown in Figure 2.

This contract requires very high engineering quality with respect to technical reliability, safety and lifetime in order to guarantee the planned performance of the VLT and to fully satisfy the high expectations of European astronomers in the scientific capabilities of their future giant telescope. For this reason, the Italian firms have decided to pool their extensive resources and experience. EIE and Ansaldo Componenti have made important contributions to the constructions of the ESO 3.5-m New Technology Telescope, including the construction of the octagonal, rotating building and the mirror cell with actuators for the computer-controlled, active-optics NTT mirror. EIE was also involved in studies of the VLT domes. Another Italian Consortium, formed by Ansaldo Componenti (leader), CRIV and INNSE, constructs the 3.5-m Galileo Telescope for Italy, a twin of the ESO NTT.

The construction of the VLT main structures will start within a few months and the parts for the first of the four 8-m telescopes will be delivered to Paranal in late 1994. The erection and testing will be ready in September 1995, whereafter the giant mirrors, which are made in Germany and polished in France, will be installed. The other three telescopes will then follow in one-year intervals, so that the entire VLT complex can be ready in 1998, just over ten years after the decision by the Council of ESO to build the world's largest optical telescope.

Next Contracts

The years 1991 and 1992 represent the culmination of the VLT planning period. During the next 12 months, another dozen VLT contracts will be awarded after the normal tendering procedure has led to the identification of the best suppliers.

Among these contracts are the M1/M3 units, the M2 units, M2 and M3 mirrors, the VLT enclosures, the civil

Figure 1: *The REOSC building at the new site in Saint-Pierre du Perray. In the foreground is the 10-m entrance door, in the background the tower for the interferometry tests. (Architect: AITEC, Construction company: IPAC).*
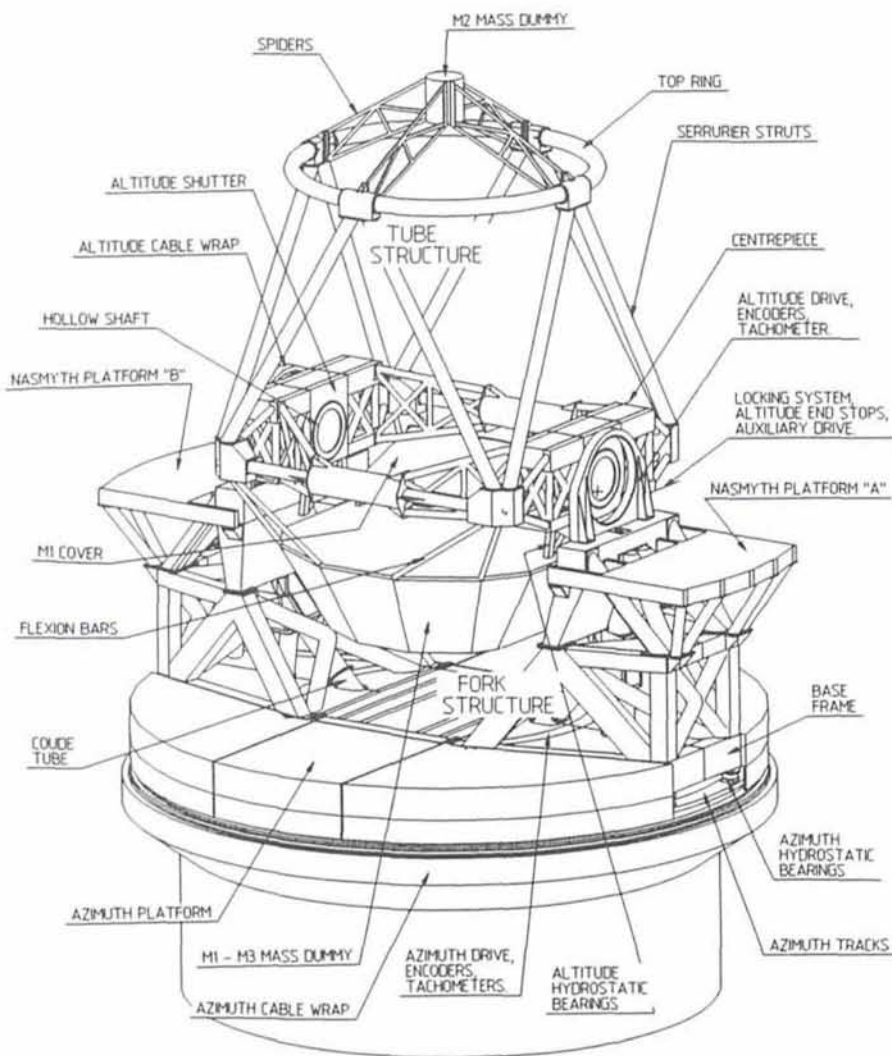
3

Figure 2: *Definition of telescope structure components and subsystems.*

engineering work including buildings, roads, site development and energy systems, the main elements of interferometry (e.g. auxiliary telescopes and delay lines). By the end of 1992, 80 per cent of the VLT capital budget is expected to be committed.

The Paranal Observatory Becomes Reality

M. J. DE JONGE, ESO

In the middle of September the first VLT contractor to execute work on the Paranal site, Interbeton from the Netherlands, started to move its earth-moving equipment and basecamp to the site.

Interbeton, contracted for the levelling and landscaping of the mountain top, had prior to beginning the actual earth-moving work, to reestablish new topographical references. The only topographical reference in the Paranal area is namely on the peak of the mountain and would disappear with the start of the levelling work.

While the survey work was going on, the base camp was finished and the contractor's staff moved into their temporary homes.

Drilling rigs, bulldozers and front loaders moved to the mountain top and started to make a first platform, of a size big enough to turn the trucks, to be used for the transport of excavation material.

The levelling work, consisting of removing approximately 250000 m³ from the mountain top to create a 20000 m² flat area on which the telescopes, the optical laboratories and the interferometer tracks will be located, had really begun.

The first drillings led to the first earth removal by explosives and on September 23 the silence of the Paranal area was broken, which initiated the VLT construction activity which will last till the end of the century.

The excavation material will almost all be used to make an artificial platform to the east side of the telescope area on which the last part of the access road will be constructed.

This platform needs to be rather large since the road requires a 12-m clearance width in order to allow the transport of large telescope parts and the main mirrors.

As from the moment the Contractor moved to the site, also ESO staff belonging to the VLT Division's Staff and Building Group installed themselves on the site in order to ensure permanent supervision of the levelling work. In particular the compacting of the road platform requires intensive follow-up and

Figure 1: *First earth removal by explosives, September 23, 1991.*

Figure 2: *The Interbeton base camp.*

Figure 3: *Drilling rig in operation, preparing the next earth removal.*

Figure 4: *Excavation material loading.*

compaction density tests are continuously made to verify that the specified loading capacity of the road, needed for the heavy transports, is obtained.

The ESO staff furthermore initiated sub-soil investigations at the location of the telescopes and started with survey work of the road leading to the Paranal area in view of improving the road, which is of paramount importance for both the construction and future operation of the VLT Observatory.

Last but not least, the ESO staff was involved in designing, contracting and in the installation of the construction base camp which provides offices, dormitories and living quarters in which they will work and live for a number of years, until the new Observatory Buildings, under design with COWI Consult in Denmark, are available.

A Report on the Second ESO Conference on High Resolution Imaging by Interferometry

J.M. BECKERS and F. MERKLE, ESO

Over 200 scientists and engineers participated in the October 15 to 18, 1991 ESO Conference on "High Resolution Imaging by Interferometry", a conference devoted to ground-based optical interferometric imaging in astronomy. This was the second conference on this topic, the first one having been held also in Garching in March 1988. In addition to four introductory and review talks, the conference included 150 contributions on single- and multiple-aperture interferometric imaging and three working sessions on adaptive optics, detectors and path-length compensation. Sixty of these contributions were given orally, the rest by means of poster presentations. To keep the size of the conference within reasonable limits and to avoid parallel sessions, the scope of the meeting excluded related topics like astrometry by interferometric means and contributed papers on astronomical adaptive optics. The latter topic will be a major topic at the April 1992 ESO meeting in Garching on "Progress in Telescope and Instrumentation Techniques". Attendees included participants from Australia, Canada, China, Japan, Mexico, the USA, the USSR, and of course many European countries.

Tutorials

As was the case in the first conference, it was preceded by a day of tutorials intended for newcomers to the field. It is becoming very clear, however, that these tutorials have a much broader function. They are also attended by "oldtimers" (old in this field means more than half a dozen years!), including a Nobel Laureate, who wanted to catch up on recent developments in the more
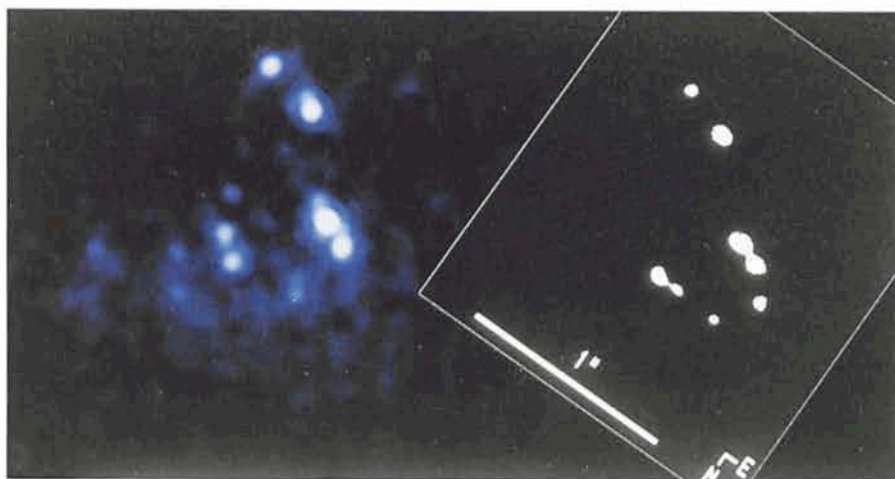
Figure 1: *Images of the object R136 in the Magellanic Clouds obtained with the Hubble Space Telescope (left, after image restoration) and by means of speckle interferometry with the La Silla 2.2-m telescope (right). (Courtesy G. Weigelt et al.)*

We here summarize the parts of the conference on speckle imaging, masked aperture imaging and multi-aperture imaging. The outline of the conference is being followed. Using a number of real-time experiments in his magnificent opening lecture, Prof. W. Martienssen of the University of Frankfurt/Main demonstrated the dual nature of light, waves and particles. It was a fascinating experience, even to the conference participants most of whom are experts in this field but who, like us, forget about the beauty of light in their quest to manipulate it.

Speckle Interferometry: Nearing Maturity?

In contrast to previous conferences and workshops on speckle interferometry, there was relatively little discussion of the many different techniques available for the analysis of speckle observations. In the past a wide variety of algorithms was always discussed and compared. The present discussions and results focussed, however, mostly on bispectrum analysis (or their analogues: speckle masking and triple correlation) for the analysis of speckle images, with a somewhat lesser attention given to the Knox & Thompson algorithms. The latter requires fewer numerical resources for data analysis, otherwise the bispectrum technique appears to be preferred. Judging from the presentation of many astronomical results one has to conclude that this type of observation is reaching a state of substantial maturity. Also the excellent agreement between the images of R136 obtained with the La Silla 2.2-m telescope with those obtained with the Hubble Space Telescope (Fig. 1) provides convincing evidence that speckle imaging has come of age.

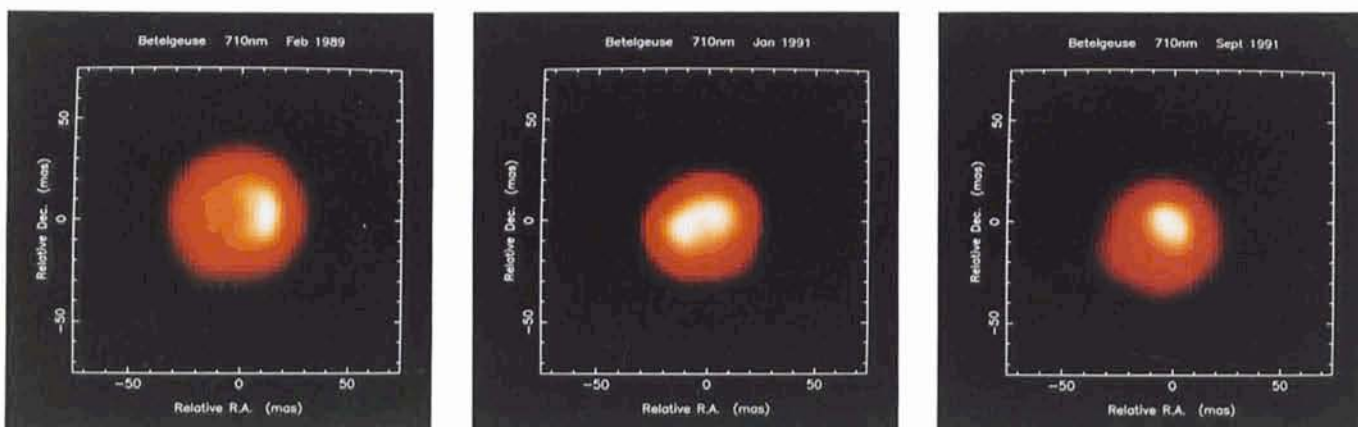At the conference results were presented of other objects, including observations of such diverse objects as

relaxed atmosphere associated with the tutorials and preceding the main conference. Over two thirds of the conference participants attended the tutorials which were given by François Roddier on Optics of the Atmosphere, Gerd Weigelt on Speckle Interferometry, John Davis on Long Baseline Optical Interferometry, and by one of us (FM) on Adaptive Optics.

The Conference Itself

Four full days were devoted to discussions on the rapid progress in the techniques of astronomical imaging by interferometric means and in the presentation of recent astronomical results. Broadly, the techniques and their results can be divided by single-aperture imaging and multi-aperture imaging. Single-telescope interferometric imaging started in 1959 with Antoine Labeyrie's pioneering work in speckle interferometry. Since then these techniques have come a long way, reaching the stage where diffraction-limited imaging can be

obtained on relatively faint, complex objects. Recently full aperture, speckle interferometry with single telescopes has been complemented with single-telescope interferometry using masks on the telescope aperture. Several results of the masked aperture observations were presented at the conference.

In terms of the development of imaging algorithms the latter provides an important step towards multi-aperture interferometric imaging in which the subapertures of the single telescope are replaced by an array of telescopes. In the resulting interference signal at the combined focus the amplitudes and closure phases are measured as is done in the single masked aperture experiments and also in radio astronomy observations. The algorithms for making images are virtually the same for all three types of observations. The trick in multi-aperture interferometry is the combination of the radiation in such a way as to obtain the highest possible sensitivity by maintaining the interference signal, or fringe, contrast.

Figure 2: *Images of the variations of the red supergiant α ORI taken with the 4-m Herschel telescope at three epochs using aperture masking. The width of the Airy disk for this telescope is about 30 milli-arcsec resulting in only 3 to 4 pixels in this 50 milli-arcsec star. (Courtesy Baldwin et al.)*
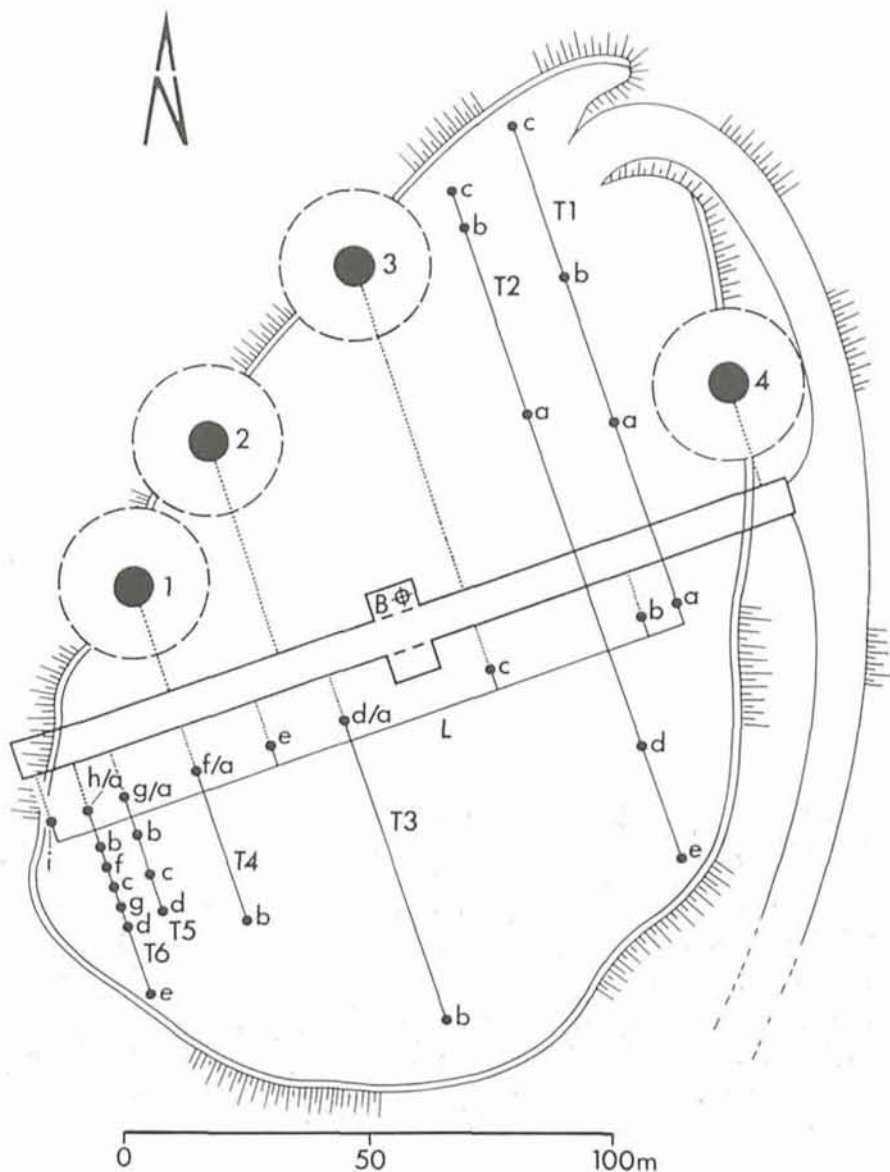
Figure 3: *Layout of the VLT Interferometer. Large dark circles indicate the locations of the 8-m telescopes. Small dark circles are the locations of the stations for the 180-cm diameter mobile auxiliary telescopes. The large rectangle is the location of the interferometric tunnel. A detailed description of the VLTI layout will appear in a future issue of the* Messenger.

a visible speckle camera (see also September 1991, *The Messenger*). Both of these cameras will make use of the unique high imaging qualities of the VLT telescopes. In their performance they will be aided by the VLT adaptive optics which can be viewed as a way of improving the astronomical seeing hence enhancing the sensitivity and limiting magnitude of the cameras.

In contributions by Roddier and one of us (JMB) the point-spread function of so-called partial adaptive optics was discussed. The VLT adaptive optics will be designed to work fully at 2 µm under median seeing conditions. At shorter wavelengths it will work partially. It is becoming very clear through numerical modelling that in such a partially functioning adaptive optics system the point-spread function consists of a spike with the characteristics of an Airy disk superposed on a broad halo with the width approximating the seeing disk. The shape of this function is not unlike that of the aberrated Hubble Space Telescope. The fraction of the total energy in the spike characterizes the point-spread function well. It amounts to 10 % or more at visible wavelengths depending on the seeing. Because of the narrowness of the spike (0.0125 arcsec at 500 nm) and the relatively large width of the halo (0.5 arcsec) the relative central intensity of the spike is large. Roddier therefore suggested that long-exposure images may be used to good advantage over speckle images to give a better limited sensitivity than speckle cameras, of course after image restoration for the background halo (à la Hubble). The VLT Visible Speckle Camera will probably be designed to accommodate this partial adaptive optics, long-exposure imaging mode.

Eta Carinae, the Seyfert galaxy NGC 1068, the Galactic Centre (see September 1991 issue of the *Messenger*) and the Sun.

Impact on the VLT Instrumentation Programme

With the 8- to 10-m diameter telescopes coming on the scene, the technique of speckle interferometry will result in images with a linear resolution 4 times larger than shown in Figure 1 (or 16 times the number of pixels per resolution element). The VLT instrumentation programme includes two instruments for diffraction-limited imaging with the individual VLT telescopes: a near-infrared camera for the 1 to 5 µm region to be built by a consortium headed by the Max-Planck-Institut für Astronomie and
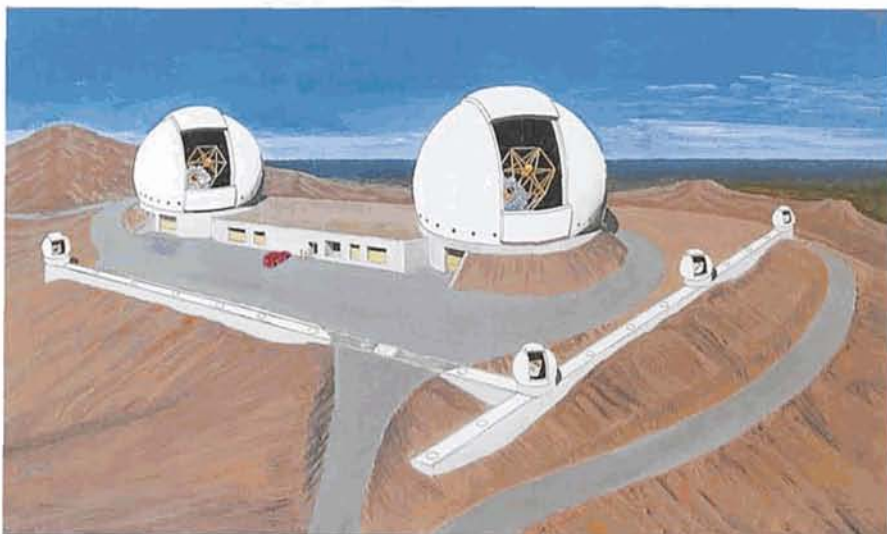

Figure 4: *Artist's view of the planned Keck Interferometric Array consisting of two 10-m telescopes and 4 movable 150-cm telescopes. (Courtesy A. Meinel et al.)*
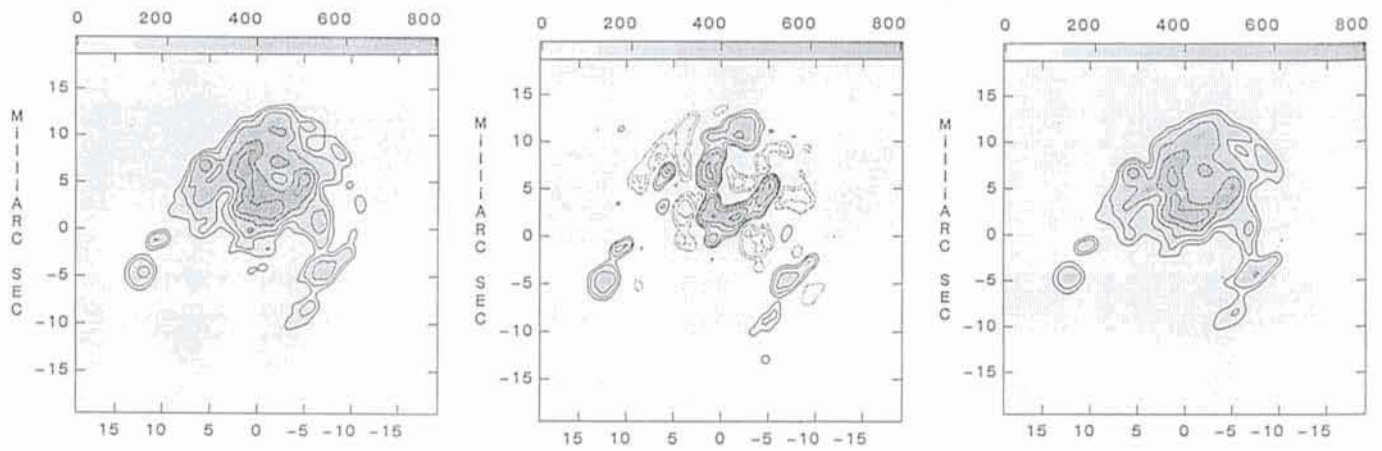
Figure 5: *Image reconstruction with the VLT Interferometer 8-m-telescope array (no auxiliary telescopes used). Left: input test image. The image is observed at 1 μm wavelength where the radius of the Airy disk is 30 milli-arcsec. The object is therefore just unresolved with the individual 8-m telescopes. Declination = 65°. Middle: image reconstructed without using the central (u,v) plane coverage resulting from a single 8-m telescope. Right: image reconstruction including the single 8-m (u. v.) plane coverage. (Courtesy R. Braun et al.)*

Aperture Masking: a Step Towards Multi-Aperture Interferometry

Many large-aperture telescopes (e.g. Hale telescope, Herschel telescope and Anglo-Australian telescope) are now being successfully used for high angular resolution imaging using aperture masks to mimic multi-aperture interferometry. Figure 2 shows a fine result of these experiments for the variable red supergiant star Betelgeuse.

These experimental observations are of great importance not only because of their astrophysical impact but also as a precursor to the imaging with multiple aperture interferometers. By using aperture masking the validity of imaging algorithms can be evaluated under realistic observing conditions, including various levels of photon noise.

Multi-Aperture Interferometry

A great deal of time was devoted to discussing the progress in multi-aperture interferometry. In contrast to speckle interferometry this is a field which is experiencing rapid advances in the development of experimental techniques but with the ability to do full two-dimensional imaging still to be realized. Interferometers in existence are now used to do astrometry (not within the topic of the conference) and to determine a limited number of parameters on stellar objects like diameters and binary orbits and separation. Table 1 lists the interferometers presently routinely in operation.

The last two interferometers in Table 1 (SUSI and COAST) have only recently come into operation and first results were reported at the conference. What is especially impressive in these new interferometers is that "first fringes" are obtained soon after the installation of the interferometer testifying to the fact that the construction of optical interferometers and delay lines with the required opto-mechanical and operational properties is well within the state of the art.
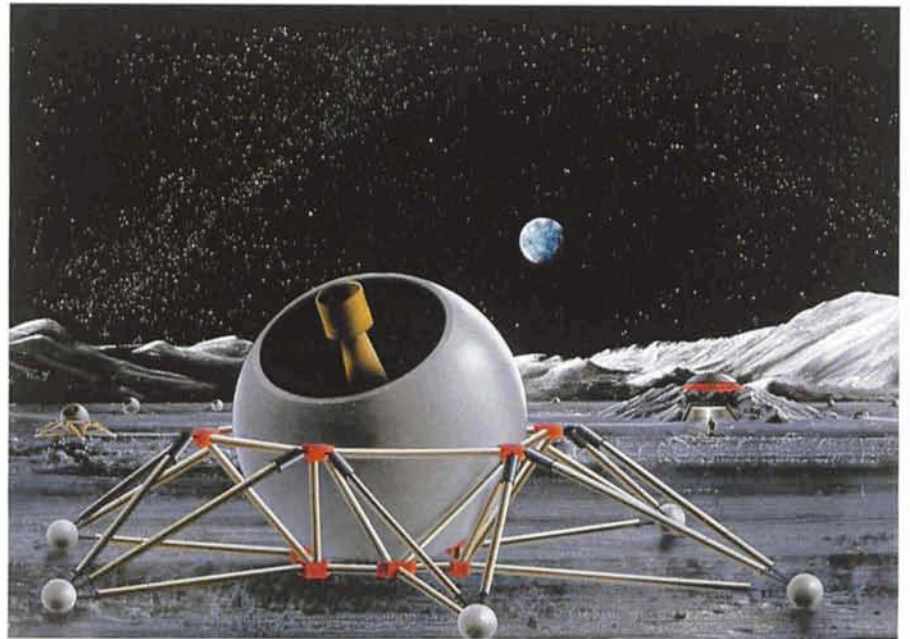
In addition to the operational inter-

Figure 6: *Artist's view of Antoine Labeyrie's proposal for a Lunar Optical Very Large Array. In foreground one of the 27 telescopes on its transporter. To the right in the background the beam-combining station. (Courtesy A. Labeyrie.)*

Table 1: *Optical Interferometers now in Operation*

Location	Maximum Baseline	Number of Telescopes[a]	Telescope Aperture
CERGA/I2T	140 m	2	26 cm
CERGA/GI2T	70 m	2	150 cm
CERGA/Soirdete	15 m	2	100 cm
MMT	5 m	6	180 cm
Mt. Wilson/Mark III	32 m	3	5 cm
Mt. Wilson/ISI	13 m	2	165 cm
Narrabri/SUSI	640 m	2	14 cm
Cambridge UK/COAST	100 m	2	40 cm

[a] = Number of telescopes in use at this time. Often more telescopes are planned.
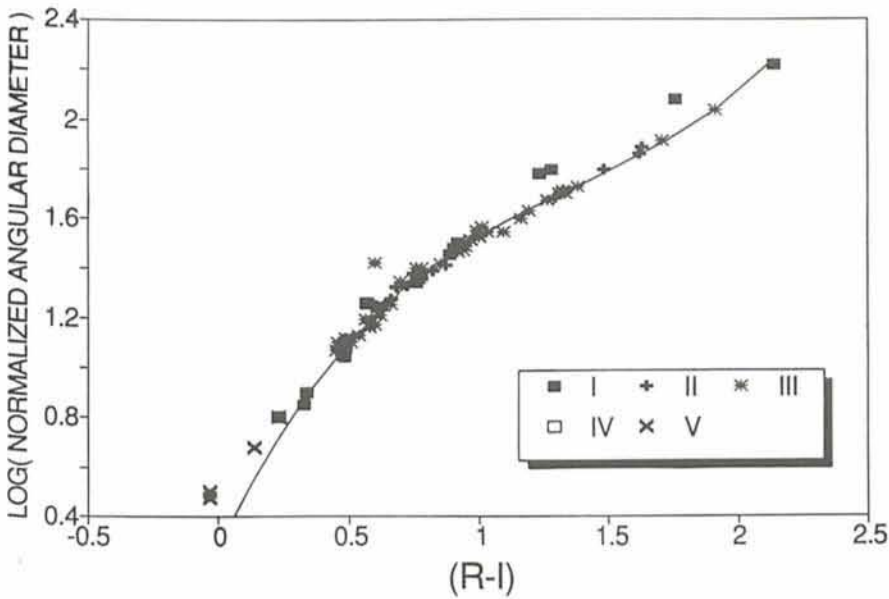
Figure 7: *Diameters of stars normalized to the same magnitude as a function of spectral type as observed with the Mark III interferometer. (Courtesy A. Quirrenbach et al.)*
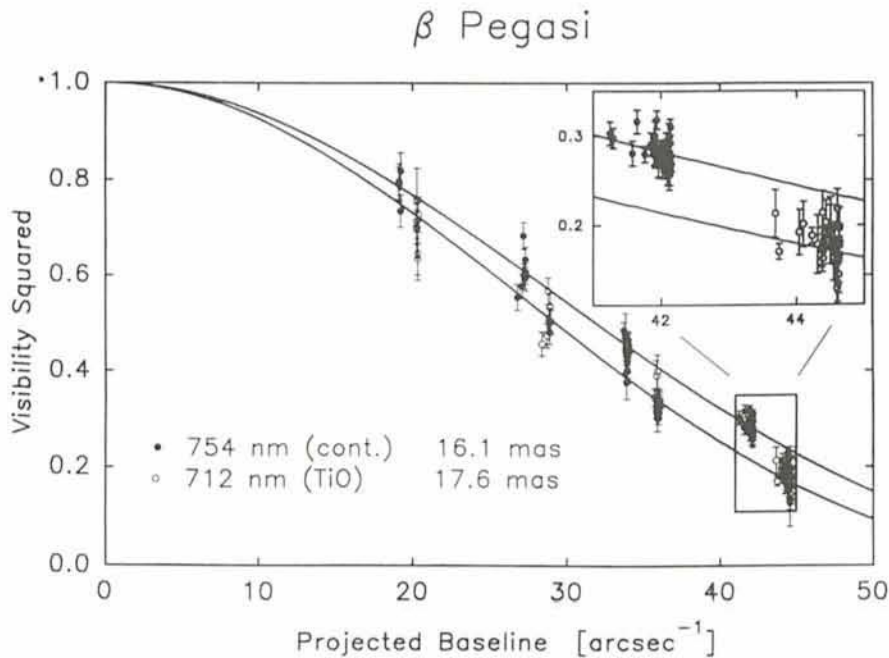

Figure 8: *The fringe visibility as a function of interferometer baseline for two spectral bands centred respectively on a TiO molecular band and the nearby continuum for the giant star β PEG. The derived diameters of respectively 0.0176 and 0.0161 arcsec have an error of ± 0.0001 arcsec so that the differences are real. The differences are an important diagnostic for the extended atmosphere. (Courtesy A. Quirrenbach et al.)*

Most of these arrays are intended to produce images in ways similar to the way this is done in radio interferometers using image synthesis techniques relying on tracking the object while it moves across the sky, thus causing the generation of a number of tracks in the (u,v) Fourier transform plane. The relatively large sizes of some of the telescopes involved causes these tracks to be relatively "fat" and to give a good (u,v) plane filling near the low frequency origin. The latter is very important in giving high quality images (see Fig. 5).

At a minimum one night is needed to generate an image as shown in Figure 5. Often more than one night might be needed if a good signal-to-noise ratio is required. An important advantage of the VLT Paranal site is the large periods of clear skies allowing uninterrupted (u, v) plane tracks. Time synthesis techniques are, however, obviously inadequate for observations of full images of objects which change on a rapid time scale (less than one day). For that type of interferometric imaging "snapshots" are desired which can only be obtained by arrays of many telescopes or by the capability to rapidly reconfigure an array with fewer telescopes. Antoine Labeyrie described his plans to construct such an Optical Very Large Array, or OVLA, containing 27, or perhaps even 130, telescopes on Earth and eventually on the Moon. Figure 6 shows an artist's view of the lunar version of OVLA. A price to pay for making snapshot images by the simultaneous use of so many telescopes at once, over an array of a few telescopes, is the loss in signal-to-noise. This results from the need to mix in optical interferometry all radiation directly, so that the signal for each two-telescope baseline contains the photon noise of the light collected by all telescopes. This is a major difference between optical and radio interferometers where such a loss does not occur.

Some Results of Multi-Aperture Interferometry

As already mentioned, full imaging with multi-aperture arrays has not been achieved yet. The results of aperture masking experiments (see Fig. 2) gives confidence that the imaging arrays now being implemented will result in astronomical images within the not too distant future. Impressive results were, however, presented at the conference on the orbit of spectroscopic binaries and on stellar diameters, including asymmetries in the shape of stars like Mira. As an example we show in Figures 7 and 8 some of the diameter observations made with the Mt. Wilson Mark III interferometer.

ferometers listed in Table 1, a number of interferometers are in the construction and planning phase. The former include the Big Optical Array (BOA) by the US Naval Research Laboratory, the US Naval Observatory Astrometric Interferometer, the ESO VLT Interferometer (see Fig. 3), the IOTA array by the Center for Astrophysics, an array at the Khazan Observatory (USSR), and the IRMA array by the University of Wyoming. In the planning phase are the Optical Very Large Array (OVLA) by Antoine Labeyrie, the Keck Interferometric Array (KIA) shown in Figure 4, the CHARA interferometer of Georgia State University, and extensions of some of the arrays listed in Table 1.

9

Major Uncertainties about the Atmospheric Wavefront Structure Function

The spatial frequency distribution of the wavefront distortions introduced by the earth atmosphere is of great importance for the behaviour of interferometers and for the wavelength dependence of the seeing disk size. Frequently it is assumed to correspond to a Kolmogoroff distribution which results in the RMS wavefront differences to grow as the baseline to the power 5/6. Serious concerns were expressed at the conference about the validity of the Kolmogoroff distribution. Observations with the two Mt. Wilson interferometers (Mark III and the ISI, see Table 1) give very different results. Whereas the Mark III interferometer indeed gives results consistent with a Kolmogoroff distribution, the ISI researchers find the exponent to decrease from $\approx 5/6$ to $\approx 1/2$ for good seeing conditions. This is a very large difference which will have a major influence on the predicted performance of interferometers and large telescopes.

Future Meetings

ESO plans to hold its next meeting in this conference series (High Resolution Imaging by Interferometry III) in the spring of 1994. The topic of adaptive optics, of major interest for interferometry, will be dealt with extensively in the April 27–30, 1992 ESO conference on "Progress in Telescope and Instrumentation Techniques". From January 11–15, 1993 the IAU Symposium No. 158 in Sydney, Australia, on "Very High Angular Resolution Imaging" will focus on interferometric imaging at both optical and radio wavelengths.

PROFILE OF A KEY PROGRAMME

Optical Identification of Celestial High Energy Sources

G. F. BIGNAMI, P.A. CARAVEO and S. MEREGHETTI, Istituto di Fisica Cosmica del CNR,
*   Milano, Italy*
J. PAUL, B. CORDIER and A. GOLDWURM, Service d'Astrophysique, Centre d'Etudes de
*   Saclay, France*
P. MANDROU, J.P. ROQUES and G. VEDRENNE, Centre d'Etude Spatiale des Rayonnements,
*   Toulouse, France*

The problem of the optical identification of high energy (X-and γ-ray) sources is a classic of modern astronomy. It is only through the optical studies that one can gain complete understanding of objects, galactic and extragalactic alike, which emit a lot of their energy, through thermal and non thermal processes, in photons 1000 or one million times more energetic than the optical ones. For hard X-rays and γ rays the problem is complicated by the source location accuracy, limited by the physics of the detection interaction. In particular, the focussing of photons is only possible if their wavelength is comparable to the surface roughness of the reflecting surface, and this happens, in practice, only up to a few keV.

This is why, in the presence of a poorly positioned high-energy source, one tries to exploit the soft X-ray domain to zero on the possible optical counterparts. Broadly, this has been the strategy adopted in our Key Programme "Optical follow up identification of hard X-ray/soft γ-ray sources discovered by the SIGMA telescope" (see also Bignami et al., 1990). About two thirds of it have already been carried out, and the first
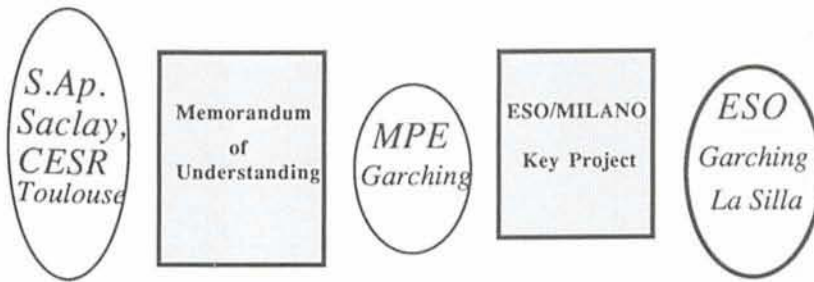
SIGMA→ROSAT→ Optical

Figure 1: *Strategy of our Key Programme.*

results can be briefly outlined in what follows.

During two observing runs in January and May 1991, we used EMMI at the (ESO) NTT telescope to perform imaging and spectroscopy in our candidate fields, selected following the strategy outlined in our original proposal. As mentioned, the idea is to bridge the gap between the SIGMA hard X-ray energy (>40 keV) range and the optical domain, taking advantage, when feasible, of the location accuracy achievable from the ROSAT soft X-ray "all sky survey". As sketched in Figure 1, this is based on an ad hoc agreement between the proposing team and the Max-Planck-Institut für Extraterrestrische Physik. This method was successfully applied for the first time to the newly discovered GRANAT source called GRS 1758−258, seen by both the French SIGMA and Soviet ART-P instruments (Sunyaev et al., 1991).

GRS 1758−258 lies only 40′ from the bright soft X-ray source GX 5−1 to which previously, for lack of resolving power, the hard radiation was erroneously attributed. Thus, the discovery of this new source is in itself a remarkable achievement of the coded mask technique, used extensively for the first time by the SIGMA and ART-P instruments. The position of the source, measured with ~1′ accuracy by the ART-P telescope, has been dramatically improved thanks to the use of the ROSAT survey data. In fact, using the well-known position of GX 5−1 as a reference, it has been possible to locate GRS1758−258 within a 10″ radius (90 % confidence) error box. Images were obtained with the EMMI red arm using R,I and z filters on May 10, 1991 with the Ford Aerospace 2048 CCD, providing a pixel size of 0.35″. The Guide Star Catalog of the HST was used to perform the astrometry of the field in order to compute the source position and superimpose the ROSAT error box. The outcome is shown in Figure 2 for a 1-m exposure in the I filter. The field is very crowded and

several candidates are present down to a limiting magnitude of ~21. The corresponding R and z exposures did not reveal any candidate with peculiar colours. Given the low galactic latitude of this field, absorption is a very critical parameter, so that the next step would be obviously to obtain near IR images of this error box.

During the May observing run, partially hampered by clouds and rain, we concentrated on 1E 1740.7−2942, a soft γ-ray source 50′ from the galactic centre line of sight. This source, already known to be the only high-energy source in the galactic centre region, has

been the target of several SIGMA observations which revealed its highly variable nature both in flux and spectral shape. In particular the presence on October 13, 1990 (Paul et al., 1991, Bouchet et al., 1991) of a significant bump in the 300−600 keV region, makes 1E 1740.7−2942 a very plausible candidate for the explanation of (at least part of) the variable e^+/e^- annihilation line measured, over more than a decade now, from the galactic centre region.

Deep images of the region of 1E 1740.7−2942 have been obtained in different filters, adding slightly offset pointings. To position the X-ray source in our images we needed stars fainter than the ones contained in the GSC distributed on CDROM, so that we had to use the original digitized GSC data, which were kindly communicated to us by D. Golombek. In Figure 3 the error circle has been superimposed to the I 14-minute image which appears to be about 3 magnitudes fainter than the SERC I plate presented by Skinner et al., 1991. In fact, stars 1 to 7 are seen here for the first time and their I magnitudes range from about 19 to 21.4.

More objects are visible in the 30 m z filter image shown in Figure 4. The very faint ones are better visible in the contour plot in Figure 5, where a marginally
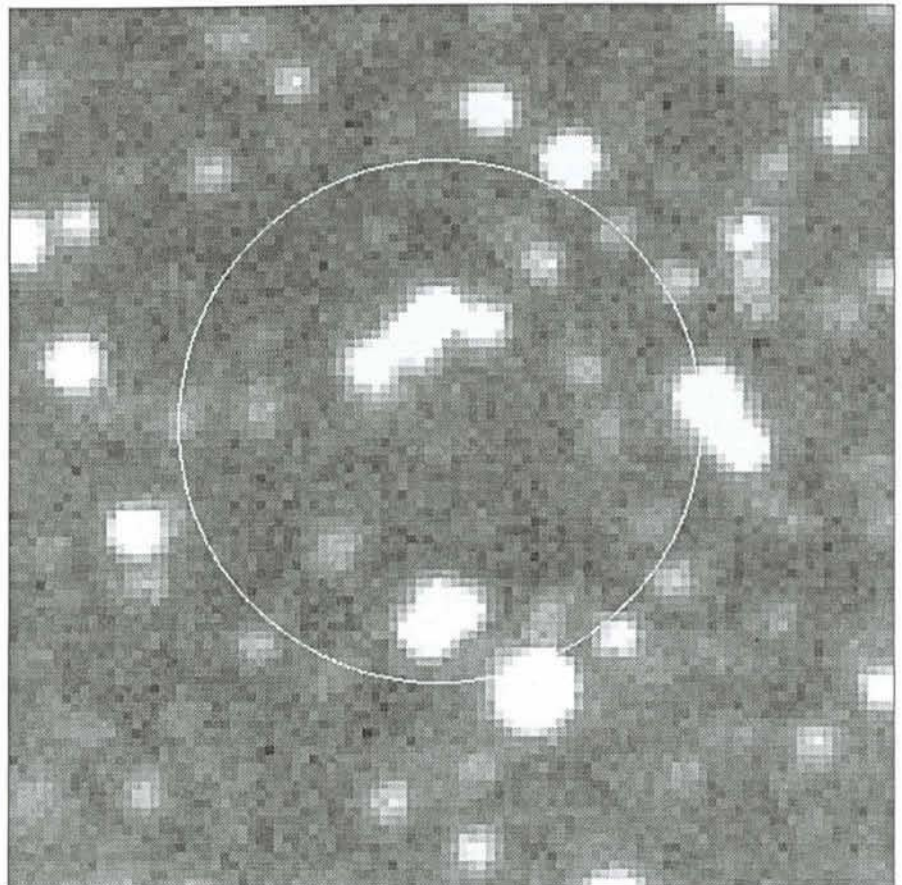

Figure 2: *I-band image of the sky region containing GRS 1758−258. The error box radius is 10 arcsec. North is to the top and East to the left.*
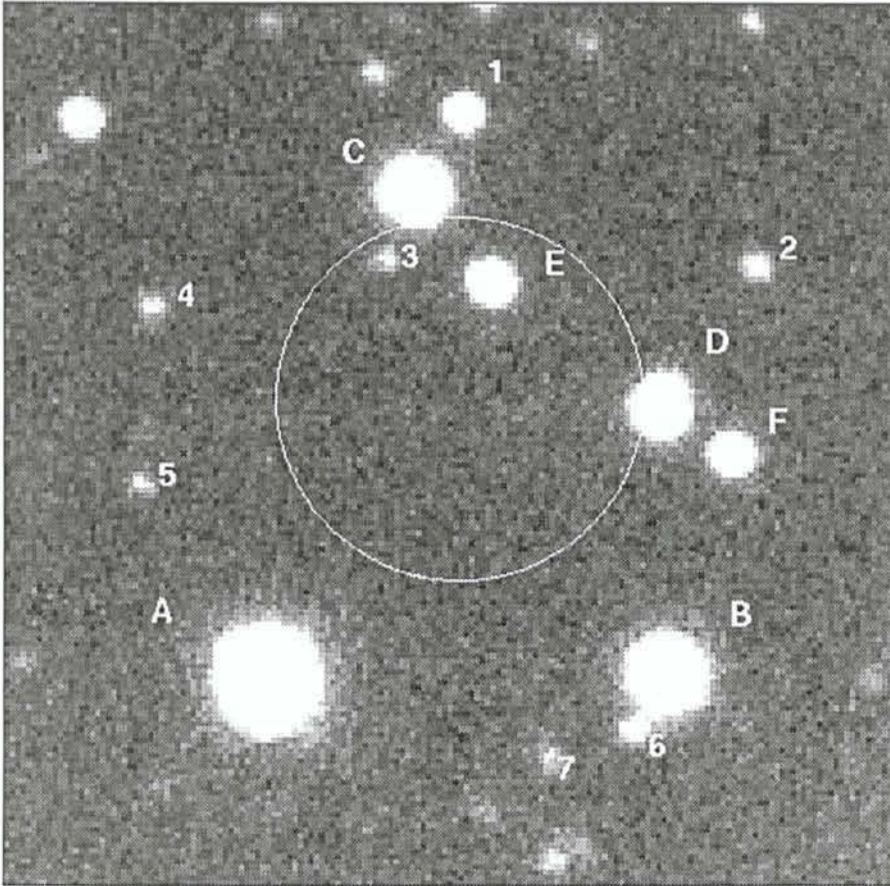
11

Figure 3: *I-band image of the sky region containing 1E 1740.7−2942. The error box radius is 12 arcsec. North is to the top and East to the left.*

molecular clouds in the centre of our galaxy, so that the search for a more standard counterpart should certainly not be abandoned.

Further detailed investigations of SIGMA sources must still await, at this time, accurate soft X-ray positioning to come mostly from the ROSAT mission. However, the case of Nova Muscae gives another example of an interesting correlation between γ-ray astronomy from Sigma data and ground-based ESO observations, as published by Della Valle et al., 1991.

In the spirit of our Key Programme we have also worked towards the understanding, through the investigation of optical counterparts, of a number of peculiar, unidentified, presumably galactic X-ray sources. This has included, among others, recently discovered GINGA-ROSAT transients, and a number of other serendipitous EXOSAT and Einstein sources. Of particular interest is the case of 1E 120723−5209.8, one of the very few remaining Einstein HRI sources with no firm optical counterpart. The source is at medium galactic latitude, in a non crowded field, and especially interesting because it is located near the geometric centre of the SNR PKS 1255−62. Previous efforts (Matsui et al. 1988) had only yielded a 17-magnitude field G dwarf inside the

detected source appears near the weak point-like VLA radio source recently discovered by Prince and Skinner (1991) and proposed as the counterpart of 1E1740.7−2942. The relative positions of our new z-object and of the 0.6 mJy VLA source are such that an association between the two cannot be excluded. Of course, chance coincidence with a field source, both galactic and extragalactic, is still possible.

More details on the optical investigations of GRS 1758−258 and 1E1740.7−2942 can be found in Mereghetti et al. (1991).

Recently, two papers (Bally and Leventhal, 1991; Mirabel et al., 1991) have appeared, suggesting in parallel a model for 1E1740.7−2942 based on a collapsed object embedded in a thick molecular cloud in the central region of the galaxy. The idea is certainly tenable and also important because, if confirmed, it would point to the first example of a new class of galactic highenergy sources. Here again better ground-based observations including IR and radio millimetric could be crucial for an understanding if not of the object itself, probably invisible, at least of its immediate surroundings. However, the chance coincidence of such scenario is rather high, owing to the high density of
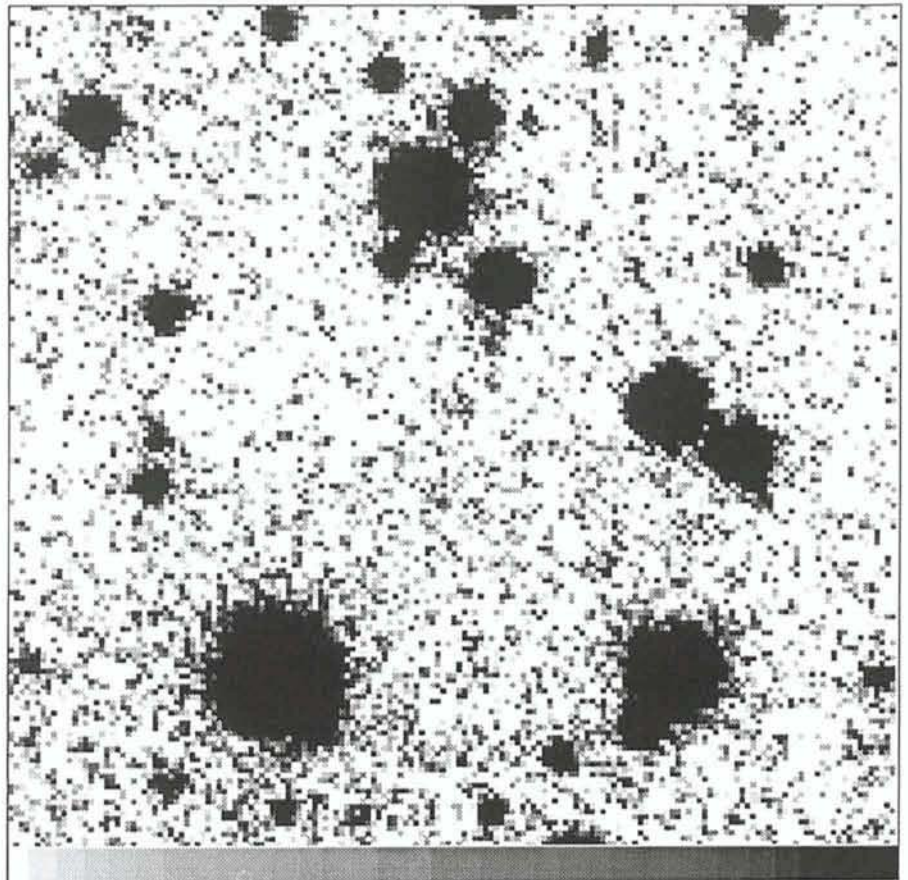

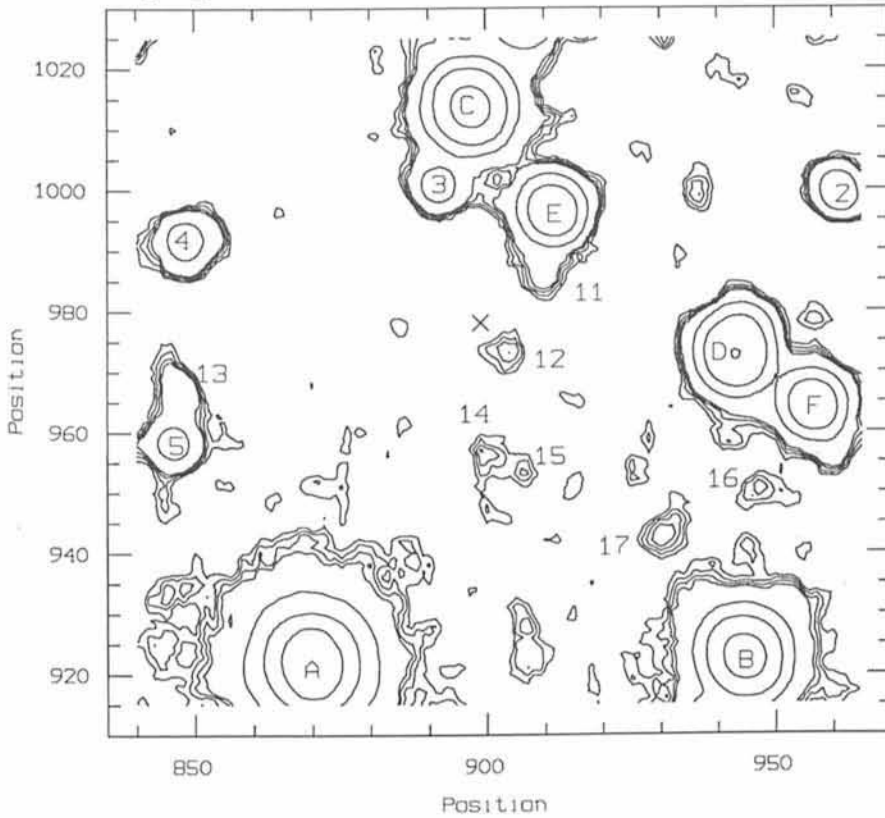Figure 4: *Image of the region of 1E 1740.7−2942 in the z filter.*

Image: gc30mZ

Figure 5: *Contour plot of the image shown in Figure 4. The cross indicates the position of the VLA radio source (α = 17 h 40 m 42.99 s, δ = –29° 43' 25" (1950)).*
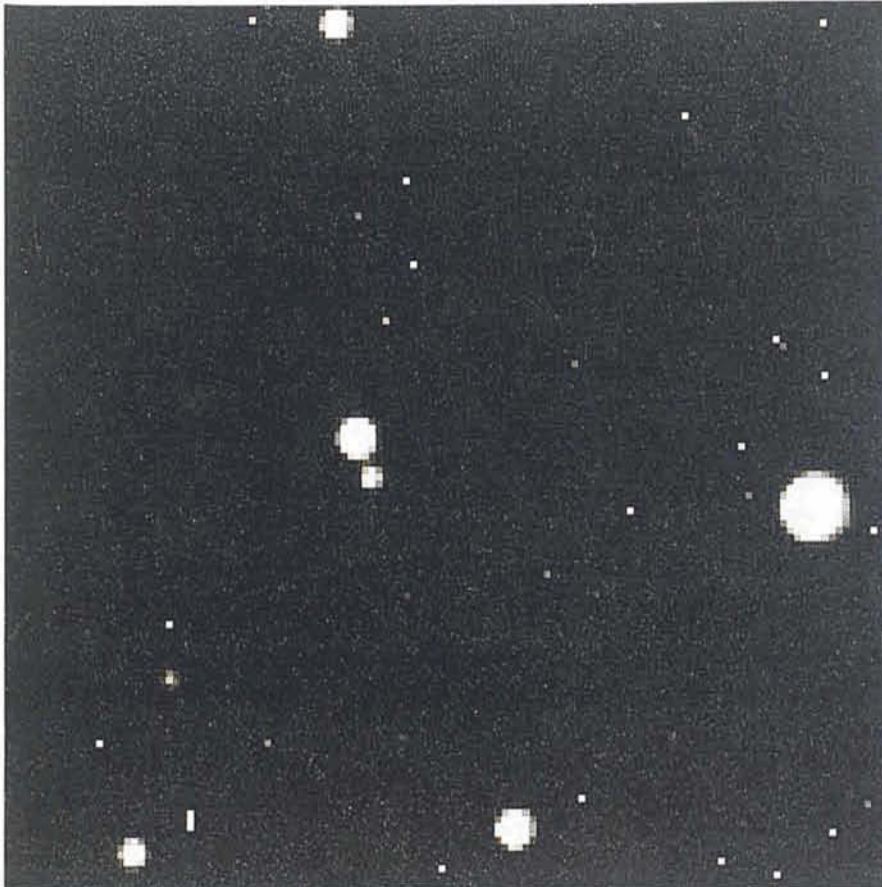

Figure 6: *NTT EFOSC2 V image of 1E120723–5209.8. The field G star (m$_v$=17.34) and the new candidate (m$_v$=19.04) are 1.8 arcsec apart. North is to the top and East to the left.*

5" HRI error box, unlikely to be responsible for the X-ray emission. Our first image with the NTT equipped with EFOSC2 in a night of good-to-moderate seeing (0.9") showed the presence of a 19-magnitude object 1.8" from the field star, and thus so far unseen. This is shown in Figure 6. The newly discovered object is very likely to be the X-ray source counterpart, although the preliminary spectrum taken at the NTT, showing no obvious signature, does not allow its immediate identification. The nature of this object could still range from a neutron star, possibly associated with the SNR, to a field BL Lac.

In conclusion, we would feel particularly happy if our Key Programme, beyond its quantitative results, had achieved its purpose of rendering the community aware of the importance of multiwavelength astronomy – from ground as well as from space – for tackling the new objects discovered by high-energy astronomy.

References

Bally, J., Leventhal M., 1991, *Nat* **353**, 234.
Bignami G., Caraveo P.A., Mereghetti S. et al., 1990, *The Messenger* **60**, 16.
Bouchet L. et al. 1991, *Ap.J.* (Letters), in press.
Della Valle M., Jarvis B.J., West R.M., 1991, *Astron. Astrophys.* **247**, L33.
Matsui Y., Long K.S., Tuohy, I.R., 1988, *Ap.J.* **329**, 837.
Mereghetti S., Caraveo P., Bignami G.F., and Belloni T., 1991, submitted to *Astron. Astrophys.*
Mirabel I.F., Morris M., Wink J. et al., 1991, *Astron. Astrophys.*, in press.
Paul J., et al., 1991, in *Gamma-Ray Line Astrophysics*, eds: Durouchoux Ph., Prantzos N. (New York: IAP), 17.
Prince T., Skinner G.K., 1991, IAU Circ. 5252.
Skinner G.K., et al., 1991, *Astron. Astrophys.*, in press.
Sunyaev R., et al., 1991, *Astron. Astrophys.* **247**, L29.

EMMI, Explorer of the Southern Sky

A new ESO video film has just become available, which describes the ESO multimode instrument, known as EMMI and now mounted at one of the NTT Nasmyth foci. The video explains in some detail the function of this instrument and how it was built. There are also some examples of the astronomical observations which have been made with EMMI.

It can be obtained from the ESO Information Service (address on last page). The cost is DM 70.–. Prepayment is required to account No. 210 2002, Commerzbank München, BLZ 700 400 41.

Trouble in the Magellanic Clouds!

First Results from the Key Programme on Coordinated Investigations of Selected Regions in the Magellanic Clouds

K. S. DE BOER, Sternwarte der Universität Bonn, Germany

F. SPITE, P. FRANÇOIS, R. CAYREL, M. SPITE, Observatoire de Paris, Meudon, France

B. BASCHEK, J. KÖPPEN, Institut für Theoretische Astrophysik, Heidelberg, Germany

B. WOLF, O. STAHL, A. JÜTTNER, Landessternwarte, Heidelberg, Germany

W. SEGGEWISS, D. J. BOMANS, E. K. GREBEL, E. H. GEYER, T. RICHTLER, A. VALLENARI, Sternwarte der Universität Bonn, Germany

J. KOORNNEEF, Space Telescope Science Institute, on assignment from ESA

F.P. ISRAEL, Sterrewacht Leiden, Netherlands

P. MOLARO, S. MONAI, G. VLADILO, Osservatorio Astronomico, Trieste, Italy

S. D'ODORICO, R. LEISY, European Southern Observatory

M. DENNEFELD, R. FERLET, A. VIDAL-MADJAR, Institut d'Astrophysique, Paris, France

G. STASINSKA, Observatoire de Paris, Meudon, France

M. AZZOPARDI, N. MEYSSONNIER, G. MURATORIO, E. REBEIROT, Observatoire de Marseille, France

J. LEQUEUX, Ecole Normale Supérieure, Paris, France

Does star formation proceed in an orderly way? How homogeneous are the Magellanic Clouds in their metal content? Is the motion of the gas complexes well behaved?

In the course of the Key Programme we started to doubt that our companion galaxies show systematic behaviour. After two fairly successful observational seasons with (except for the slitless spectroscopy and the photometry) good observing conditions, conflicting evidence on some of the fundamental questions has been obtained.

Our Key Programme was among the first to be accepted and has as speciality those two southern-sky galaxies which unfortunately can be observed under good conditions only in the southern summer. This means that the observational progress is slower than in programmes of survey nature. In addition, although our Key Programme does require a fairly large amount of telescope time, it consists of small subprogrammes, each of which takes a number of nights equal to that of any regular ESO proposal. In short, especially the coordination aspect is important, both time-wise and with respect to the objects (Regions) where the research is carried out. The regions had been selected on scientific grounds (see de Boer et al., 1989; here we show pictures of the Magellanic Clouds with the Regions marked (Fig. 1).

The subprojects we are working on are the following: (1) spectroscopic survey with EFOSC (Marseille, Paris, Uppsala); (2) CCD photometry in small fields within the regions (Bonn); (3) IRAC photometry of the same (Baltimore, Leiden); (4) stellar spectroscopy for the study of element abundances in the hot stars (Heidelberg) and cool stars (Meudon) of field and clusters; (5) the investigation of the interstellar absorption lines (Trieste, Paris); (6) the study of the spectra of emission nebulae (Paris). All these projects are carried out in coordination and it is this aspect which promises (and starts to show) new scientific results.

During our first observing runs we concentrated on two of the regions with the young clusters NGC 330 and NGC 1818. But also in Region E in the upper edge of supershell LMC 4, in which one finds an old cluster and young stars, as well as in the supernova field observations were carried out. In all cases puzzling effects have been found. A review of earlier work and of new results also from our Key Programme may be found in the conference proceedings edited by de Boer, Spite and Stasinska (1989) and by Haynes and Milne (1991) respectively.

Age Versus Metallicity

Region A in the SMC contains the young cluster NGC 330 which stands out from the field. Its age derived from our CCD photometry is of approximately 10 Myr. The surrounding field population (if homogeneous) has an age of at least a factor of 10 larger. The cluster contains blue supergiants, while the field is almost devoid of these. Observations of the cluster area have been performed with EFOSC1 in the slitless mode using a grism and an Hα+[NII] interference filter. Thanks to special software routines (Muratorio and Azzopardi, 1990) this survey resulted in the identification of about twice as many new Hα emission-line objects as in the Curtis-Schmidt telescope spectroscopic survey of the same field. This led to estimate the total number of Hα emission-line objects in the SMC to about 40,000 (Meyssonnier and Azzopardi, 1991). In particular, about sixty Hα emission-line stars have been discovered in the cluster NGC 330 (Fig. 2), while only 10 were known to Feast (1972). With the normal BVR CCD observations, also an Hα wide filter was used for a few exposures. Including also Strömgren photometry, Grebel developed in her Diploma thesis an elegant method to isolate the Be stars in the sample. Her identifications could be confirmed completely with the EFOSC data. From the final account of that work (Grebel et al., 1991) we show the colour-colour plot (Fig. 3), demonstrating an exceptional high Be star fraction in that SMC cluster.

Metallicity problems with NGC 330 emerged in a combination of studies. Spite, Richtler and Spite (1991) and Barbuy et al. (1991) confirmed results of work carried out before the Key Programme, in showing that the metal content of red supergiants in NGC 330 is −1.0 to −1.1 dex. Very similar results
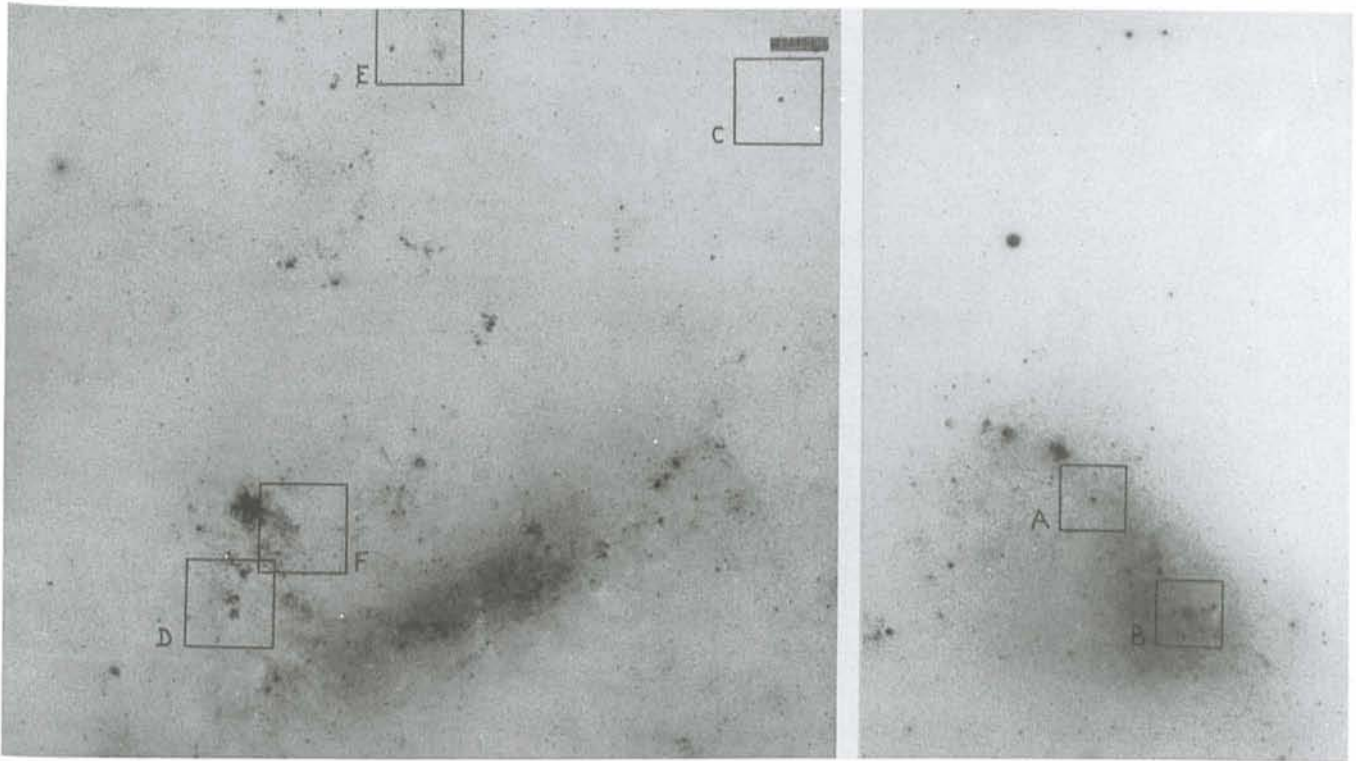
Figure 1: *In the SMC and the LMC a total of six regions have been defined where all studies of our Key Programme are concentrated. Region A: NGC 330 and field, poor in gas and dust; Region B: N27 and crowded field, rich in gas and dust; Region C: NGC 1818 and field, poor in gas and dust; Region D: N 159 and field, rich in gas and dust; Region E: NGC 1978, NGC 1948, and N49, some gas and dust; Region F: SN 1987A and field, gas and dust. (Picture with thanks to Reiner Donarski, ESO.)*

have been obtained from one hot star in NGC 330 (see Reitermann et al., 1990. Jüttner et al., 1991). For work on hot stars it was necessary to obtain also IUE spectra to get reliable effective temperatures. For the field stars, earlier data by Spite, Barbuy and Spite (1989) and by Russell and Bessell (1989) from Mt. Stromlo, indicated that the field has a metal content of −0.6 to −0.7 dex. This was confirmed in a related study, where Grebel and Richtler (1991) could show from CCD Strömgren photometry that the red giants and supergiants in NGC 330 have indeed a lower metallicity than those in the surrounding field, the difference being of the order of 0.5 dex. In short, the cluster NGC 330 is younger than the surrounding field stars but with a metallicity clearly below that of the field. This means that the SMC must be chemically very inhomogeneous! A similar effect had been found spectroscopically in Region C in the LMC which contains NGC 1818 (Richtler, Spite and Spite, 1989; Reitermann et al., 1990). Here the data could not yet be substantiated through photometry.

The abundance pattern of the elements in the Magellanic Clouds (Table 1) is in general not well understood. The large carbon deficiency found in the SMC HII regions (Dufour et al., 1982) is neither found in the stars of NGC 330 (Barbuy et al., 1991) nor in those of the surrounding field. The question thus is: are the analyses of the

stars wrong or those of the HII regions, or perhaps both? Or is C still depleted in HII-region dust? The emission-line object sub-project (which was started late in the Key Programme) should soon give additional information. Type I planetary nebulae will be studied (C-N-O processes) and IUE data are being collected. How does the C abundance affect the dust content and the molecule formation in the Clouds? A related interesting result is that europium (an r-process element) is relatively enhanced in the stars of NGC 330 (Spite, Richtler and Spite, 1991). Does this indicate a more primitive phase of chemical evolution in the Clouds (Westerlund, 1990)?

The values for the extinction in the Clouds cause trouble too. For the study of the abundance in the red supergiant stars it is of utmost importance to have a very accurate temperature determination and here the photometry group has

provided some input. But also the extinction may play a role. Recently, Bessell (1991) has critically analysed the information available on the extinction toward the SMC. He found that E(B−V) is rather of the order 0.1 than negligibly small. In an effort to contribute to the discussion with our Key Programme, the strengths of the interstellar sodium lines in the spectra obtained for our stars in and near NGC 330 were analysed. It is found by Molaro and collaborators that the foreground E(B−V), as derived from the strengths of the NaI lines and the correlation of N(NaI) with E(B−V), amounts to 0.08 to 0.1 mag. Even a small contribution by the SMC gas would bring the total E (B−V) near 0.11 mag. This new result indicates that some of the earlier abundance studies may have to be reworked!

Region E in the LMC, in the NW corner of the larger LMC-4 supershell,

Table 1. *Derived metal abundances relative to solar*

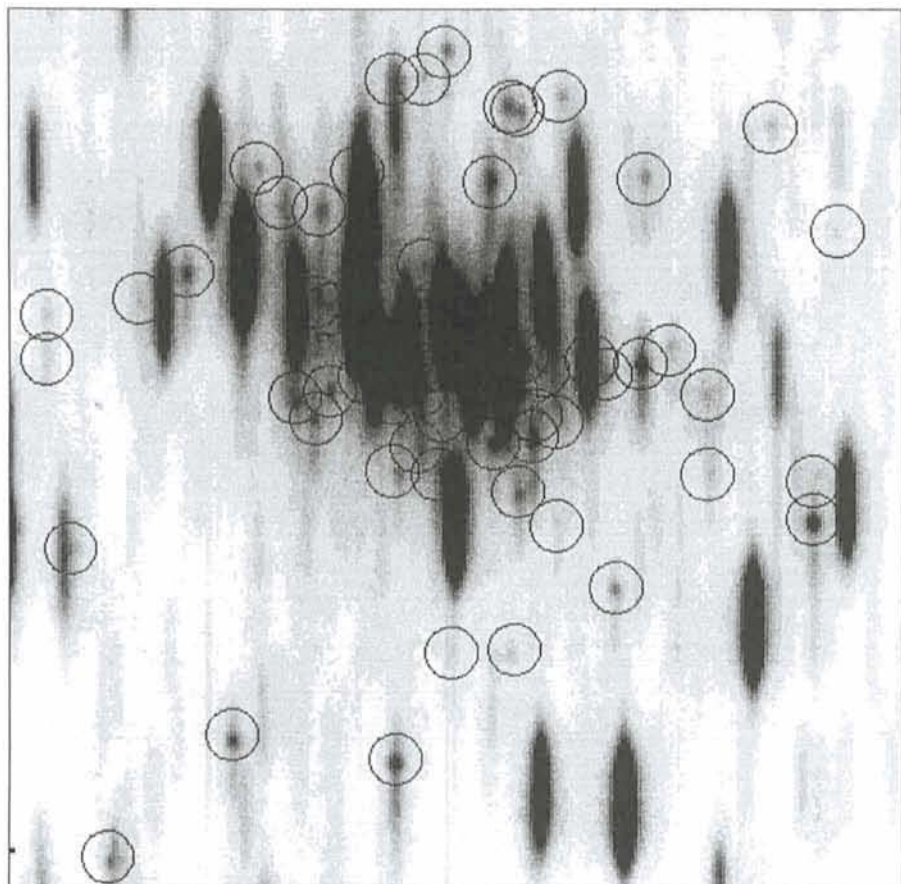|			C/H	O/H	Fe/H	Eu/Fe
SMC	Region A	cluster	− 0.9	− 1.1	− 1.0	+ 0.7
		field	− 0.9	− 0.8	− 0.6	+ 0.4
		HII regions	− 1.5	− 0.8	−	−
LMC	Region E	cluster	−	− 0.5	− 0.9	+ 0.6
		field	− 0.5	−	− 0.3	−
		HII regions	− 0.8	− 0.5	−	−

HII-region data from Dufour et al. (1982)

15

Figure 2: *Slitless spectroscopy of the young globular cluster NGC 330 with EFOSC (900 sec. exposure) through the red 300 grism (270 Å/mm) and an Hα+[NII] filter (6569Å/100Å). Emission-line objects (see open circles) show up clearly due to the Hα line (Azzopardi et al., in preparation).*

contains the old cluster NGC 1978, the young association NGC 1948 and the more compact young cluster with the emission nebula N 49. From spectra of a few stars we learned that the metallicity is about −0.4 but with an overabundance of Si in the sense [Si/Fe] = 0.4. Field spectroscopy is now available as well as CCD photometry in a strip covering NGC 1978 and NGC 1948. Field spectroscopy led to the detection of several new faint Hα emission-line objects including a few compact HII regions. In addition, EFOSC slitless spectroscopy (using the B1000 grism giving 850 Å/mm dispersion and a 1025 Å band-width interference filter at 4885 Å) resulted in the identification of a new faint planetary nebula and of some new carbon star candidates in NGC 1978 and its surrounding field. The large and most elliptical of all the LMC clusters, NGC 1978, is definitely older than 2 Gyr (Bomans et al., in prep.). In this strip the brighter part of the young population of the underlying field has an age of about 1 Gyr, but there are also stars which formed only 70 Myr ago. The association NGC 1948 is prominent due to its larger surface density of stars and its lower age of about 20 Myr. Synthetic colour-magnitude diagrams generated (Vallenari et al., in prep.) indicate that

most likely there has been a longer period of star formation and not just a recent single burst.

Measurements in the infrared with IRAC have not been possible yet because the new detectors did not arrive in time on La Silla to be adequately used by our Key Programme. The field spectroscopy and the photometry have suffered substantially from bad weather.

The first spectra of planetary nebulae and HII regions have been obtained, but it is too early to comment on abundances.

Approaching Gas Clouds?

The investigation of the interstellar medium was, due to its imminent importance, concentrated in the first period of the Region F around SN 1987A. Very good CaII and NaI interstellar line profiles have been obtained for more than a dozen of stars. The line profiles provide unique information on the structure of the ISM and many separate absorbing clouds can be recognized. One of our goals is to define the depth structure of the gas. For this the absorption lines are compared with HI 21-cm emission-line data available in the literature. From the 21-cm data it has been known for a long time that

there are three main gas complexes in the LMC, based on their radial velocities. These are at about 240, 270 and 300 km s^{-1} (heliocentric). All these components are present in the area of 30 Dor and thus in the field of the SN 1987A. Vladilo et al. (1991) could show that the 270 km s^{-1}, gas is not seen in absorption so that one must conclude that it is in the background of the LMC. Since the bulk of the material is near 290 to 300 km s^{-1}, one witnesses in the 270 km s^{-1} gas a large amount of mass approaching the rear of the LMC! The nature of our data as well as the essentials of this result can be seen in Figure 4.

The depths of the stars can now also be inferred from the IS data. Simply speaking, the more absorption components are seen, the deeper into the LMC the stars are located. Here also extinction studies will help, in the same way as others have shown that the SN 1987A itself was rather in the rear of the LMC. This line of approach is now also being used in Region E, and results will be available in the near future.

Interactions of Programmes

One very important aspect of the workings of the Key Programme collaboration is that data are being obtained in the same regions and on the same fields for the mutual benefit. Several examples can be given.

The spectroscopic surveys together with the CCD photometry provide input for the groups doing high-resolution stellar spectroscopy for abundance determinations. Indications for the spectral type are needed, but in particular also colour and brightness is of great value

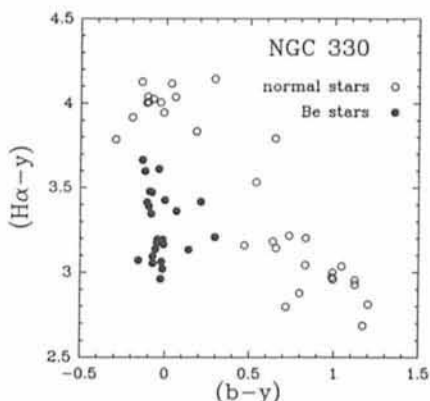Figure 3: *In a two-colour plot, involving Hα wide and Strömgren b and y, the normal stars show up along a line just below the diagonal in the diagram. Stars having Hα emission lines are bright at Hα (thus giving in 2.5 log (I(Hα)/I(y)) a smaller value) and appear below the sequence of normal stars (data from Grebel, Richtler and de Boer, 1991). This plot illustrates the exceedingly large fraction of Be stars in NGC 330.*

for the classification of the stars as main sequence or evolved star as well as with respect to the suitability for stellar and interstellar spectroscopy. In the spectroscopic survey data hitherto unknown emission-line objects have been discovered, objects to be further investigated by the emission nebula project.

The stellar spectra give in many cases preliminary information on the interstellar absorption lines, although often extra observations are required because of the very high resolution needed. And, as indicated before, the IS work helps to determine the value of the extinction, an essential parameter in the abundance studies.

The very existence of our Key Programme has stimulated others to pool efforts and work on the same regions as defined by us.

The abundance studies of hot and cool stars have benefitted much from the collaboration with M. Bessell from Mt. Stromlo. Not only are observing programmes coordinated, but the fact that Bessell analysed thus far stars of spectral type not addressed by us adds weight to our mutual research.

Right from the beginning, it was foreseen that our Key Programme would interact strongly with the ESO Key Programme on SEST CO observations of the Magellanic Clouds coordinated by Lequeux and Israel. For Regions C, D, and F the 12CO (1–0) observations are complete and some exist for the 12CO (2–1) transition. Region B has been partly covered and Region E is being planned.

In New Zealand, W. Tobin started patrolling some of our CCD fields in search for variable stars. The Mt. John University Observatory (see Tobin, 1991) is farther to the south than any other easily accessible facility, albeit with on average poorer weather conditions, but with better conditions for long-term monitoring programmes.

Finally, in cooperation with our Key Programme, observing programmes are being carried out with ROSAT on the MCs. In particular the Regions in the LMC will get good coverage being so near to the orbital pole of that satellite.

Figure 4: *The interstellar NaI spectrum obtained at a resolution of 100,000 in an exposure of 5400 sec. with the 3.6-m shows the great detail of the structure of the interstellar medium in the LMC in Region F. For comparison the HI 21-cm profile from Rohlfs et al. (1984) is shown to demonstrate that (as in all lines of sight in Region E) the strong HI 21-cm emission 270 km s⁻¹ component is essentially absent in absorption. Since most of the material in this direction has a velocity near 300 km s⁻¹, the 270 km s⁻¹ gas must be approaching this part of the LMC from the rear (Vladilo et al., 1991).*

References

Barbuy, B., Spite, M., Spite, F., Milone A. 1991, *Astron. Astrophys.*, in press.

Bessell, M.S. 1991, *Astron. Astrophys.*, **242**, L17.

de Boer, K.S. et al. 1989, *The Messenger* **57**, 27.

de Boer, K.S., Spite, F., Stasinska, G., Editors. 1989, *Recent Developments in Magellanic Cloud Research*, Obs. de Paris.

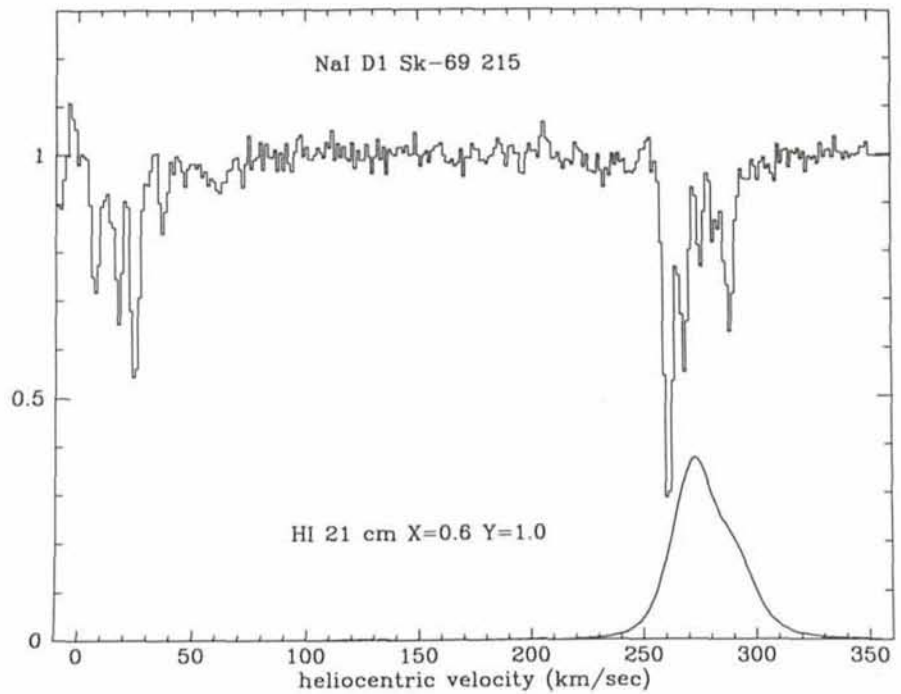Dufour, R.J., Shields, G.A., Talbot, R.J. 1982, *Ap.J.* **252**, 461.

Feast, W.W. 1972, *M.N.R.A.S.* **159**, 113.

Grebel, E.K., Richtler, T. 1991, *The Messenger* **64**, p. 56.

Grebel, E.K., Richtler, T. 1991, *Astron. Astrophys.* in press.

Grebel, E.K., Richtler, T., de Boer, K.S. 1991, *Astron. Astrophys.* submitted.

Haynes, R., Milne, D., Editors. 1991, IAU Symp 148, *The Magellanic Clouds*, Kluwer.

Jüttner, A., Stahl, O., Wolf, B., Baschek, B. 1991, in prep.

Meyssonnier, N., Azzopardi, M. 1991, IAU Symp "MCs", p. 196.

Molaro, P., Vladilo, G., D'Odorico, S., Dennefeld, M., Ferlet, R., Vidal-Madjar, A. 1991, *IAU Symp.* **148**, p. 434.

Muratorio, G., Azzopardi, M. 1990, Proc. 2nd ESO/ST-ECF Data Analysis Workshop, p. 6.

Russell, S.C., Bessell, M.S. 1989, *Ap.J.S.* **70**, 865.

Reitermann, A., Baschek, B., Stahl, O., Wolf, B. 1990 *Astron. Astrophys.* **234**, 109.

Rohlfs, K., Kreitschmann, J., Siegmann, B.C., Feitzinger, J.V. 1984, *Astron. Astrophys.* **137**, 343.

Spite, M., Barbuy, B., Spite, F. 1989, *Astron. Astrophys.* **222**, 35.

Spite, F., Richtler, T., Spite, M. 1991, *Astron. Astrophys.* subm.

Tobin, W. 1991, Pacific Reg. IAU Meeting, Proc. Astr. Soc. Australia, in press.

Vladilo, G., Molaro, P., Monai, S., D'Odorico, S., Dennefeld, M., Ferlet, R., Vidal-Madjar, A. 1991, in prep.

Westerlund, B.E. 1990, *Astron. Astrophys. Rev.* **2**, 29.

Visit to the ESO Headquarters

ESO was pleased to receive high-level visitors from Germany and Switzerland at the Headquarters in Garching, near Munich.

On October 31, 1991 Ministerialdirigent Dr. H. Strub and Ministerialrätin Dr. A. Hansen (ESO Council delegates) spent a day with ESO staff to inform themselves about the latest developments at ESO, in particular about the VLT project.

Presentations were made by senior ESO staff, and the guests from Bonn received detailed replies to their various questions. At the end of the day Drs. Hansen and Strub met with the German staff members in the auditorium where a very useful exchange of views took place.

On November 13, the new Swiss Consul General, Mr. P.A. Studer, and Vice Consul, Mr. R. Bloch, came to the ESO Headquarters to learn about ESO-Swiss interactions. They were very pleased to become better acquainted with our organization, and ESO was happy to learn about the interest of the local Swiss authorities in promoting good political and industrial contacts between ESO and their home country.

Unusual Solar Halos Over La Silla

D. HUTSEMEKERS, Institut d'Astrophysique, Université de Liège, Belgium

Most of the halo phenomena associated with the sun, or the moon, are caused by reflection or refraction of light in ice crystals which are hexagonal in cross-section, usually in cirrus-type clouds. The amazing variety of halos produced by these simple crystals is nicely explained in Greenler's book "Rainbows, halos and glories".

Halos are not infrequently seen over La Silla and, from time to time, interesting displays may be recorded like the series of pictures in Figure 1 which illustrate the evolution of a brightly coloured circumzenithal arc as the sun progressively sets down.

On January 27, 1990, we had the chance to photograph a rare and impressive combination of solar halos. The phenomenon appeared around 2 p.m. and lasted less than 1 h. It is partly illustrated in Figures 2 and 3, the different halos being identified in Figure 5. The coloured ring around the sun is the 22° refraction halo. It is particularly sharp and remarkable for its brightness and high contrast. Downwards, we successively encounter a part of the great 46° halo and the relatively rare circumhorizontal arc well detached from the former. Despite being fainter, both were significantly coloured. The striking feature was the small parhelic circle inside and tangent to the 22° halo. This halo surrounding the zenith and passing through the sun is due to reflected sunlight, as indicated by its whitish colour. Parallel to the horizon at the solar elevation, it is generally much more extended across the sky (see Fig. 8); as far as we know, this is one of the smallest parhelic circles ever reported (Cardon, 1977, discussed the observation of an unusual paraselenic circle whose diameter is comparable to that of the 22° halo). The peculiar aspect of this halo combination is due to the fact that at the moment of observation, the zenithal distance of the sun was exactly half the angular radius of the 22° halo, a situation which cannot occur at any latitude nor at any moment. After a few hours of interruption, the phenomena continued until sunset with the progressive apparition of the sun dogs and the circumzenithal arc. Figures 4 and 6 illustrate the complex of halos, unfortunately fainter, for a sun elevation of ~36°: the parhelic circle is much more extended. Two sun dogs are also present, located on the parhelic circle and well detached from the 22° halo.

It is quite remarkable that all the phenomena described before may be

Figure 1: *From top to bottom, this sequence of photos, obtained on February 20, 1990, illustrates the evolution of the circumzenithal arc as the sun progressively sets down. The circumzenithal arc is a refraction halo which appears around the zenith, high in the sky, and only for a sun elevation lower than 32° (see Fig. 8). It is one of the most brilliantly coloured halos caused by ice crystals, the purity of its colours often surpassing that of the rainbow. This occurs because the circumzenithal arc is not caused by a minimum deviation effect like for other halos (Fig. 7).*
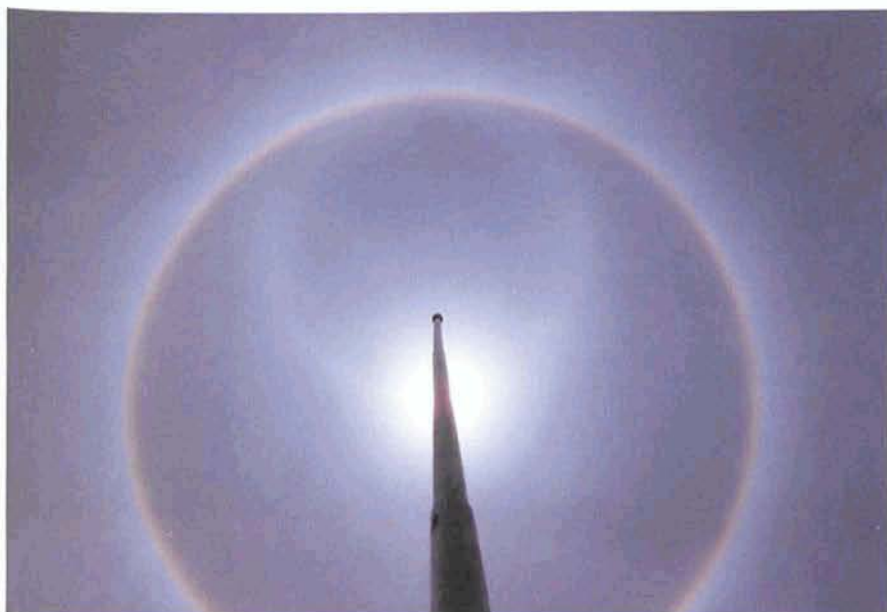
Figure 2: *The 22° halo and, inside, the very unusual parhelic circle photographed for a sun elevation of ~79° on January 27, 1990, about 2 p.m. local time. The colours indicate that the greatest halo is due to refraction while the parhelic (whitish) circle is due to reflected sunlight.*

simulations of Greenler et al. (1979, 1980). For the unusual parhelic circle seen in Figure 2, we have computed the theoretical brightness distribution along the perimeter. Fresnel formulae for reflectance times of the reflecting faces predict the intensity to be nearly constant along the perimeter except near the sun where it decreases to zero (see also Lynch, 1979). We find good agreement, but overexposure hampers a detailed comparison close to the sun. Finally, taking account of the angular diameter of the sun, the remarkable sharpness of the parhelic circle indicates that the oriented plate crystals producing it are aligned to better than 0.2°!

Apart from their aesthetic interest, observations of unusual halos or combination of halos may certainly contribute to a better understanding of ice crystal physics and ultimately one could hope to derive some characteristics of the atmosphere by simply analysing the observed halos. From the astronomical point of view, the halo phenomena may provide a unique tool for detecting crystals (not only ice) in planetary atmospheres (Whalley and McLaurin, 1984). This was first pointed out by O'Leary (1966) who suggested to measure the changes of Venus polarization near inferior conjunction when it passes the 22° scattering angle.

La Silla being located in a site where unique climatic conditions prevail and visited by many people equipped with

Figure 3: *The lower part of the halo complex illustrated in Figure 2. It was recorded at the same moment. In addition to the 22° halo, we can identify a portion of the 46° halo and the circumhorizontal arc.*

Figure 4: *The halo phenomena photographed a few hours later (about 5ʰ 40ᵐ p.m.) for a sun elevation of ~36°. The parhelic circle is now widely opened (see Figs. 6 and 8). Two parhelia or sun dogs are present, well detached from the 22° halo as can be expected for this elevation of the sun.* ▼

explained by the presence in the atmosphere of only one type of ice crystals: the plate-form crystals; pencil-shaped crystals if present would have produced additional halos like the circumscribed halo or the upper tangent arc (Greenler and Mallmann, 1972). The presence of a portion of the great 46° halo also suggests that plate crystals dominate (Plattloch and Tränkle, 1984). Figure 7 illustrates the different light rays which may explain the observed halos; most of the phenomena are in agreement with the
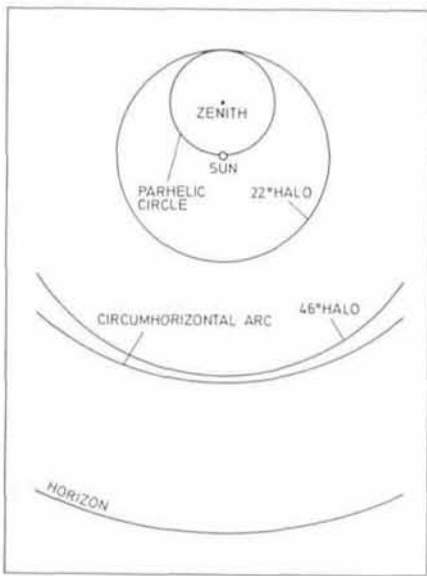
Figure 5: *Schematic zenith-centred projection illustrating the halo phenomena observed around 2 p.m. (Figs. 2 and 3).*

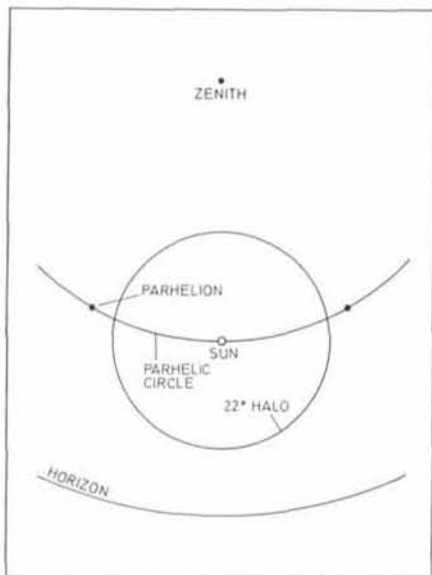Figure 6: *Schematic zenith-centred projection illustrating the halo phenomena observed around 5ʰ 40ᵐ p.m. (Fig. 4).*

Figure 7: *This figure illustrates the light rays passing through plate-form hexagonal ice crystals which are thought to be responsible for all the halo phenomena observed on*

January 27, 1990. For the refracted rays A and B, the crystals act as 60° and 90° prisms, respectively. The light therefore concentrates near the minimum deviation, i.e., for ice, near 22° and 46°. If the crystals are randomly oriented in the sky, these rays are at the origin of the 22° and 46° ring halos. The shape of these halos is independent of the sun elevation. Falling in the air, some of these crystals, the largest ones, tend to have their flat bases oriented horizontally. Through this subset of oriented crystals, rays of type A produce the light condensations called sun dogs or parhelia. For sun elevations close to 0°, the rays enter normal to the crystals and produce sun dogs located at the sun elevation on each side of the 22° halo. For higher sun elevations, the rays penetrate the oriented crystal with increasing skewness. The minimum angle of deviation through a prism being higher for skew rays, the sun dogs therefore appear detached from the 22° halo for moderately large sun elevations (Fig. 4). Interacting with the same subset of oriented crystals, the refracted rays C and D produce the circumhorizontal and circumzenithal arcs while rays E, reflected on vertical faces, are at the origin of the parhelic circle. For a given solar elevation, it is easy to realize that the light rays C, D, E apparently come from arcs or circles which are centred on the zenith and lie at constant elevation above the horizon (see Fig. 8), the only degree of freedom for the oriented crystals being rotation around their vertical axis. The parhelic circle passes through the sun and may be seen for any sun elevation. On the contrary, due to internal reflection, the circumzenithal (resp. circumhorizontal) arc cannot be seen for sun elevations greater than 32° (lower than 58°).
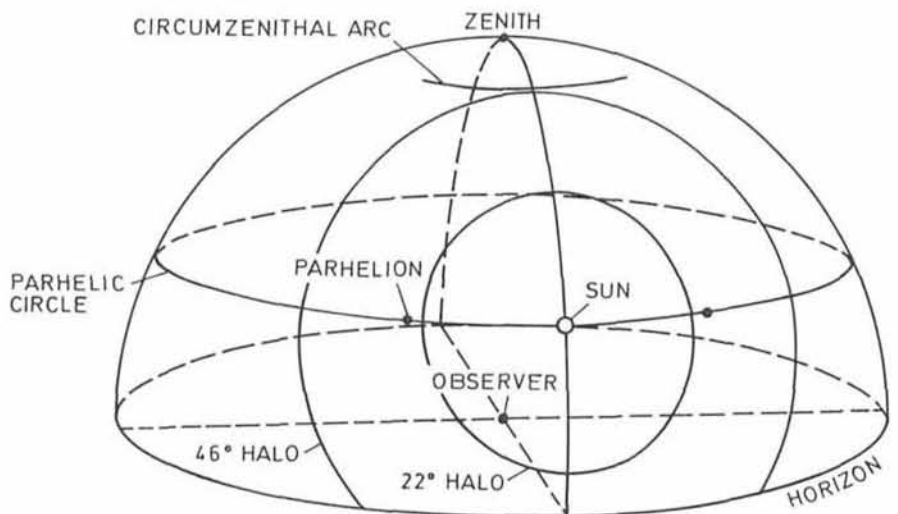
Figure 8: *A schematic perspective view of some halos discussed in this paper.*

cameras, it is clear that very interesting effects could be recorded. For example, halos of radii different from 22° and 46°, or those occurring 180° away from the sun are not yet clearly understood because of a lack of good photographic records. Photometry and polarization measurements are even scarcer. Halo observations could be a nice goal for astronomers lucky enough to get cloudy weather!

It is a pleasure to thank my friends and colleagues Marc Remy, Jean Surdej and Eddy Van Drom for their comments and enthusiasm.
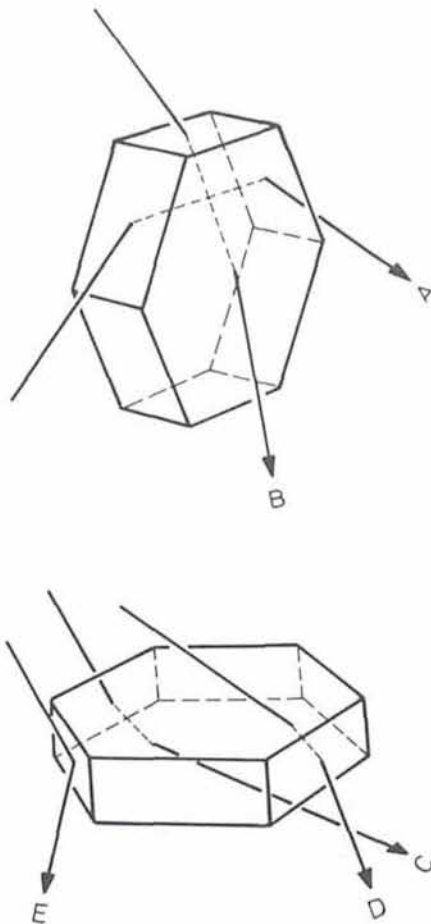
References

Cardon, B.L.: 1977, *Am. J. Physics* **45**, 331.
Greenler, R.: 1980, *Rainbows, halos, and glories*, Cambridge University Press.
Greenler, R., Mallmann, A.J.: 1972, *Science* **176**, 128.
Greenler, R., Mueller, J.R., Hahn, W., Mall-mann, A.J.: 1979, *Science* **206**, 643.
Lynch, D.K.: 1979, *J. Opt. Soc. Am.* **69**, 1100.
O'Leary, B.T.: 1966, *Ap.J.* **146**, 754.
Pattloch, F., Tränkle, E.: 1984, *J. Opt. Soc. Am. A* **1**, 520.
Whalley, E., McLaurin, G.E.: 1984, *J. Opt. Soc. Am. A* **1**, 1166.

Flower Power at La Silla

D. HOFSTADT and M. MORNHINWEG, ESO, La Silla

Periodically a rainy winter hits the "Norte Chico" of Chile. Winter 1991 was one of them and generated some unhappiness among the La Silla observers.

For tourism and botany however the interest was greatly enhanced. Down in the valley near the airstrip the *Palo Santo* (Fig. 1) opened the exhibition in August. The shrubs, frustrated by con-secutive years of drought, dressed up in tiny green leaves and delicate yellow flowers. Above the Pelicano quebrada the evergreen *Carbonillo* (Fig. 2) began a long sequence of white flowering which will last till summer. Its branches are often chopped down for charcoal and it is now in danger of extinction. Fortunately the La Silla territory remains a preservation area. The carbonillo pro-duces a small almond-flavoured nut highly appreciated by the Vizcacha rabbits. In the same area we find the *Algarrobilla* (Fig. 5), another bush ex-posed to intensive exploitation. Its thick bean-shaped fruit has a very high content of tanin and is exported to the leath-er tanneries abroad.

The really spectacular sceneries how-ever appeared in September when the
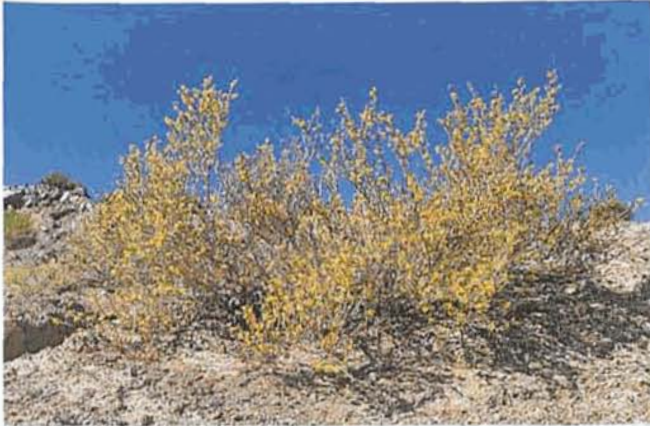
Figure 1: Palo Santo *(Porliera chilensis)*

Figure 4: Espino *(Acacia caven)*

Figure 2: Carbonillo *(Cordia decandra)*

Figure 5: Algarrobilla *(Balsamocarpon brevifolium)*

Figure 3: Chañar (Geoffroea decorticans)

Figure 6: Algarrobo *(Prosopis chilensis)*

Figure 7: Soldadillo (Tropaeolum looserii)

Figure 10: Mariposa blanca (Schizanthus candidus)

Figure 8: Rosita (Cruckshanksia)
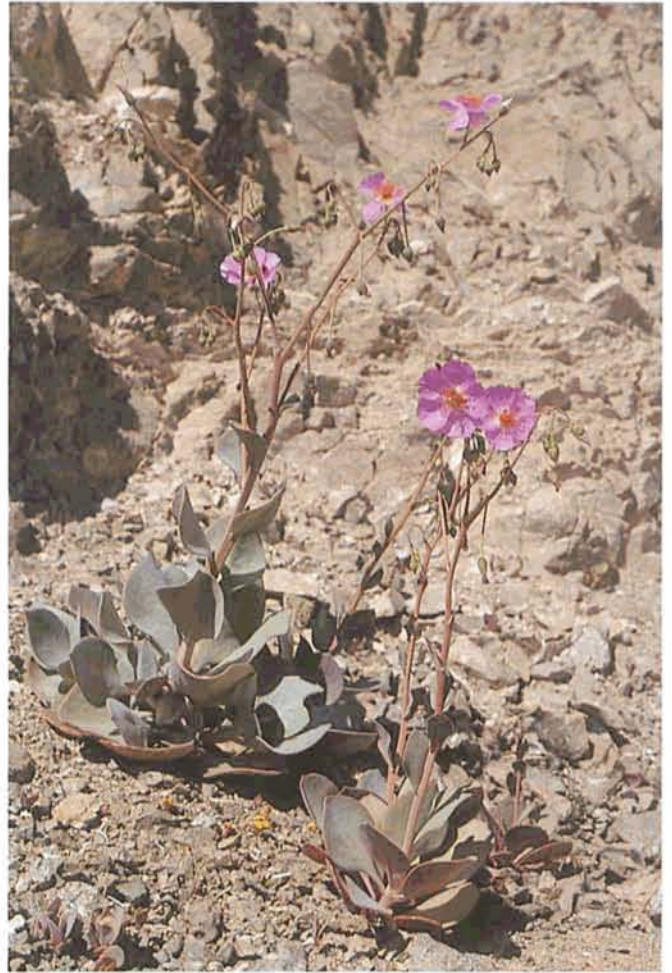
Figure 11: Pata de Guanaco (Calandrinia longiscapa)
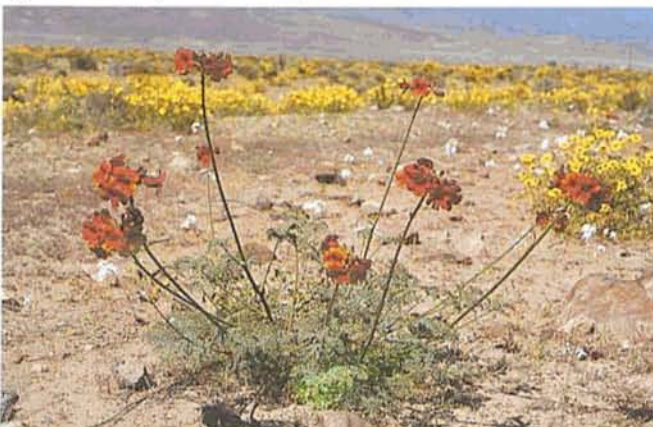
Figure 9: Terciopelo (Argylia radiata)

Figure 12: Viola del Campo (Viola asterias)

purple *Pata de Guanaco* (Fig. 11), covered large extensions of fields alternating with the yellow *Violas del Campo* (Fig. 12) and the *Rositas* (Fig. 8). This is the time when photographic cameras get inspired and the telescopes emerge from unusual green surroundings. The curious visitor will spot the *Terciopelos* (Fig. 9) whose colours range from yellow-orange to dark brown. The velvet flowers make a point of growing on bare ground where other plants cannot compete.

Of the two native trees which grow in our region the *Chañar* (Fig. 3) is the most spectacular one during the flowering season. It shrouds itself in orange blossoms and attracts thousands of bees. The tree has lent its name to hundreds of places in Chile where the villages of Chañar and Chañarcillo compete in numbers with the Algarrobos and Algarrobillos. The elegant and thorny *Algarrobo* tree (Fig. 6) populates the quebradas and has invaded Mr. Schumann's garden located five hundred metres below the mountain top. It is moderate in water consumption and will eventually outnumber the ever thirsty poplars and eucalipti, thriving on our waste waters.

On the road to La Silla the flower festival is led by the *Encelias* which Chileans identify with the lovely name of the *Coronilla del fraile* (the friar's crown).

On the mountain itself the *Soldadillos* (little soldiers – Fig. 7) line up. They are the mountain cousins of the garden Capucins. Several of those wild species *(tropaeolums)* exist in Chile and the coastal slopes harbour a magnificent three-colour version.

The white crosspetal *Schizopetalon* deserves a special mention as it is adapted to our activities. It opens up at sunset and sends its honey smell through the night before closing in the morning.

Many more wild flowers grow on our slopes: the candid *Mariposas blancas* (Fig 10), *Adesmias, Senecios, Malvillas* and magnificent *Alstromerias*.

Dr. Grenon, our walking encyclopedia, has identified over 150 endemic species in our surroundings. Who said La Silla is a desert . . .?

New Aspects of the Binary Planet Pluto-Charon

V. BURWITZ[1], K. REINSCH[1], M.W. PAKULL[2], P. BOUCHET[3]

[1]*Institut für Astronomie und Astrophysik, Technische Universität Berlin, Germany;* [2]*Landessternwarte Heidelberg, Germany;* [3]*ESO, La Silla, Chile*

Introduction

Never since the discovery of Pluto in 1930 has our knowledge about this tiny far-out planet improved so rapidly as during the past five years. The coincidence of two rare opportunities that occur together only once every 250 years kept astronomers around the world busy to solve the puzzle of Pluto and its satellite Charon.

In 1987/88, the plane of Charon's highly inclined orbit around Pluto swept over the inner solar system. This gave rise to a series of mutual occultations and transits of the planetary disks that were observable from Earth between 1985 and 1990 (cf. Fig. 1). Nearly at the same time, on September 5, 1989, Pluto reached the perihelion of its eccentric orbit around the Sun which placed the binary system within range for photometry with medium-sized telescopes.

The shapes and the timings of the mutual eclipse light curves not only reflect the geometry of the system (which had been scarcely known before) but also provide information about the gross albedo distribution on Pluto and Charon.

In an earlier issue of the *Messenger* (Pakull and Reinsch, 1986), we reported the analysis of the first eclipse light curves observed in 1985 and 1986 which revealed that the diameter of Pluto was much smaller than previously believed.

Thanks to generous allocation of ESO time we were able to continue our study of the mutual eclipse light curves.

Eclipse Observations

As the aspect of Charon's orbit around Pluto as seen from Earth varies with time, different areas on Pluto are occulted during the eclipses (Fig. 2). The eclipse series started in early 1985 with occultations of the north polar region on Pluto. While in 1986 and 1987 large fractions of the northern hemisphere were covered as Charon crossed in front of Pluto, Pluto's southern hemisphere was involved in the eclipses throughout the rest of the series until 1990.

To exploit the full information provided by the mutual eclipses it was therefore necessary to spread observations over the whole period of eclipse phenomena. Due to the fact that the binary system is in a bound rotation it is, however, only possible to derive the gross albedo distribution on one hemisphere of Pluto and Charon, respectively.

From 1985 to 1990 we successfully observed six transits of Charon in front of Pluto (inferior events) and eight occultations of Charon by Pluto (superior events). The photometry was obtained with the ESO/MPI 2.2-m and the Danish 1.5-m telescopes, respectively, using CCD direct imaging techniques which allow high-precision differential photometry even if sky conditions are not strictly photometric. Our data base was supplemented by published light curves of eleven further events (Binzel et al., 1985; Tholen et al., 1987 b; Binzel, 1988, Tholen and Buie, 1988; Tholen and Hubbard, 1988).

While the first grazing eclipse light curves could be analysed using models for eclipsing binary stars, more sophisticated algorithms were required as the eclipse series continued. The light curves were then complicated by shadow transits which occurred displaced in time relative to the eclipse events (Fig. 3).

The analytical model developed by Dunbar and Tedesco (1986) to derive the physical parameters of a binary
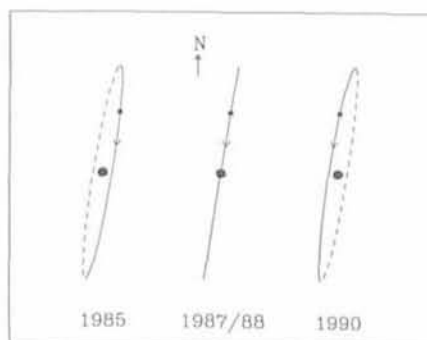

Figure 1: *Apparent view of Charon's 6.4-day orbit around Pluto between 1985 and 1990.*
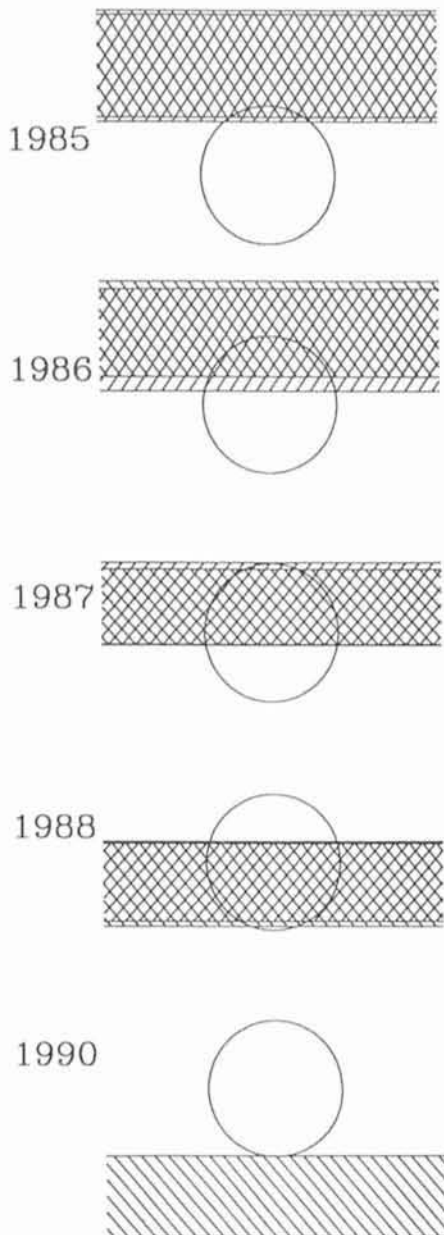
23

1985

1986

1987

1988

1990

Figure 2: *Projected paths of Charon and its shadow across Pluto. The northern and southern extremes of the observed transits are displayed for each year.*

Table 1: *Physical parameters and orbital elements of the Pluto-Charon system derived from the least-squares fit of our analytical model.*

	Pluto	Charon
Radius r [km]	1151 ± 20	591 ± 11
Mean density ϱ [g/cm^3]	2.032 ± 0.040	
Mass m [10^{22} kg]	1.47 ± 0.07	
Absolute brightness V (1,0)	-0.648 ± 0.010	1.350 ± 0.010
Mean geometric albedo p_v	0.618 ± 0.020	0.372 ± 0.012
Apparent inclination (17.4.87) i [degrees]	90.710 ± 0.032	
Sidereal orbital period P [days]	6.387244 ± 0.000007	

The radii of (1151 ± 20) km derived for Pluto and (591 ± 11) km for Charon are in good agreement with our earlier results (Pakull and Reinsch, 1986). They confirm that the radii are significantly lower than those found by previous observers using speckle interferometric techniques. The error uncertainties could be reduced by more than a factor of 3, and the slight discrepancies in the results of different eclipse observers could be solved (cf. Dunbar and Tedesco, 1986; Tholen et al., 1987 a; Reinsch and Pakull, 1987; Tholen and Buie, 1990).

A comparison of our best-fitting model with the observed light curves reveals that systematic differences still remain. These must be attributed to local deviations from the assumed constant albedo of Charon and of Pluto's northern and southern hemispheres (cf. Fig. 4).

Based on our improved physical parameters of the system, we chose a numerical approach to derive individual albedo values for a grid of surface areas on Pluto. The boundaries of the surface elements were selected to match in latitude with the five groups of eclipse paths and to suit time-resolution of our data (longitudinal strips).

We found that the significant surface structures needed to fit the photometry are already described by a grid of 17 surface elements. The albedo distribution derived is independent of the particular method used to define the grid (longitudinal or rectangular division, cf. Fig. 5).

Our albedo map reveals that areas of high contrast must coexist on the Charon-facing hemisphere of Pluto. The highest contrast found was that between the two polar caps. While the south polar region appears to be the brightest area on the planet, we found that the north polar region has the lowest albedo. This is a surprising result because the south polar region is the one that has been exposed to perma-

planet from eclipse light curves was adapted to our problem. In a first-order approach, we assumed a constant albedo for Pluto and Charon, respectively. The light curves obtained with this model showed that the albedos of the northern and southern hemisphere were significantly different. Therefore, we modified our first-order model introducing separate parameters for the albedos of the northern and southern hemisphere.

We performed a multi-parameter least-squares fit to our data using the analytical model light curves. Adopting the orbital radius of 19640 ± 320 km for Charon determined by Buie and Tholen (1990) the best solution of our fit yielded the improved physical parameters of the system given in Table 1.

Figure 3: *Series of reconstructed images showing the transit of Charon and its shadow across Pluto on May 1, 1988.*
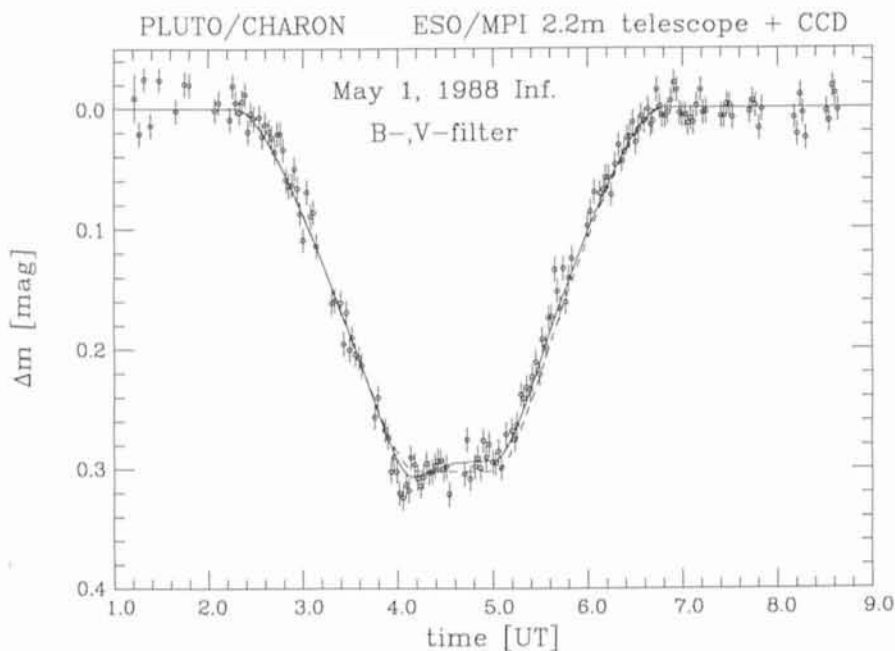
Figure 4: *Example of an eclipse light curve observed on May 1, 1988 with the ESO/MPI 2.2-m telescope (combination of B- and V-filter measurements). The two lines superimposed on the data represent our purely geometrical model (dashed line) and our albedo model (continuous line), respectively.*

nent irradiation from the Sun as Pluto approached perihelion.

From simultaneous observations in different colour bands we found no systematic colour variations of the surface structures on Pluto. The eclipse depths were, however, detected to be colour dependent for occultations of Charon. In this case the eclipses observed in the B-filter were slightly deeper than those observed in the V-filter.

The Rotational Light Curve of Pluto

The variation of Pluto's visual brightness with a period of 6.4 days (cf. Fig. 6) was first detected by Walker and Hardie (1955) and has been interpreted as the rotational period of the planet. This rotational light curve contains independent information about the albedo distribution on Pluto.
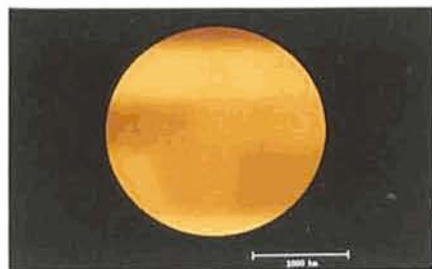

Figure 5: *Albedo map of Pluto reconstructed from a grid of 17 surface elements. The albedo distribution has been smoothed to reproduce the spatial resolution obtained. The north pole is to the top.*

It has been noted that the "absolute" mean brightness V(1,0) of the planet has increased by 0.3 mag since 1954. At the same time, the amplitude of the rotational light variation has become significantly larger.

Attempts to model the albedo distribution on Pluto have already been published using the information provided by this secular variation of the rotational light curve (Marcialis, 1988; Buie and Tholen, 1989). Buie and Tholen derived two distinct configurations of dark and bright spots on Pluto that fit the out-of-eclipse photometry equally well (models 'MAX' and 'SHELF').

Whereas these models assume that the surface structures have not changed during the past 35 years, there is some evidence from the detection of a substantial atmosphere of Pluto (Elliot et al., 1989) that a cyclic methane sublimation and freeze-out may occur during Pluto's eccentric orbit (Stern et al., 1988). This would be an alternative explanation of the rotational light curve changes and implies that the albedo distribution on Pluto could be variable on a time scale $\gtrsim 10$ years.

A straightforward method to derive the albedo distribution on Pluto has become available during recent years. As we have viewed the equator of Pluto nearly edge-on around 1987/88 a deconvolution of the rotational light curve yields the instantaneous longitudinal albedo distribution on Pluto without requiring further assumptions.

Besides the eclipse observations we have, therefore, obtained absolute pho-

tometry of Pluto's rotational light curve between 1982 and 1990 using the Walraven photometer attached to the Dutch 0.91-m telescope and the single-channel photometer at the ESO 1-m telescope. The observations have been reduced to the "absolute" brightness V(1,0) corresponding to unit distances Pluto-Sun and Pluto-Earth and to a phase angle of 0° (cf. Fig. 6).

From information theory it is known that the deconvolution of a light curve is numerically instable if the low frequency intensity variations are largely contaminated by statistical fluctuations. The low and high frequencies can, however, be separated by computing the Fourier transformation of our light curve. We found that our original light curve is already well described by its first two Fourier components within the statistical errors of the data (see Fig. 6). We have deconvolved this analytical light curve to derive the longitudinal albedo variation on Pluto (Fig. 7). The albedo distribution obtained shows a double peaked structure. The maximum of the latitude averaged albedo is attributed to the longitudinal strip which faces towards Earth at rotational phase 0.65. The minimum albedo corresponds to the region being in front at phase 0.95.

While the features of our longitudinal albedo distribution resemble most of those implied by the 'SHELF' model (e.g. maximum and minimum albedo), the existence of a second maximum at rotational phase 0.2 is neither supported by the 'SHELF' model nor by our eclipse map.

We found no colour dependence of the rotational light curve and, consequently, of the longitudinal albedo distribution. The colour difference for the Pluto-Charon system is $(B-V)_{Pl/Ch} = 0.846 \pm 0.010$ and does not vary with the rotational phase. From the depths of the superior events where Charon is totally eclipsed we computed the colour differences for Pluto $(B-V)_{Pl} = 0.871 \pm 0.014$ and for Charon $(B-V)_{Ch} = 0.701 \pm 0.014$ which show that Pluto is redder than Charon.

Discussion

Our finding of a dark north polar cap on Pluto is in contrast with the bright polar caps required by the models of Marcialis (1988) and Buie and Tholen (1989) to account for the secular variation of Pluto's rotational light curve. The existence of a dark polar cap can, however, be understood if we assume that the surface structures have changed during the past 35 years as suggested by the model of Stern et al. (1988). It will therefore be important to continue monitoring the out-of-eclipse brightness
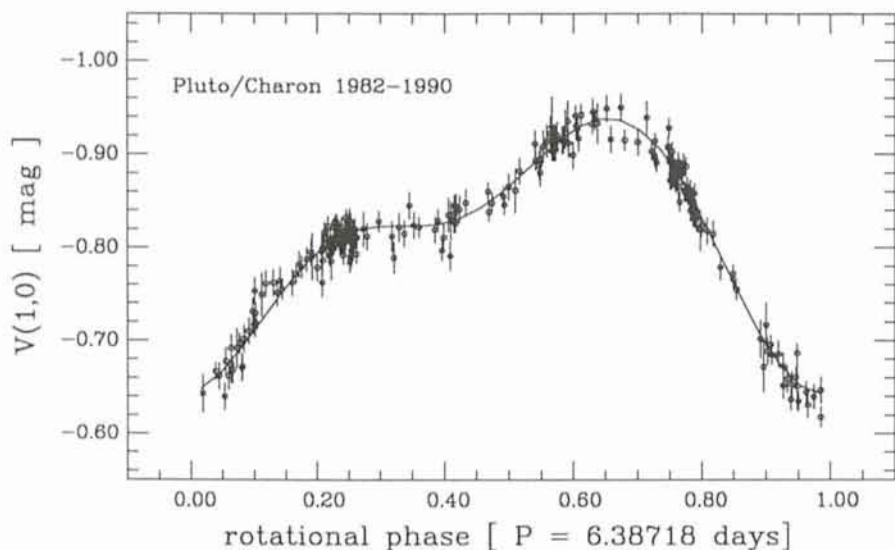
25

Figure 6: *The rotational light curve of Pluto and Charon observed between 1982 and 1990. The continuous line represents our analytical description of the light curve used for the deconvolution.*

Figure 7: *Longitudinal albedo distribution on Pluto derived by deconvolving the rotational light curve in Figure 6.*

References

Binzel, R.P., Tholen, D.J., Tedesco, E.F., Buratti, B.J., Nelson, R.M., 1985, *Sci* **228**, 1193.

Binzel, R.P., 1988, *Sci* **241**, 1070.

Buie, M.W., Tholen, D.J., 1989, *Icarus* **79**, 23.

Dunbar, R.S., Tedesco, E.F., 1986 *AJ* **92**, 1201.

Elliot, J.L., Dunham, E.W., Bosh, A.S., et al., 1989, *Icarus* **77**, 148.

Marcialis, R.L., 1988, *AJ* **95**, 941.

Pakull, M.W., Reinsch, K., 1986, *The Messenger* **46**, 3.

Reinsch, K., Pakull, M.W., 1987, *Astron. Astrophys.* **177**, L43.

Stern, S.A., Trafton, L.M., Gladstone, G.R., 1988, *Icarus* **75**, 485.

Tholen, D.J., Buie, M.W., Swift, C.E., 1987a, *AJ* **92**, 244.

Tholen, D.J., Buie, M.W., Binzel, R.P., Frueh, M.L., 1987b, *Sci* **237**, 512.

Tholen, D.J., Buie, M.W., 1988, *AJ* **96**, 1977.

Tholen, D.J., Hubbard, W.B., 1988, *Astron. Astrophys.* **204**, L5.

Tholen, D.J., Buie, M.W., 1990, *BAAS* **22**, 1129.

Walker, M.F., Hardie, R., 1955, *PASP* **67**, 224.

of Pluto with high precision photometry to track the secular variation of the rotational light curve. The 'SHELF' model of Buie and Tholen (1989) predicts an immediate reversal of the secular variation (i.e. general brightening and a reduction in amplitude of the rotational light curve) whereas Stern et al. (1988) predict that the reversal should take place 7–17 years after passing perihelion due to the thermal inertia of Pluto's surface.

The physical parameters of the Pluto-Charon system seem to be well established now. The largest uncertainty that remains lies in the exact determination of the semi-major axis of the system which measures only 0.9″ on the sky. This is the scaling factor of the diameters and the total mass of the binary components. Future observations with high spatial resolution (e.g. with the HST or the ESO-NTT) will allow a more accurate determination of Charon's orbit. One physical parameter which is independent of this scaling length is the mean density of the system that can be calculated from the binary period and the dimensions of Pluto and Charon relative to the binary separation. The mean density of about 2 g/cm³ indicates that the Pluto-Charon system has a high rock mass fraction similar to that of the larger satellites of the giant planets.

The mutual eclipse series of Pluto and Charon has provided us with many new aspects of the binary planet Pluto-Charon. The albedo maps computed by different observers will hopefully converge as the data of all observers will be combined. The spatial resolution that can be obtained by eclipse mapping is superior to that offered by the HST even if it would be working to design specifications. It will not be before the end of the first decades of the next century that space probes may provide more detailed pictures of the surfaces of Pluto and Charon.

Acknowledgements

ESO's Early History

The readers of the *Messenger* will be pleased to learn that the recent series of eleven articles about the early history of ESO, written by Professor Adriaan Blaauw, have now been collected in a book. The text has been thoroughly revised and includes photos which were not in the *Messenger* articles.

The narrative begins with the developments in the early 1950's when leading European astronomers initiated a search for the best possible observatory site under the comparatively unexplored southern sky. Ten years later, in 1962, ESO was established by an international convention and soon thereafter a remote mountain top in the Chilean Atacama desert, La Silla, was acquired. It took another decade to transform this site into the world's largest optical observatory.

ESO exemplifies the highly successful European integration in a fundamental field of science, providing European scientists with modern facilities for front-line investigations beyond the capacities of the individual member states.

Professor Adriaan Blaauw, well-known Dutch astronomer, has been closely associated with ESO during all of this time. He actively participated in many of the events described and as a former Director General of ESO (1970–74) he possesses first-hand knowledge of the organization and the way it works. A scientist of international renown, Professor Blaauw is also a noted amateur historian in his home country.
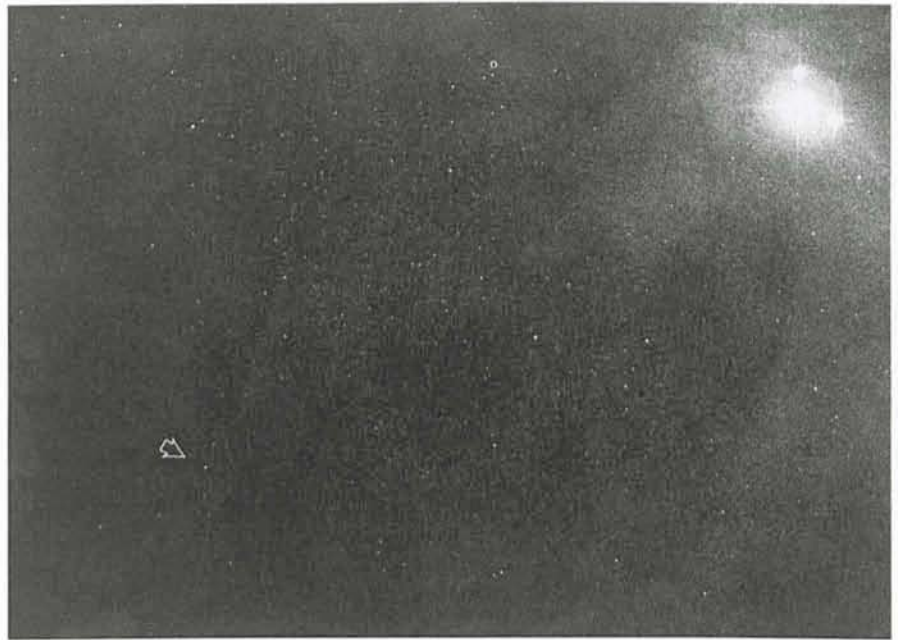
The book is available from ESO (address on the last page); the price is 25 DM, which must be prepaid by cheque or bank transfer to ESO account No. 2102002 at the Commerzbank in Munich (BLZ 70040041). Please be sure to indicate "ESO History" in your order.

A Visit to Gaspra

This is a ground-based photo of the first minor planet ever to be visited by a spacecraft. On October 29, 1991, the NASA spacecraft Galileo flew past minor planet No. 951 Gaspra on its way to Jupiter where it will arrive in December 1995. The distance to Gaspra from the Earth was 410 million km at the time of the fly-by. Although Galileo's high-gain antenna has not yet been unfolded and could therefore not be used, JPL engineers succeeded in getting a 300-line image via the low-gain antenna; the others will be sent when Galileo is again near the Earth. The first image showed the irregular form of Gaspra and several craters on its surface with a resolution of about 130 metres. The diameter was measured as 16 kilometres.

Gaspra was discovered on July 30, 1916 at the Simeis Observatory in the mountains of Crimea, the Russia. The discoverer was the well-known Russian astronomer Grigorij Nikolaevich Neujmin (born 1886 in Tbilisi, Georgia; died 1946 in Leningrad), who later became Director of that observatory (1925–1931 and 1936–1941) and Director of the Pulkovo Observatory near St. Petersburg (1944–1946). During three decades he discovered 72 minor planets and 6 comets.

Neujmin's dedication for (951) Gaspra reads as follows: "Named after the re-sort on the southern coast of Crimea, in which the famous Russian writer Lev Nikolaevich Tolstoy (1828–1910) spent many years of his life." The village of Gaspra is located about 10 km south-west of Yalta.

The present photo was obtained with the 1-metre ESO Schmidt telescope at La Silla on April 9, 1991 and served to measure an accurate position of Gaspra, in support of the navigation of Galileo. The exposure lasted 10 minutes and Gaspra is indicated with an arrow. On this date, its distance from the Earth was 262 million km and the magnitude was about 15.

The background of the photo is a region in the southern constellation Ophiochus (the Serpent-holder) which is characterized by relatively few stars, but many bright and dark nebulae. The brightest of the three stars in the top right corner is the 5th-magnitude Rho Ophiuchi, a hot and young double star. It is surrounded by nebulosity that reflects the light from the stars.

New ESO Preprints

(September–November 1991)

Scientific Preprints

789. F. Bertola, G. Galletta and W.W. Zeilinger: The Minor-Axis Dust-Lane Elliptical NGC 1947. *Astronomy and Astrophysics.*

790. P. Padovani and C.M. Urry: Luminosity Functions, Relativistic Beaming, and Unified Theories of High-Luminosity Radio Sources. *Astrophysical Journal.*

791. G. Bertin, F. Bertola, L.M. Buson, I.J. Danziger, H. Dejonghe, E.M. Sadler, R.P. Saglia, P.T. de Zeeuw and W.W. Zeilinger: The ESO Key Programme: A Search for Dark Matter in Elliptical Galaxies. Presented by F. Bertola at the 2nd DAEC meeting "The Distribution of Matter in the Universe", Observatoire de Meudon.

792. D. Baade: Binary Be Stars and Be Binaries. Invited talk presented at IAU Symp. 151 "Evolutionary Processes in Interacting Binary Stars", held Aug. 5–8, 1991 in Cordoba, Argentina.

793. A. Smette, J. Surdej, P.A. Shaver, C.B. Foltz, F.H. Chaffee, R.J. Weymann, R.E. Williams and P. Magain: A Spectros-copic Study of UM673 A&B: on the Size of Lyman-α Clouds. *Astrophysical Journal.*

794. P. Møller and P. Kjærgaard: The Expected Ionization of HI by Line of Sight Neighbour Quasars: Measuring the Quasar Beaming. *Astronomy and Astrophysics.*

795. M.R. Rosa, H. Zinnecker, A. Moneti and J. Melnick: The Galactic Center in the Far-Red. *Astronomy and Astrophysics.*

796. M. Bersanelli, P. Bouchet, R. Falomo and E.G. Tanzi: Homogeneous J, H, K, L Photometry of a Sample of BL Lac Objects. *The Astronomical Journal.*

797. T. Prusti, H.-M. Adorf and E.J.A. Meurs: Young Stellar Objects in the IRAS Point Source Catalog. *Astronomy and Astrophysics.*

798. R.M. West and R.H. McNaught: Earliest Photometry of SN 1987A. *Astronomy and Astrophysics.*

799. M. Della Valle: Nova LMC 1991: Evidence for a Super-Bright Nova Population. *Astronomy and Astrophysics*, Letters.

800. M. Fulle, F. Pasian and P. Benvenuti: HST Observations of the Inner Coma of Comet Levy 1990c. *Anuales Geophysicae.*

801. Bo Reipurth, S. Heathcote and Frederick Vrba: Star Formation in Bok Globules and Low-Mass Clouds. IV. Herbig-Haro Objects in B335. *Astronomy and Astrophysics.*

802. Bo Reipurth, A.C. Raga and S. Heathcote: Structure and Kinematics of the HH 111 Jet. *Astrophysical Journal.*

Technical Preprints

34. P. Dierickx: Optical Performance of Large Ground-Based Telescopes. *Journal of Modern Optics.*

35. W. Schröder, H. Dahlmann, B. Huber, L. Schüssele, F. Merkle and M. Ravensbergen: Telescope Pointing and Tracking with Optical Gyros. To be published in the Proceedings of SPIE, Vol. 1585 (1991).

36. B. Lopez and M. Sarazin: Optimum Exposure Times for Interferometry. ESO Conference on High Resolution Imaging by Interferometry II, Garching, Oct. 14–18, 1991.

New ESO Scientific Report

No. 10 – October 1991. M.-P. Véron-Cetty and P. Véron: A Catalogue of Quasars and Active Nuclei (5th Edition).

A Survey of Optical Knots in Kepler's SNR

R. BANDIERA, *Osservatorio Astrofisico di Arcetri, Firenze, Italy*
S. VAN DEN BERGH, *Dominion Astrophysical Observatory, Victoria, Canada*

1. Introduction

Kepler's supernova remnant (SNR) is an ideal object for a direct investigation of the interaction of a blast wave with a highly inhomogeneous medium. Most of the optical emission comes from dense ($n \sim 10^3 - 10^4$ cm^{-3}) and compact ($r \sim 10^{16} - 10^{17}$ cm) knots recently hit by the main shock. The physics of the interaction is complex and involves the formation of secondary shocks, cloud crushing and evaporation by saturated conduction (see McKee, 1988 for a review).

We here present some results of a long-term project on Kepler's SNR, directed towards the study of links between the kinematical, morphological and spectroscopical properties of a knot, and the phase of its interaction with the supernova blast wave. Kepler's SNR is a very young object (less than 400 yr old), and contains features that evolve with time-scales considerably shorter than a human lifetime. For this reason it represents one of those rare cases in which the evolution can be followed "in real time".

2. Morphology

After Kepler's supernova (SN 1604) faded away, more than three centuries passed before its remnant was discovered. In 1941 Baade (1943) first detected some nebulosity near the supernova position that was deduced from the historical records. He described Kepler's SNR as "a broken mass of bright knots and filaments covering a fan-shaped area", but actually detected only the N-W brightest part of the optical remnant.

In fact the location of this remnant is far from ideal for optical observations. It is highly reddened, and very crowded by field stars. Therefore faint filaments may be overwhelmed by the background, while some optical knots can be mistaken for stars. Deeper images of the nebular emission can be obtained only after a careful subtraction of the stellar continuum from narrow-band frames centred on conspicuous emission lines, like Hα+[N II] (D'Odorico et al., 1986), but also [S II], [O I] or [O III] (Blair, Long and Vancura 1991).

Such images reveal a great deal of structure. In addition to the brightest complex located on the N-W side of the remnant, there are some clumps of knots lying along the edge of the rem-

nant, and spanning directions from N-E to West (clockwise). Other groups of knots are located closer to the remnant centre. Fainter diffuse emission is also present along most of the northern rim of this SNR, as well as in the surroundings of the central groups of knots. No optical emission can be detected along the southern rim of the remnant.

Actually the optical images are not the most suitable for defining centre and size of Kepler's SNR; but one could use radio and X-ray images (Matsui et al., 1984), where the remnant looks pretty circular. However also at these wavelengths it shows a strong asymmetry in the emission, with a N-W limb considerably brighter than the rest of the remnant.

3. Kinematics – A Bow Shock Model?

By a comparison of plates covering the period 1942–1976, van den Bergh and Kamper (1977) were able to measure proper motions for 19 knots. Furthermore they collected radial velocity measurements for a few knots.

Their data were consistent with an "expansion age" of less than 2×10^4 yr. Therefore it became clear that the optical knots in Kepler's SNR have not been ejected by the supernova. On the other hand they are too dense and clumped to be interstellar (recall that the remnant is located about 500 pc above the Galactic plane, for a distance of 4.5 kpc). Very likely the optical knots originated from a wind of the stellar progenitor. This hypothesis is also supported by the presence of a slight nitrogen overabundance (Dennefeld, 1982; Leibowitz and Danziger, 1983). In some respects the knots resemble the "Quasi Stationary Flocculi" in Cassiopeia A.

Knot velocities, typically only some hundred km/s, can be interpreted as random motions added to a common translation, pointing towards the N-W. Bandiera (1987) noticed that such a translation points to the direction where the remnant is brightest, in the optical as well as in radio and X rays, and explained this in the following way:

Assuming that this material originated from a stellar wind, its common motion may reflect the motion of the supernova progenitor. During that mass-loss phase, the wind was interacting with the interstellar medium, and formed a bow

shock in the direction of the stellar motion. In the bow shock the gas was compressed, allowing the condensation of dense clumps. Now the supernova blast wave moves through this dense and inhomogeneous medium. The effect of this is an enhanced emission in radio and X rays on that side. When the most compact clumps are "ignited" by the arrival of the blast wave they become visible as optically emitting knots.

Since the time-scale for the evolution of knots is considerably shorter than the remnant age, the optical knots trace the actual position of the supernova blast wave. Knots are visible only on an annulus at the intersection of the bow shock with the blast wave. Since the common translation also has a radial component, the bow shock geometry is seen from an oblique perspective, and this annulus appears as an ellipse. On this hypothesis the knots projected near the central regions of the SNR are actually part of this (distorted) ellipse. With the expansion of the blast wave, new knots will appear on an ellipse that increases in size and shifts in position as well.

This geometry allows one to predict where new knots will appear. A non-trivial prediction concerns the central knots. These new knots should brighten to the south of those already existing (Bandiera 1988).

4. The Restoration of Old Plates

Here we shall describe the most important phases of a work (Bandiera and van den Bergh, 1991a), that allowed us to obtain cleaner and deeper images, and to follow in detail the motions of many knots and the evolution of their intensities over the last half century.

We used plates taken with the Hooker 2.5-m reflector (1941–1943) and with the Hale 5-m telescope (1950–1983). As already mentioned in Section 2, the nebular emission is immersed in a crowded stellar field. This is particularly evident on old plates, exposed with broad-band filters. As a first step, we decided to "restore" these plates, by subtraction of the stellar continuum, with the aim of also extracting from them information that was originally hidden. This requires an off-line reference image for the subtraction. However we did not expect the stellar field to have experienced significant changes
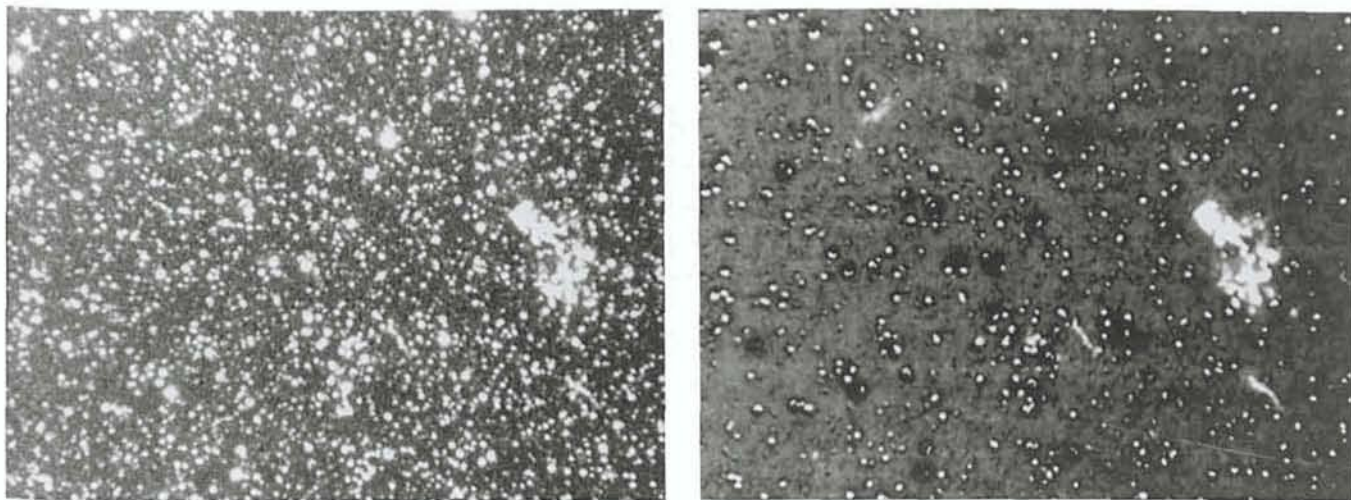
Figure 1: *(a) good-quality photographic plate of Kepler's SNR (Hale 5-m telescope, May 1950); (b) the same after restoration by subtraction of the stellar continuum.*

over the last decades. We therefore decided to use an image taken recently.

Observations were carried out in 1989 with the 1.5-m Danish telescope on La Silla, with the RCA CCD No. 15, using broad-band as well as interference filters centred on Hα+[N II], [S II] lines, and on the nearby continuum. Our aim was to produce a reference image for the stellar field with a spectral response similar to that of the old plates. In this respect a Bessell R filter was found to give the best results. We first obtained Hα+[N II] and [S II] images of the nebular emission, by subtracting the stellar continuum, after a proper alignment of the frames and an approximate equalization of the point spread functions. They were then used for subtracting the nebular component from the frame with the Bessell R filter. In all the steps of the reduction procedure we stressed the production of images that were as clean as possible, while deemphasizing the detection of very faint structures.

The next step was the subtraction of the stellar continuum from the old plates. This stellar subtraction can be carried out only after a linearization of the characteristic curve of the photographic plates. Since this was unknown, we had to derive it from the plate itself, by comparison with the (linear) CCD frame. This is a difficult task, mainly because the point spread functions of the two images are also different. We solved the problem in an approximate way by comparing the intensities of a set of stars selected independently on the plate and on the CCD reference frame, using the INVENTORY routine, implemented in MIDAS. By this procedure the image of the bright stars cannot be completely removed. However, for fainter stars which are more numerous, the characteristic curve of the plate can be fitted with greater accu-

racy, resulting in a more efficient stellar subtraction. As an example, Figure 1a shows the appearence of a photographic image of Kepler's SNR, obtained in 1950 with a broad-band red filter. Figure 1b shows the same image, after the stellar subtraction procedure described above.

5. A Catalogue of Optical Knots

After "cleaning" the old plates from stellar contamination, following the evolution of the nebular emission becomes an easier task. The complete set of restored images has been published by Bandiera and van den Bergh (1991a). Some knots are seen to brighten considerably. Most of these lie on the external part of the northern rim, but some are also located in the central regions of the remnant. The evolution of knots is of particular interest for the understanding of the geometry of this object. Newer knots brightened to the south of those already existing; in qualitative agreement with the predictions of the bow shock model (Bandiera and van den Bergh, 1991b) described in Section 3.

The quality of the images is good enough to also allow a quantitative analysis of the evolution of the optical remnant. As a first step, a catalogue of emitting knots has been prepared. In Kepler's SNR optical knots usually look to be well defined. When filamentary structures are present, they usually consist of a group of aligned knots. In order to avoid selection effects produced by manual recognition and centring of knots, we preferred to perform an automatic search (by INVENTORY) in the region where knots are present. Furthermore, this search was performed independently on the different plates. We retained as real only those knots that were detected independently on most of

the plates. On average a knot was detected on 9 of the 12 available frames. Our catalogue was not intended to be complete. Even a few rather bright knots were discarded because they were almost coincident with a poorly subtracted star. Furthermore, a few very recent knots were not included, because they were only present on a few images. Our catalogue lists only knots whose parameters can be determined with some accuracy. The total number of knots in our catalogue is 50 compared to the 19 knots catalogued by van den Bergh and Kamper (1977), who used a similar set of plates.

INVENTORY gives both positions and intensities of sources. These positions can be used to determine astrometric motions of individual knots. Proper motions are combined to measure the amount of common translation, as well as expansion velocity. After correcting for Galactic rotation the components of the average knots motion are 117 ± 10 km/s and 105 ± 11 km/s, toward West and North, respectively; the expansion velocity is instead 67 ± 26 km/s (for a distance of 4.5 kpc). These values are consistent with those of van den Bergh and Kamper (1977), but have a much higher accuracy.

Approximate photometry has been obtained by comparing the intensities of corresponding knots in different images, after additional corrections for effects of the residual non-linearity in the restored images. Absolute calibration is provided by the knot fluxes given by D'Odorico et al. (1986). At the end of this reduction we obtained light curves (basically in Hα+[N II] emission) for all catalogued knots over a period of 40–50 yr. The relative accuracy on the intensity estimates is about 30%.

Bandiera and van den Bergh (1991a) present all available quantitative infor-
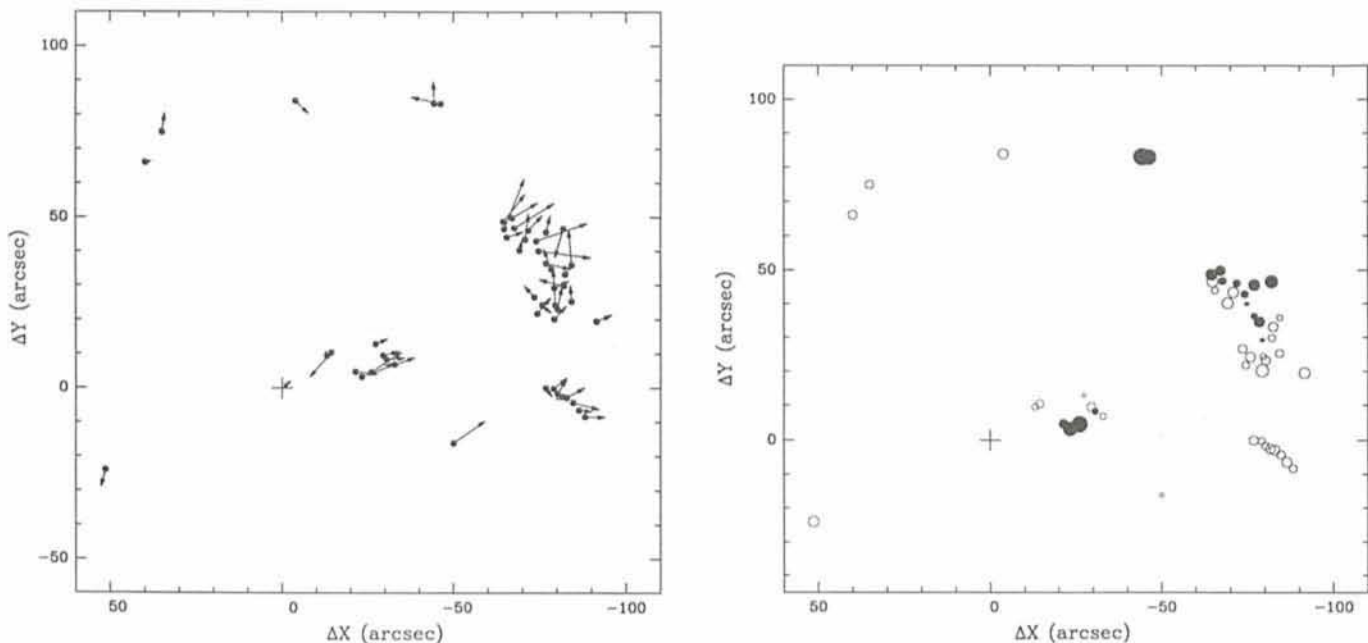
Figure 2: *Mapping (a) of proper motions and (b) of evolution in brightness of catalogued knots in Kepler's SNR (see text).*

mation derived from astrometry and photometry of the catalogued knots. Our Figures 2a and 2b give a synoptic picture of the proper motions of knots and of their evolution in brightness, respectively. In Figure 2a each arrow represents the proper motion of a knot over 400 yr (the present SNR age). The cross indicates the position of the centre of the radio and X-ray image, and the arrow from its centre indicates the common translation of the pattern of knots. In Figure 2b a circle centred at the position of each catalogued knot represents its evolutionary phase: filled circles indicate brightening (newer knots), while open circles indicate fading (older

knots). Larger circles indicate faster evolution. As already discussed above, newer knots brightened on the northern rim central regions of Kepler's SNR. Most knots are fading, with time-scales generally longer than those of the brightening ones (e-fold time-scales are up to 10 yr for brightening, and up to 30 yr for fading).

6. Effects of the Evolution on the Knots' Properties

Purpose of this Section is to give the reader a qualitative feeling of how the properties of knots depend on the phase of their evolution. Here we shall

present preliminary results based on images obtained with SUSI at the New Technology Telescope (May 1991), using narrow-band filters centred on $H\alpha+[NII]$, [SII] and [OIII] lines, respectively. For each of these three filters, after the subtraction of the stellar continuum, the relative intensities of knots catalogued by Bandiera and van den Bergh (1991a) have been measured.

In Figures 3a and 3b knot intensities in different lines are plotted ([SII] vs. $H\alpha+[NII]$, and [OIII] vs. [SII], respectively). Each knot is represented by a circle, whose characteristics indicate the evolutive phase of that knot, according to the conventions already used in Fig-
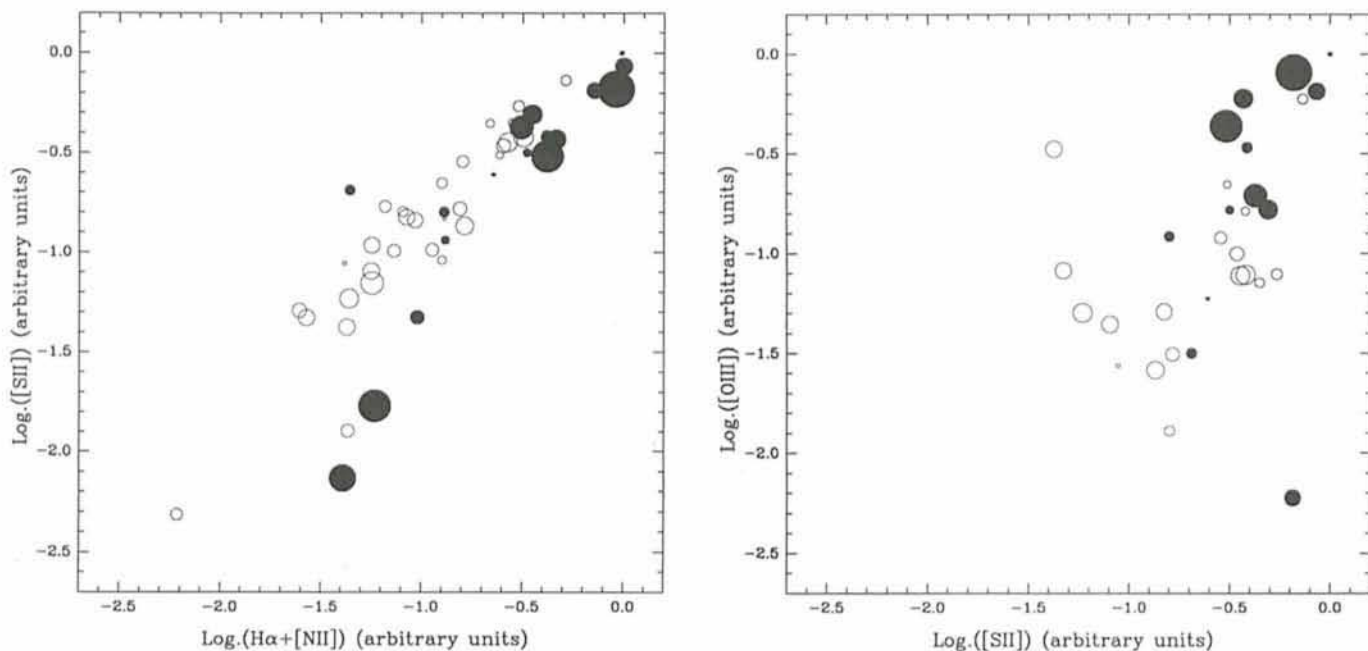

Figure 3: *Distribution of knots at different evolutionary phases in the (a) (Hα+[N II]) – [S II] and (b) [S II] – [O III] intensity-planes (see text).*

ure 2b. Figure 3b contains only 30 knots, because the INVENTORY routine failed to detect [O III] emission from the others.

From both figures it is seen that the regions containing younger knots (filled circles) are separated from those containing older knots (open circles). In Figure 3a the correlation between [S II] and Hα+[N II] intensities is rather good, but older knots are typically brighter in [S II]. However, in Figure 3b this correlation is poor. Most of the brighter knots in [O III] are young, while this is not so for [S II].

These results qualitively agree with a scenario in which the knots are initially at a higher ionization level, which then decreases with time. However, quantitative conclusions are beyond the scope of this discussion which is still based on incomplete data.

7. What's Next?

We have shown that a spectroscopic survey of optical knots, if combined with the present knowledge on their evolution, can provide a wealth of information on the temporal behaviour of the interaction of a blast wave with dense and compact clumps. Therefore, it might represent a useful benchmark for theoretical models of this interaction. The next step in this programme is to obtain a complete set of spectra for all catalogued knots. Intensity information on many lines would allow one to see how physical quantities, like densities and temperatures, evolve with time. A further goal is to discriminate those spectral features that mostly depend on evolutionary phase from those directly related to the intrinsic properties of a knot, like original density, size, etc. . . .

A detailed mapping of the radial velocities of knots is also planned. With Kepler's SNR we are at present in the paradoxical situation that proper motions are known in more detail than radial velocities. These two components, once combined, will give a 3-dimensional picture of the kinematics of this object. Such a study could provide valuable information on the structure and possibly also on the nature of this remnant.

The present advanced stage of our investigation is mostly due to observations taken at La Silla. The equipment present at La Silla is particularly suitable for a completion of the survey with a reasonably short observing time. Multi-Object-Spectroscopy facilities are the most suitable for optimizing observing time when spectra are needed for a large number of nearby objects. A private instrument (but well integrated in La Silla environment) like CIGALE Fabry-Perot scanning interferometer from

Marseille Observatory (Boulesteix et al., 1984), however, is ideal for radial velocity mapping.

References

Baade, W. 1943, Ap.J., **97**, 119.
Bandiera, R. 1987, Ap.J., **319**, 885.
Bandiera, R. 1988, In *Supernova shells and their birth events*, ed. W. Kundt, Lecture Notes in Physics Series, Springer Verlag, Berlin, p. 81.
Bandiera, R., van den Bergh, S. 1991a, Ap. J., **374**, 186.
Bandiera, R., van den Bergh, S. 1991b, In *SN 1987A and other Supernovae*, Proceedings of ESO/EIPC Workshop, eds. I.J. Danziger and K. Kjär, p. 661.
Blair, W.P., Long, K.S., Vancura, O. 1991, Ap. J., **366**, 484.
Boulesteix, J., Georgelin, Y.P., Marcelin, M., Monnet, G., 1984, In *Instrumentation in Astronomy*, Proc. SPIE 445, eds. V.A. Boksenberg, and D.L. Crawford, p. 37.
Dennefeld, M. 1982, Astron. Astrophys. **112**, 215.
D'Odorico, S., Bandiera, R., Danziger, J., Focardi, P. 1986, Astr. J., **91**, 1382.
Leibowitz, E.M., Danziger, I.J. 1983, M.N.R.A.S., **204**, 273.
Matsui, Y., Long, K.S., Dickel, J.R., Greisen, E.W. 1984. Ap. J., **287**, 295.
McKee, C. 1988. In *Supernova Remnants and the Interstellar Medium*, IAU Coll. 101, eds. R.S. Roger, and T.L. Landecker, Cambridge Univ. Press, New York, p. 205.
van den Bergh, S. Kamper, K.W. 1977, Ap. J., **218**, 617.

Subarcsecond Structures in Kepler's SNR

Narrow-band frames of Kepler's SNR have been obtained on May 15, 1991, using SUSI at the New Technology Telescope, during an official run devoted to imaging and spectroscopy of this object. Here we present images of the most conspicuous clusters of optical knots. These images are based on a 10-min exposure frame, taken with a narrowband filter centred on Hα + [N II] lines; the seeing was 0.7 arcsec.

After standard reduction, the stellar continuum has been subtracted using another 10-min exposure with an off-line narrow-band filter, obtained in similar seeing conditions. Before stellar subtraction the two point-spread functions have been carefully equalized, taking care of degrading the resolution as little

as possible. In the resulting image the residuals are about 7% (peak-to-peak) of the original stellar images, while the seeing has been degraded to 0.8 arcsec.

In order to extract details on the fine structure of the optical knots, we digitally simulated an unsharp-masking procedure. We convolved the image with a gaussian function of 1.8 arcsec FWHM, and added a constant value of 1.5 times the sky background. We finally divided the original image by this "mask". The effect of such a procedure is that of depressing the diffuse emission, as well as that of compressing the dynamical range. The dynamical compression allows us to see at the same time knots that originally were differing in intensity even by a factor 100. The results are
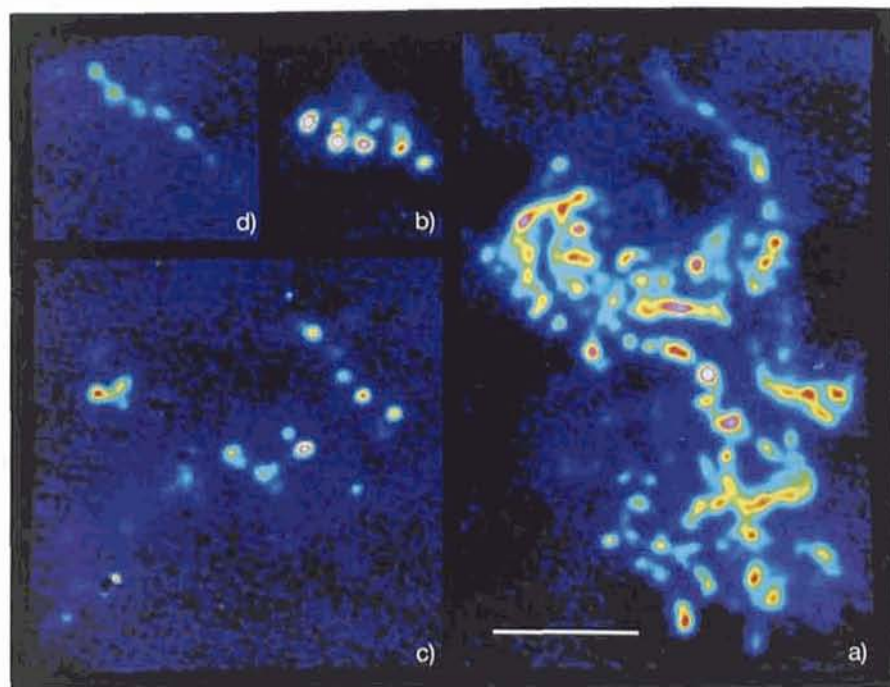
displayed in the figure, for four groups of knots in Kepler's SNR. Window (a) contains the brightest complex of knots, located on the N-W side; in window (b) there is a compact group of knots, that appeared only about 20 yr ago: region (c) is projected near the remnant centre, while region (d) is located on the West side. The white rule in the figure corresponds to 10 arcsec on the sky.

The most striking characteristics of these images is that they show that virtually all the filamentary structures visible in previous images are actually arrays of compact knots. This is very clear for the "filaments" in regions (c) and (d). The situation is similar also for region (a), even though the pattern of knots is very complex there: various structures seem to be just the intersection of different filamentary structures, as if we observe the projection of a 3-dimensional network. Knots are arranged rather regularly along filaments, with a typical separation of about 2 arcsec: this scale length does not seem to vary along the remnant (just compare region (c) with region (d)). The sizes of most individual knots are near the resolution limit. For instance, most knots in region (c), when deconvolved with a stellar PSF, result to have typical sizes of 0.3−0.5 arcsec. This, at a distance of 4.5 kpc, translates into a typical knot size of $2-3\times10^{16}$ cm.

R. BANDIERA, Osservatorio Astrofisico
di Arcetri, Italy
M. DELLA VALLE, ESO, La Silla

A Large Disk-Like Structure Around the Young Stellar Object Z CMa

F. MALBET[1,2], P. LÉNA[1,3], C. BERTOUT[2]

[1]Observatoire de Paris; [2]Observatoire de Grenoble; [3]Université Paris VII, France

We report here on the first observations of the luminous young stellar object Z Canis Majoris obtained with the adaptive optics COME-ON system.

Z CMa was originally thought to belong to the class of Herbig Ae/Be stars, the intermediate mass counterparts of T Tauri stars. Its optical spectrum displays strong emission lines with P Cygni profiles indicating outflow velocities of about 1000 km/s, but shows no photospheric absorption lines. Hartmann et al. (1989: Ap.J. 338, 1001) recognized Z CMa to be an FU Orionis star, i.e., a young, presumably low-mass stellar object undergoing strong mass-accretion via an accretion disk. Models of the optical and near-infrared energy distribution of Z CMa show that these spectral regions are entirely dominated by emission from the disk and suggest a record mass-accretion rate of some 10^{-3} M$_\odot$/yr, which makes Z CMa the most luminous FU Orionis star known to date. Poetzel, Mundt, and Ray (1989; Astron. Astrophys., 224, L13) discovered a high-velocity gaseous bipolar outflow (traced by an optical jet including at least fifteen Herbig-Haro objects) that emanates from Z CMa and extends to about 2 pc ($\approx$ 3') on each side of the star at P.A. 60°. Since the connection between accretion disks and outflows in young stellar objects is well documented (if not yet understood), it is not too surprising that such spectacular outflow manifestations are associated with indirect evidence of an accretion disk in this FU Ori object.

As one of the brightest young stellar objects in the sky, and an interesting one too, Z CMa is an obvious candidate for high spatial resolution work. Recent speckle interferometry in the near-infrared reveals that Z CMa is in fact a binary with separation about 0.1" (Christou et al., 1991; Proc. of ESO Conference on High Resolution Imaging by Interferometry). This finding is confirmed by Koresko et al. (1991; preprint), who show that the visible object (the inferred
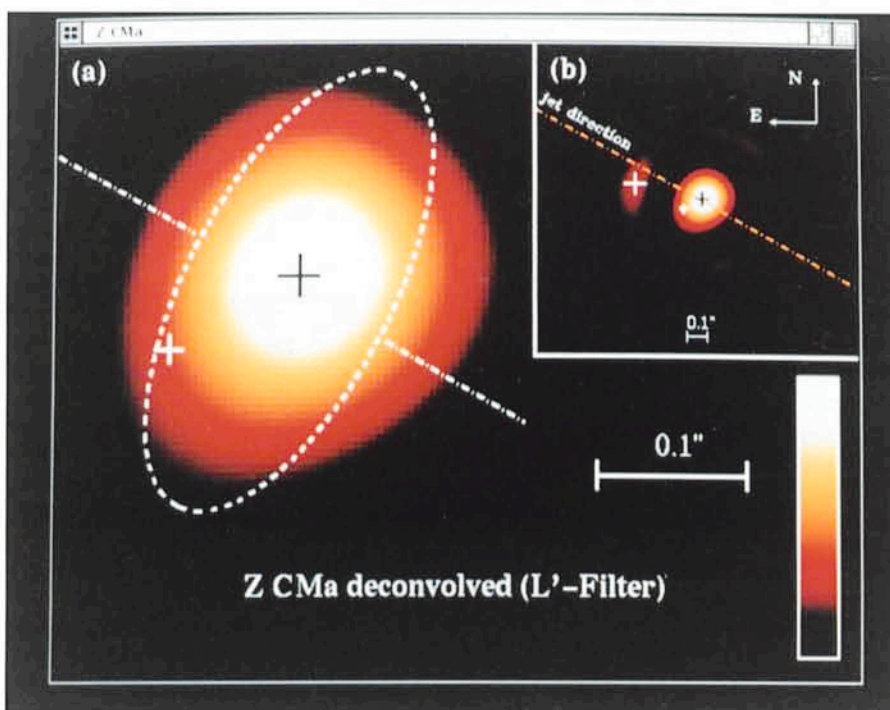

Figure 1: Deconvolved images of Z CMa at L' = 3.87µm, with superimposed components derived by best-fit model.
(a) The binaries are located at (+): the visible component at SE, the infrared at NW. The ellipse shows the best-fit disk-like structure, centred at the L' optical barycentre of the binaries, having a gaussian radial brightness profile in all directions: The dashed ellipse represents the 0.5 value of the gaussian. The intensity profile is linear on the colour scale. The direction of the Herbig-Haro objects and of the optical jet is indicated: see Figure (b).
(b) The same image as in Figure (a) on a larger scale. A third component may be present (+), but has to be confirmed. The dashed-dotted line gives the direction of the large-scale optical jet towards the Herbig-Haro objects and detected by the VLA.

FU Ori accretion disk) is located South-east (P.A. 120°) of the infrared compan-ion, which remains a somewhat mysteri-ous, probably protostellar object having a higher bolometric luminosity. How-ever, the binary system alone cannot account for the large far-infrared flux originating from the Z CMa region, a fact which leads Koresko et al. to speculate about the existence of a cool, extended structure surrounding the binary. The observations reported here reveal this condensation, and demonstrate that it is elongated in the direction perpendicular to the jet.

These observations use COME-ON at the Cassegrain focus of the ESO 3.6-m telescope, the adaptive optics VLT prototype described by Rigaut et al. (1991 a+b; *Astron. Astrophys.*, in press, and are part of its continued scientific use (Eta Carinae: *The Messenger* **63**; Ceres: *The Messenger* **65**). The imaging camera is a 32×32 InSb array with a 0.108″ pixel size on the sky. Standard image processing is applied and then followed by image reconstruction using a classical deconvolution algorithm from the complex visibilities. The de-convolved image at $L' = 3.87$ μm is shown in Figure 1 together with the var-ious components needed to get a re-sonable fit of the visibilities (using χ^2 minimization techniques). We find that the most probable model of this com-plex object is indeed a binary system surrounded by an extended, flattened structure. The positions of the optical and infrared binary components were assumed to be those found in speckle work, and the geometric properties of the extended structure were consid-ered as free parameters in order to fit the observed complex visibilities. The centre of the disk-like structure is taken at the optical barycentre of the binary at L'. The inferred diameter of the disk-like strukture is 0.4 ± 0.06″. It is oriented at P.A. 153 ± 8°, whereas the outflow direction is at P.A. ≈ 60° (dashed-dotted line in the insert of Fig-ure 1). We therefore suspect that the observed disk-like structure, which re-mains unresolved in the direction paral-lel to the jet, is in fact a large-scale disk, perpendicular to the outflow axis and surrounding both components of Z CMa. It is likely that this large-scale disk fuels the FU Orionis accretion disk that surrounds the visible component and provides a density gradient in the flow direction that helps to collimate the jet. In order to get the best possible fit to the visibilities, the presence of yet another component must be assumed, to account for the relative maximum of intensity seen on the diffraction ring at P.A. 70° (see insert of Figure 1). The brightness of this third component is

much lower than that of either binary members; if confirmed by further work, this may represent either an emission knot in the jet or a stellar object.

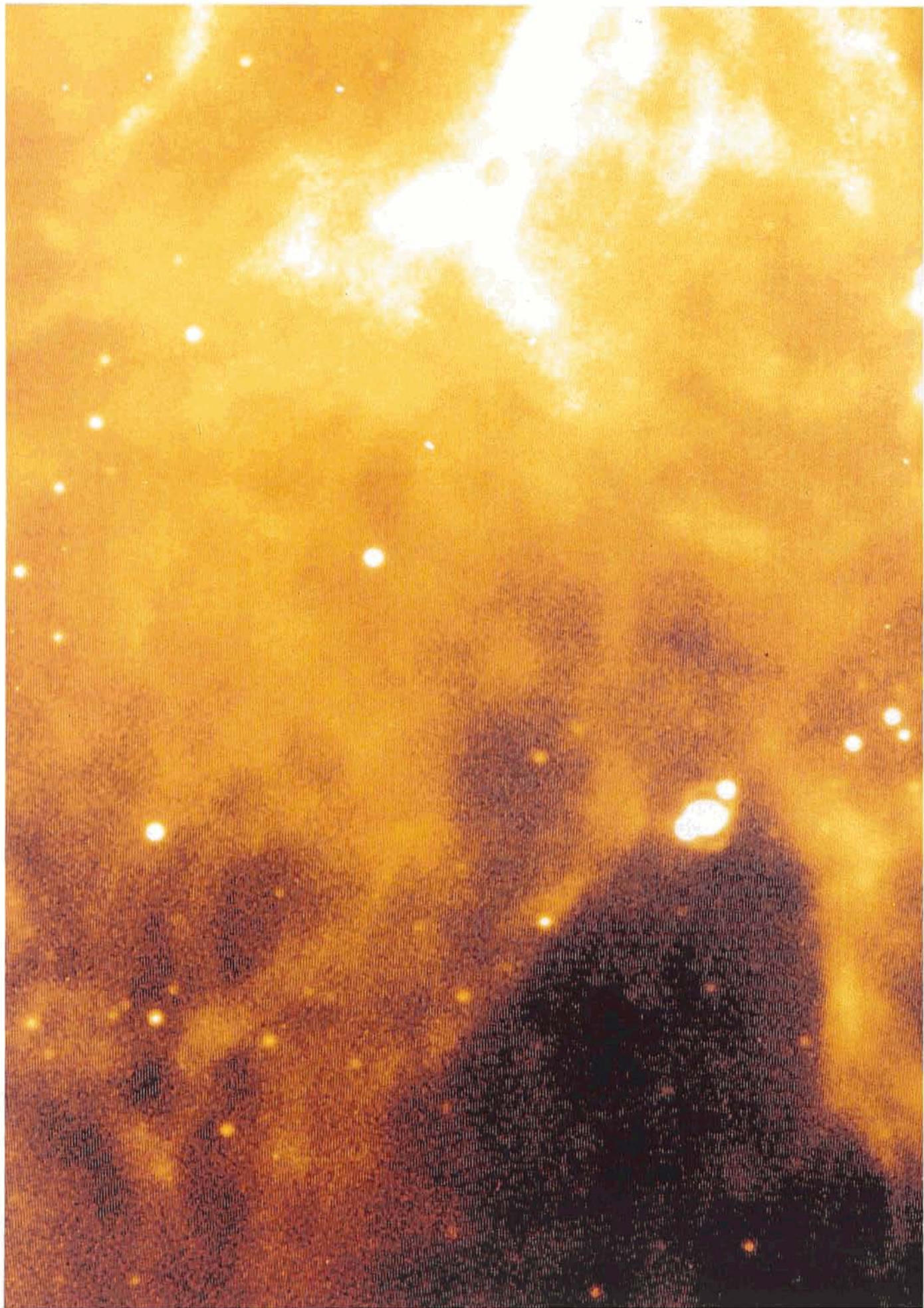This new result reveals the power of the adaptive optics technique to explore the close surroundings of young stellar objects. They appear more complex than anticipated, as demonstrated by this first direct image of a disk-like structure surrounding a binary (100 A.U.). Further instrumental develop-ments are under way, including the use of coronographic techniques.

With modern observatories being moved to ever more remote sites, fewer and fewer European students have ready access to up-to-date observing facilities. As one step towards balancing this obvious shortcoming in the training of young European astronomers, the ESO/OHP Summer School offers the opportunity to gain practical experience under realistic conditions.

In groups of three students, each guided by an experienced observer, the participants will prepare a small observing programme to be carried out with telescopes of 1.2–1.9 m aperture (direct imaging and spectroscopy) at OHP. The data reduction will be done with MIDAS, on-line also with IHAP. In a micro workshop at the end of the school each group will present their results, including additional pertinent information from the literature, to the other participants.

The preparation of the practical work will be supplemented by a series of 90-minute lectures which will be given by invited specialists. The subjects foreseen include (a) modern telescope layout, (b) charge-coupled devices, (c) design principles of high-throughput optical instruments, (d) crowded-field photometry, (e) high-resolution spectroscopy, (f) low-resolution and slitless spectroscopy, (g) astronomical infrared technology, and (h) data-reduction strategies. As a scientific highlight, a talk on a cosmological subject is foreseen. The working language at the summer school will be English. (Reports on the two previous ESO/OHP Summer Schools appeared in *The Messenger*: see No. **53**, p. 11 and No. **61**, p. 8.)

Applications are invited from graduate students working on an astronomi-cal Ph.D. thesis at an institute in one of the ESO member countries. Applica-tion forms can be obtained from the organizers. The deadline by which applications must have been received is March 31, 1992. A letter of recom-mendation by a senior scientist who is familiar with the applicant's work will be required at the same time. Up to eighteen participants will be selected and have their travel and living expenses fully covered by ESO and OHP.

The Organizers:

M.P. Véron
Observatoire de Haute-Provence
F-04870 Saint-Michel-l'Observatoire
France
Internet: MIRA@OBSHPA.DNET.
        NASA.GOV
EARN/Bitnet:
PSI-mail:
PSI%0208004042183::MIRA
SPAN: OBSHPA::MIRA

D. Baade
European Southern Observatory
Karl-Schwarzschild-Str. 2
W-8046 Garching, Germany
VISAS@ESO.ORG

VISAS@DGAESO51

ESO::VISAS

RECTIFICATION

The VLT Adaptive Optics Programme (*The Messenger* No. 65, p. 13)

The true value of the inclination of the projected rotation axis of Ceres with respect to the normal to the ecliptic plane is 4±6° and not 20 to 30 as erroneously given in Figure 1.   *M. COMBES, O. SAINT-PÉ, DESPA-Paris Observatory*

Supernova 1987A in the LMC

Almost 5 years after the explosion, this NTT exposure (left) in the light of Hα was obtained by ESO astronomers Christian Gouiffes and Massimo Della Valle on December 1, 1991. Both the inner oval nebula and the outer filaments are clearly visible. The exposure time was 10 minutes with a seeing of approximately 0.65 arsec.

SN 1987A is situated SW of the Tarantula Nebula in a complex region containing extended emission nebulosities. Just south of it is a darker area of higher absorption, possibly the interstellar cloud in which the young star SK −69° 202 was formed, some million years ago.

The frame below is an enlargement of an [NII] image, processed to better show the details of the SN 1987A surroundings.

The small frame at the bottom shows the same area in continuum light, in a spectral region with no emission lines. The magnitude of the supernova itself has now decreased to about 18, and it has become significantly fainter than the two stars in the multiple system SK −69°202, in which the brightest star exploded on February 23, 1987.
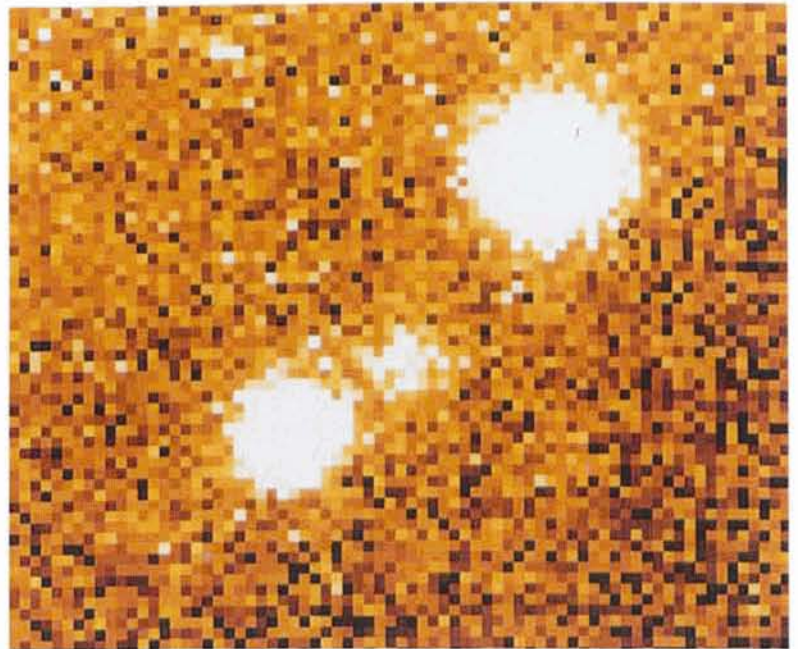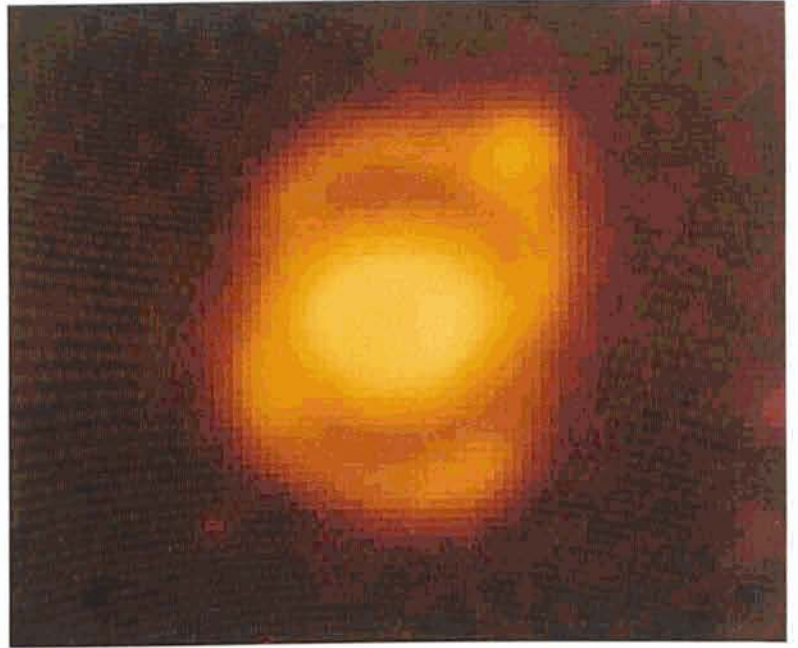
Asteroseismology

W.W. WEISS[1], H. SCHNEIDER[2]

[1]*Institut für Astronomie, Vienna, Austria;* [2]*Universitätssternwarte Göttingen, Germany*

Introduction

Probably the most convincing definition for what *asteroseismology* actually is, was given by Däppen, Dziembowski and Sienkiewicz (IAU Symp. No. 123, p. 233, 1988) as a method of testing stellar structure and evolution theory, using *all* available pulsation data (including also growth rates, phases, the fact that mode exists, and sometimes are transient, etc.), and not just observed frequencies.

Asteroseismology probably opens the accessible parameter space well beyond the classical instability strips, if solar-type oscillations can be observed for a large variety of stars. It has become an increasingly accepted opinion that pulsation (probably mostly in the form of non-radial pulsation) is the rule, rather than the exception. Unfortunately, the observable quantities tend to be extremely small and new instrumentation is needed, for ground-based observations as well as for observations from space. The prospects, however, are magnificent since it appears to be possible to test stellar interior and evolution over most of the parameter space of the HR diagram. Stars where relativistic effects are not important and which might therefore be classified as 'normal', will probably serve as most common targets for asteroseismology.

'Normal' stars are very interesting astronomical objects in themselves and certainly are not 'boring'. They play a crucial role in the chemical evolution of the Universe. Stars on the Main Sequence and close to it are by far the most frequent and easily observable ingredients of the Universe. All our understanding of the Cosmos is based on calibrations (age, distance, mass, etc.) obtained from our closest neighbours. We will not be able to appreciate our Cosmos until we fully understand its constituent stars. Understanding stellar evolution is fundamental for a coherent picture of the Universe, because the life of galaxies largely depends on the life of their basic, luminous constituents: the stars.

For many years, astronomers have struggled with the problem posed by these 'simple' objects, but find themselves still far from the goal anticipated by Eddington who, in 1926, finished his book on *The Internal Constitution of the Stars* with the sentence: "... but it is reasonable to hope that in a not too distant future we shall be competent to understand so simple a thing as a star."

These 'normal' stars are best suited for significant tests for various aspects of fundamental stellar physics. Confronting realistic stellar models with high-quality observations will tell us much about the underlaying physics.

In addition, stars constitute essential laboratories for studying important aspects of basic physics (convection, MHD, nuclear reactions, equation of states, transport processes, etc. . . .) under conditions which cannot be reproduced in terrestrial laboratories. For extremely high and low temperatures and densities, this stellar laboratory is indispensable for testing physical theories. These are just a few examples for the significance of stellar physics to what may be called laboratory physics.

Not surprisingly, many international conferences have been devoted in recent years to helio- and asteroseismology. IAU Colloquium No. 137 (Vienna, April 13 to 17, 1992) will be devoted, among others, to aspects raised in the present article and is entitled "Inside the Stars".

A short overview over the last 30 years of stellar astrophysics illustrates the immense increase of knowledge about how stars are working, but also about the serious shortcomings in our physical concepts and accuracy of our data.

In the sixties, a very important step in stellar modelling was achieved by qualitatively explaining the structure of the HR diagram at the level of accuracy of the observational data. In the late seventies and in the eighties the development of solar neutrino astronomy as well as helioseismology showed that there is not yet a satisfactory model which can predict the observed quantities at the very high level of accuracy meanwhile achieved. The immense progress in this field, accelerated by successful space experiments, suffers from a lack of generality, as was demonstrated, e.g., at IAU Colloquium No. 121, "Inside the Sun". New steps forward are needed to constrain theories by studying stars with different physical parameters (effective temperature, luminosity, chemical composition, rotation rate, magnetic fields, etc.).

In the nineties, still more accurate observational techniques are being developed which are suited to challenge theories in a parameter space more complex than the two-dimensional HR diagram. The most prominent new tools are:

- precise distances, measured by the Hipparcos satellite,
- pulsation periods, observed with ground-based telescope networks and with space experiments,
- rotational velocities and magnetic fields, derived from surface imaging techniques,
- new powerful detectors which help to increase the S/N of observations significantly,
- dramatic advances in computer technology.

Scientific Goals

The key issue of asteroseismology is the theory of stellar structure and evolution. In the present status of the theory, a stellar model is typically characterized by five parameters (mass, age, initial compositions in helium and metals, and mixing length – a parameter describing the convective transport of energy) for which we usually have only two observables (luminosity and surface gravity). Consequently, stellar models cannot be adequately tested. Moreover, we have some reasons not to trust our description of stellar interiors. Let us take two examples.

- When ensembles of stars (like open clusters or binary systems) are observed for which independent constraints on some astrophysical parameters are available (same age and same initial composition for each star in the ensemble), it is usually impossible to reproduce the observed properties of the stars with the same value of the mixing length. This may indicate that the representation of convective transport by the mixing length theory is not adequate.
- The observed solar neutrino flux is much lower than expected, which indicates that modelling of the solar interior is incomplete.

Already these two examples demonstrate that an improvement of stellar modelling is absolutely necessary. However, such an improvement is possible only if adequate tests for current models can be provided. Asteroseismology is a new tool for this purpose.

Pulsation

Classical pulsating stars have already been known since 1784, when δ Cephei

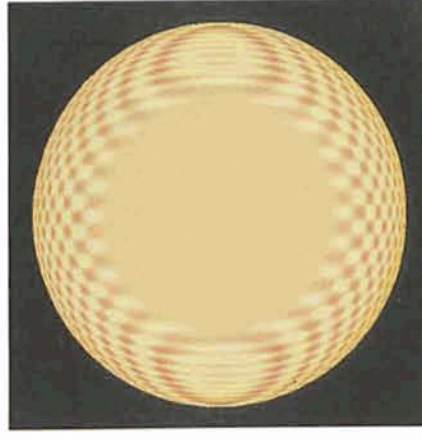Figure 1: *Solar p-modes, equatorial cross section l=40, m=40, v=3.175 mHz.*

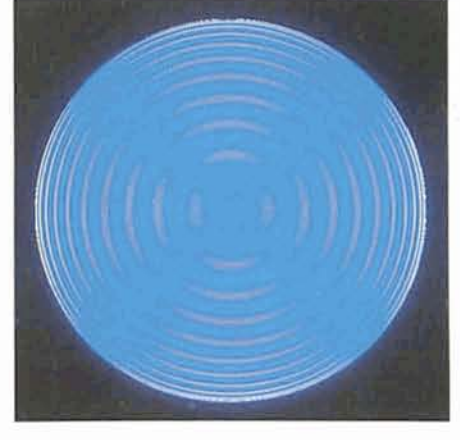Figure 2: *Solar p-modes, equatorial cross section l=40, m=0, v=3.175 mHz.*

Figure 3: *Solar p-modes, equatorial cross section l=2, m=2, v=3.147 mHz.*

was discovered as a variable star. It took nearly 200 more years to understand the reasons for this type of stellar variability.

Eigenmodes of pulsations carry a wealth of information on the state of the interior of stars. A mode of a given degree l is confined to a given cavity within the star. High-degree modes, like the one represented in Figures 1 and 2, are restricted to sub-surface layers, while low-degree modes, as shown in Figure 3, propagate all the way to the centre of the star. The Figures 1 to 3 are equatorial cross sections through vibrating solar models and have been kindly provided by S. Frandsen (Astronomisk Institut, Aarhus). Amplitudes of the displacement vectors of the solar p-modes are colour coded. Another illustration of non-radial pulsation modes is given in Weiss and Schneider (*The Messenger*, No. **33**). For distant stars, ony low-degree modes can be detected because of the lack of spatial resolution. Fortunately, these modes are precisely those that probe the structure from surface to centre.

The roots of asteroseismology are, of course, the same as for the theory of classical pulsating stars. This can be best illustrated in the asymptotic case, when the degree l of a pulsation mode is much smaller than the order (overtone) of this pulsation n. Tassoult (1980) has derived an asymptotic solution for p-modes:

$$\nu_{n,\ell} = \Delta\nu_0 \cdot \{n + \frac{\ell}{2} + \epsilon - \delta_{n,\ell}\}$$

with $\quad \delta_{n,\ell} = \frac{\ell(\ell+1)\alpha+\beta}{n+\frac{\ell}{2}+\epsilon},\quad$ and

$$\Delta\nu_0 = \{2\int_0^R \frac{dr}{c}\}^{-1}.$$

The polytropic index of the model is 2ϵ, whereas α and β are constants depending on the internal structure of the

star, and c is the travel speed of sound.

For a rotating star, the unperturbed frequency $\nu_{n,l}$, as observed from the earth, is further split in a symmetric frequency multiplet according to:

$$\nu^{rot}_{m,n,\ell} = m \cdot (1 - C_{\ell,n}) \cdot \Omega,$$

with $-l<m<l$, m being an integer, Ω the stellar rotation frequency, and C a constant which strongly depends on the stellar structure.

In addition, the global magnetic field structure of a star also influences the eigenfrequencies and pulsation amplitudes. Hence, amplitude ratios of frequency multiplets allow to derive information on this magnetic field structure.

As is evident, a full mode identification (n, l and m) is necessary in order to compare any observed pulsation frequency with predictions. For most of the classical pulsating stars only one pulsation frequency has been observed, sometimes two, very rarely three frequencies. Frequently, the observed frequencies do only poorly correspond to those predicted by models. The solution to this discrepancy is often prevented by an unknown full mode identification.

Asteroseismology – a New Tool

In asteroseismology the analysis of the stellar structure will not be based on the observation of one or two frequencies, but on a frequency spectrum which allows the determination of characteristic periodic structures within such a spectrum. No individual mode identification is necessary in this case.

The kind of results we can expect for distant stars are illustrated by the full disk solar power spectrum obtained by the Iphir experiment on board the Phobos probe towards Mars (Fig. 4). In this power spectrum of the Sun – seen as a star –, we can distinguish up to 30 low-degree modes. Two quantities can

be measured to a very high accuracy in such a power spectrum: the "large" and the "small" separations. The large separation $\Delta\nu_0$ is the frequency difference between two modes of same degree l, but of quantum numbers n differing by one. The small separation δ_{nl} is the frequency difference between mode n, l and mode n−1, l+2. It turns out that $\Delta\nu_0$ depends on the "average" sound speed in the stellar interior, and therefore carries information on the "average" structure, while δ_{nl} is sensitive to the details of the stellar structure close to the core.

Once the large and the small separations have been measured to a high accuracy for a given star, one can, for example, locate them in the so-called asteroseismological HR diagram, where the structure constant D_0, proportional to the small separation, is plotted versus the large separation $\Delta\nu_0$. This diagram was introduced into asteroseismology by J. Christensen-Dalsgaard (Aarhus). In such a diagram (Fig. 5), lines of constant mass (full lines) and lines of constant central hydrogen content (dashed lines) can be drawn. The central hydrogen content is an excellent age indicator. By placing the measured large and small separations in the asteroseismological HR diagram, one can derive with a good accuracy the mass and age of a star.

Further diagnostics is provided in an 'echelle' diagram (Fig. 6) in which the frequencies are plotted modulo $\Delta\nu_0$. The curvature of the lines appearing in an echelle diagram (one line for each value of l) is very sensitive to the details of the structure just below the stellar surface. Thus, low-degree modes can also be used to probe these regions.

Finally, and as was already mentioned, a further dependence of the frequencies on the azimuthal order m is introduced when a star rotates, known as the rotational splitting. This splitting depends on the integral of the internal
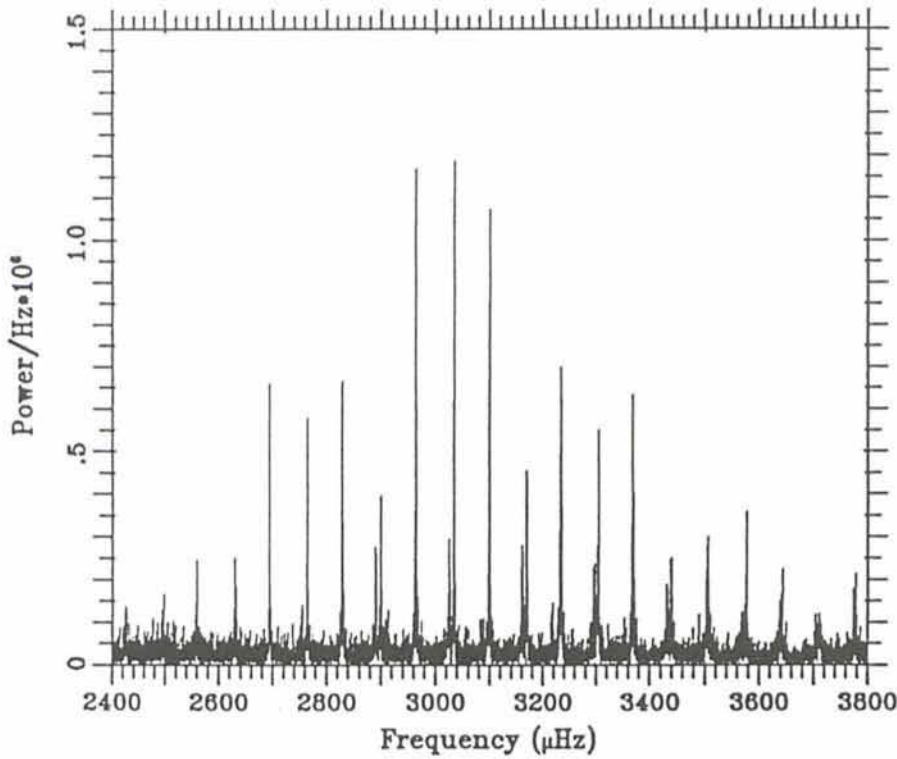
37

Figure 4: *Power spectrum of the low-degree p-modes from 160 days of the IPHIR experiment.*

spectral resolution and the high S/N ratio required. They are also limited to very slow rotators, because sharp spectral lines are needed to reach the desired accuracy. Unfortunately, slow rotators are not the most interesting objects to study (no measurable rotational splitting, not efficient dynamo), and therefore the first class of methods should be preferred for a systematic study.

Although we are concentrating here on 'normal' stars, it has to be mentioned that more exotic objects, like white dwarfs and nuclei of planetary nebulae, have benefitted enormously from asteroseismology.

In conclusion we can say that asteroseismology is a powerful tool to probe the internal structure and dynamics of stars, and therefore to contribute to the solution of the current basic problems of stellar physics by providing two independent observables ($\Delta\nu_o$ and δ_{nl}). However, as current stellar evolution theories characterize a star by five independent parameters (mass, initial mass fraction of Helium (Y) and metals (Z), age and mixing length), additional data have to be provided for a full test of stellar interior and evolution models. Hitherto, in most cases only the effective temperature and luminosity can be measured, accounting for two further independent parameters, out of the total of five needed.

Scientific Impact of Asteroseismology

In the following sections we will try to highlight the most prominent aspects of stellar physics which will benefit – and have already benefitted – from asteroseismological projects.

rotation over the region crossed by the mode under consideration (i.e. for most of the stars the low-degree modes), and hence can provide an estimate of the internal rotation.

Seismological techniques have been applied extensively to the Sun, and helioseismology has brought an enormous amount of information about the solar interior. Among other results, it was shown that solar p-mode frequencies are not compatible with presently assumed core mixing, with the existence of Weakly Interacting Massive Particles (WIMPS), that there is no fast spinning core in the Sun, and that solar internal rotation is not constant on cylinders, as suggested by some theories.

For other solar-type stars on the contrary, only very few results have been obtained so far. In fact, only marginal detection of pulsation has been claimed for two very bright slow rotators (Gelly, Grec, Fossat: 1986, *Astron. Astrophys.* **164**, 383): α CMi (Procyon) and α Cen (Rigil Kent). In the respective power spectra for the radial velocity variations, no clear evidence for $\Delta\nu_o$ and δ_{nl} emerge and therefore no reliable information can be extracted about the internal structure of these two stars.

This lack of clear asteroseismological results is caused by the extremely low signal that must be detected in the case of, e.g., solar-type stars. Two observable quantities can be used for asteroseismology:

● Brightness fluctuations induced by the pulsations: These fluctuations amount to only 10^{-6} mag. for typical solar-type stars. As will be shown later, photometric measurements down to this accuracy are not possible from the ground.

● Velocity fluctuations induced by the pulsations: These are of the order of 10 cm s^{-1} for solar-type stars, and this type of measurements represent an important technological challenge, not totally out of scope, though. However, these measurements are limited to only a few very bright objects, because of the high
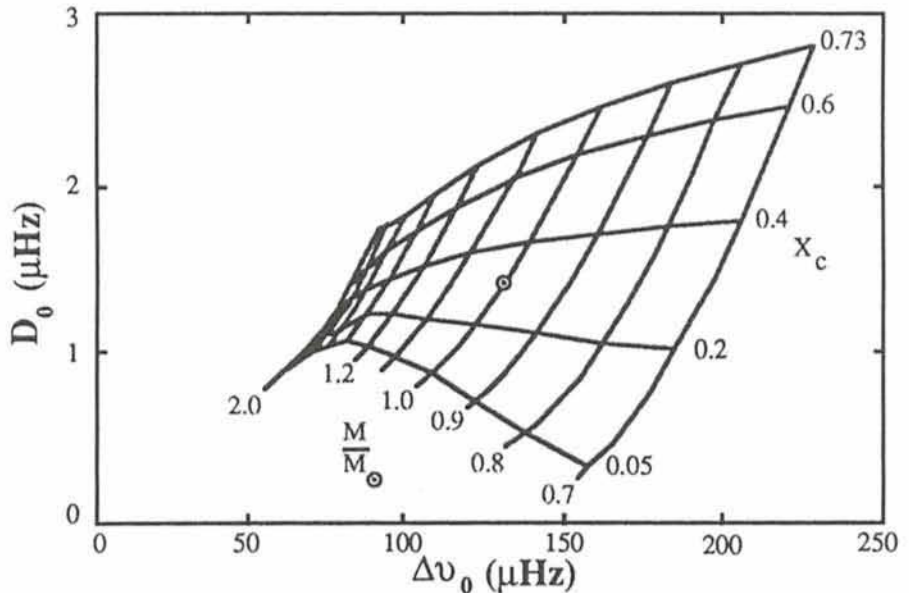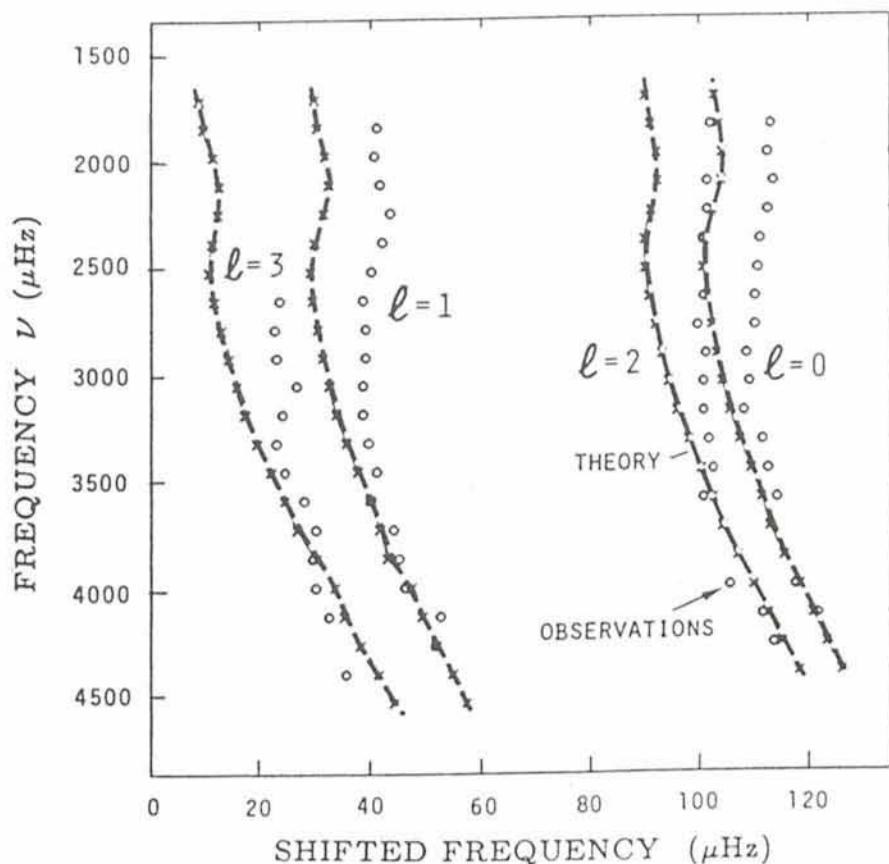

Figure 5: *The asteroseismological HR Diagram.*

Figure 6: *Echelle-diagram for the solar p-mode oscillations.*

● *Stellar interior:* For individual stars, as mentioned above, we usually have 2 observables: the absolute luminosity, which can now be known to a high accuracy thanks to the Hipparcos satellite, and the surface gravity, known to a much lower accuracy. The mode frequencies provided by the asteroseismological data will yield additional observables to test stellar models. In particular, the large and the small separations will be measured to a very high accuracy. These two observables are directly sensitive to the details of internal structure, while the usual observables are surface properties of the stars and are only indirectly sensitive to the internal structure.

● *Stellar evolution:* With the availability of very precise frequency measurements it will be possible to detect stellar evolution effects even within an active life time of a scientist. This has been investigated, among others, for white dwarfs by D. Winget, for roAp stars by St. Kawaler, and for δ Scuti stars by M. Breger.

● *Excitation and convection:* Convection is thought to be responsible for mode excitation in solar-type stars. Therefore, measuring mode amplitudes and life-times of stars of different types and ages will have a very important impact on the theories of

mode excitation, and as a consequence on our understanding of stellar convection.

● *Angular momentum distribution and transport:* The problem of angular momentum is among the most important in stellar physics. The issue is to understand how stars get rid of their initial angular momentum, how angular momentum is distributed and is transported in stellar interiors during a star's life. Providing an estimate of internal rotation through rotational splittings and a measurement of surface rotation through observed rotational modulation of white light as well as of UV lines will give a hint about angular momentum distribution within stars. The differences seen between stars of different ages will tell us how angular momentum is transported during stellar evolution.

● *Dynamo theories:* The mode frequencies and the separations provide an estimate of stellar ages and masses. The frequencies and separations, with the addition of mode amplitudes and life-times, will result in constraints on the structure of convective zones. Moreover, as indicated previously, the simultaneous estimates of internal rotation (rotational splittings) and of surface rotation (rotational modulation) will provide an estimate of the angular ve-

locity gradient, and a hint on the rotational shear at the base of the convection zone.

Asteroseismology at La Silla

Already since the early stages of asteroseismology ESO has granted telescope time to various projects in this field. In the following we can only give a very brief summary which will be biased towards our own activity and is based mainly on after-dinner 'shop talks' at La Silla. We apologize for being ignorant of other important projects.

One group of stars which contributed to the boom in asteroseismology is the group of pulsating magnetic CP2 stars, also called, but less precisely, rapidly oscillating Ap (roAp) stars. Soon after the discovery of the first member of this group with periods of about 10 minutes by Don Kurtz (South Africa) in 1979, confirming observations were gathered at La Silla with the 50-cm Danish telescope in Strömgren and Hβ colours. The full story is already told in *The Messenger*, No. **33**.

In the beginning of the eighties, some surveys had already been initiated to check CP2 stars for stability against δ Scuti type pulsation with few hours period. Our survey at La Silla, e.g., is still ongoing and uses mainly small telescopes (50-cm telescopes, 0.9-m Dutch telescope and the 1-m ESO telescope). The recently descoped Walraven photometer proved to be particularly useful, because it allowed to obtain simultaneous 5-colour data. The potential of multicolour information on mode identification is illustrated in *The Messenger*, No. **34**, p. 9. Furthermore, Matthews, Wehlau and Walker (*Astrophys. J. Lett.*, **365**, L81) have shown that such observations, supplemented by data from the IR, allow to derive the atmospheric temperature stratification. The first observations of roAp stars in the near IR have also been obtained at La Silla.

La Silla usually plays an important role in observing campaigns organized to obtain long and uninterrupted data sets which are not affected by the day-night cycle. Several such campaigns have already been successful for various δ Scuti (e.g. M. Breger with Bochum observers) and roAp stars.

The observations of solar-type oscillations of Procyon and α Cen, mentioned earlier in this article, have been obtained by the Nice group primarily at La Silla. Other very important activities in asteroseismology are currently ongoing at the Danish 1.5-m telescope, where S. Frandsen (Aarhus) and his colleagues investigate various clusters of different age for δ Scuti stars. The Geneva group has accumulated and

published a lot of data related to micro-variability, δ Scuti, β Cephei and RR Lyr variables. Similar holds true for the Leiden group, using the famous Walraven photometer. Very probably, this list of photometric and spectroscopic projects carried out at La Silla is incomplete, but yet suited to illustrate the significance of the excellent ESO site for asteroseismology, as well as for the importance and effectivity of small and medium sized telescopes. "Big Science" not always demands "Big Telescopes".

Finally, we would like to briefly touch on our future projects at La Silla related to asteroseismology, in addition to continuing our survey and participating in world-wide observing campaigns.

As has been clearly demonstrated by a recent ESA Assessment Study for project PRISMA (*ESA SCI* (**91**) 5, asteroseismology will enter a new era, if observations can be done from space.

The elimination of atmospheric noise and the possibilities of very long, continuous data strings with a large duty cycle are the main reasons. One such asteroseismological space experiment is already approved for the Sovjet MARS-94 probe and has the acronym EVRIS. The other space project, more versatile, elaborate and powerful, is presently in Phase A study at ESA and is called PRISMA (Probing Rotation and Interior of Stars: Microvariability and Activity).

As already shown earlier in this article, supplementing ground-based observations are mandatory for a full exploitation of the scientific potential of asteroseismology. In the case of EVRIS, basic stellar data of sufficient accuracy, like effective temperature, log g and luminosity are missing for many EVRIS target stars. Furthermore, a careful investigation of the immediate vicinity of the very bright target stars is necessary

in order to avoid a poor target choice. Photometric problems may arise from even very faint background sources which drift in and out of the photometer aperture due to satellite jitter. To our surprise, there are presently no data archives available which would allow to extract the required astrometric and photometric information for EVRIS. As a consequence, all the candidate target fields have to be carefully observed in various colours with CCD techniques.

This synergy between space- and ground-based observations is another example for the necessity to develop both and not to ignore one at the expenses of the other.

Multi-Wavelength Observations of Infrared-Bright Carbon Stars

M.A.T. GROENEWEGEN[1] *and T. DE JONG*[1,2]

[1]*Astronomical Institute 'Anton Pannekoek', Amsterdam, the Netherlands*
[2]*SRON, Laboratory for Space Research, Groningen, the Netherlands*

1. Introduction

The carbon star phase is one of the last phases of evolution of intermediate mass stars (1-8 solar masses). Carbon stars reside on the Asymptotic Giant Branch (AGB) in the Hertzsprung-Russell diagram. The carbon is produced in thermal pulses, short periods of explosive He-shell burning, and transported to the surface by convective mixing. Many of the physical processes that play a role in the formation and evolution of carbon stars are still poorly understood, e.g. the production and dredge-up of carbon, the origin and evolution of the mass loss. Here we briefly report on an observational study of infrared-bright carbon stars.

In a recent paper Groenewegen et al. (1991) have studied an infrared-complete sample of bright carbon stars containing all 109 carbon stars with $S_{12}>100$ Jy in the IRAS PSC. This sample is more complete than others previously studied in that both optical and infrared carbon stars are included.

Using near-infrared photometry from the literature they derived near-infrared colour temperatures and from the ener-

gy distribution they calculated infrared bolometric corrections. Distances were derived assuming $M_{bol}=-4.9$, corresponding to $L=7050$ $L_{\odot}$. From available CO data mass-loss rates were calculated for about 80 stars in their sample.

The sample was divided into five groups depending on their infrared properties, extending the classification of carbon stars of Willems and de Jong (1988). Group I stars show the silicate feature in their LRS spectra, possibly because they are very recently formed carbon stars. Since none of the known Group I stars is bright enough to have made it into the sample they will not be discussed further. Group II stars have a pronounced 60-μm excess, high near-infrared temperatures, small bolometric correction and low mass-loss rates. They probably turned into a carbon star quite recently and their excess at 60-μm is due to a cool circumstellar shell, probably the oxygen-rich remnant of the preceding high mass loss phase. From group III to V the mass-loss rate of carbon stars steadily increases, and as a consequence the near-infrared temperatures decrease and the bolometric corrections increase.

Using average bolometric corrections for each group the infrared-complete sample was transformed into a volume-complete one. The scale height of carbon stars is found to be 190 pc and their local space density equals 185 kpc^{-3}.

From the calculated space densities of carbon stars in each group relative timescales are derived. Adopting a lifetime of 20,000 years for group II stars from model calculations, Groenewegen et al. find a total lifetime of the carbon star phase of about 26,000 years, uncertain to a factor 2. The total mass lost during the carbon star phase equals about 0.04 $M_{\odot}$. This number is uncertain to a factor 5, a factor 2 arising from the uncertainty in the lifetime of group II stars and a factor 2.5 arising from the uncertainty in the mass-loss rates. For an adopted average white dwarf mass of 0.65 $M_{\odot}$ this implies that most stars are already of low mass when they turn into carbon stars, probably around 0.69$_{\odot}$ and certainly less than 0.85 $M_{\odot}$.

The location of the 109 stars in the IRAS colour-colour diagram is shown in Figure 1. The colours $C_{21}=2.5$ log(S_{25}/S_{12}) and $C_{32}=2.5$ log(S_{60}/S_{25}) are indicated along the axes. As discussed
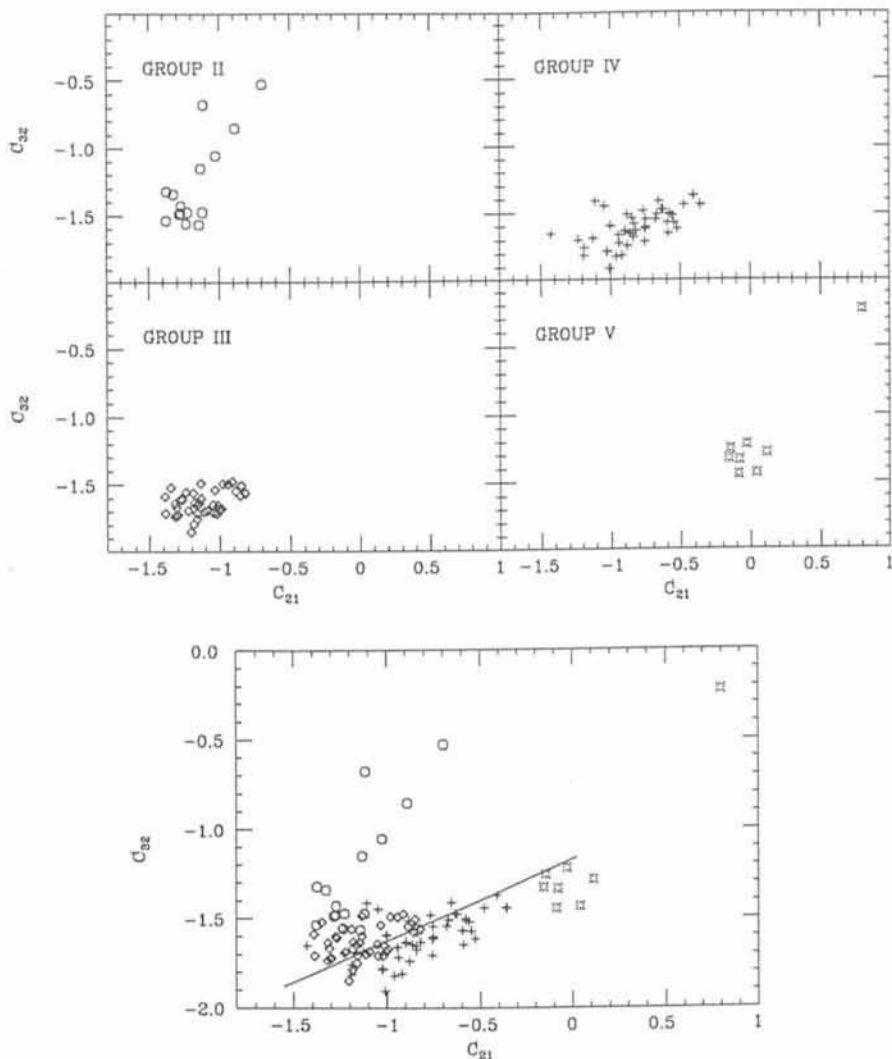
Figure 1: *The location of the 109 carbon stars in the IRAS colour-colour diagram. In the top four figures the sample is divided into the different evolutionary groups. In the bottom figure the total sample is plotted. The solid line indicates the location of the blackbody line.*

the 2.2-m telescope as well as HCN (1–0) data from the SEST.

In section 2 we present the data obtained for three stars in our sample for which we obtained NIR photometry and CVF spectra as well as CO and HCN data. They are 08074–3615 (a group IV star), 11318–7256 (group III) and 13477–6532 (group IV). Several observed parameters like galactic longitude and latitude, colour-corrected IRAS fluxes, C_{21} and C_{32}, LRS classification and VAR index are listed in Table 1. In sections 3 and 4 we derive mass-loss rates from the CO line profiles and fit the energy distribution using a radiative transfer model. The results are briefly discussed in section 5.

2. The Data

Near-infrared photometry was obtained on February 17–18, 1991 at the ESO 1.0-m telescope and on February 25–28 at the ESO/MPI 2.2-m telescope. We used the standard INSB photometer with apertures of 15″ and 8″ and a throw of 20″ and 15″ at the 1.0-m and 2.2-m, respectively. Standard stars were observed from the list of Bouchet et al. (1991). The reduction was done at La Silla using the reduction programme written by P. Bouchet. The results are given in Table 2.

The 3-μm spectra were obtained at the 2.2-m telescope with a Circular Variable Filter wheel. After observing a programme star, a nearby standard star was observed. We used the standard reduction technique of dividing the source spectrum by the standard star spectrum and then multiply either by the assumed blackbody temperature of the standard or the known continuum flux in case of G-dwarfs (Koornneef, 1983). Absolute calibration was achieved by adopting a K magnitude for the standard. The standard stars used with their adopted magnitudes are listed in Table 2. The calibrated spectra are shown in Figure 2.

All three stars show the characteristic carbon star feature at 3.1 μm attributed to photospheric HCN and C_2H_2 (Ridgway et al., 1978). For 11318–7256 this is not surprising since it is a known optical carbon star (C3062 in Stephenson's 1989 catalogue of carbon stars) with an IRAS LRS classification of 44. For 08074–3615 and 13477–6532 these ob-

above, available near-infrared (NIR) data were used to calculate bolometric corrections and CO data to calculate mass-loss rates. Searching in the literature we noticed that existing observations are biased against infrared carbon stars (groups IV and V). For example, NIR data existed in the literature for 14 out of the 15 group II stars, but 10 out of 48 group IV stars (~20 %) did not have NIR photometry. Likewise for the CO data. For group II stars, 13 out of 15 have been measured in either CO(1–0) or CO(2–1), for group IV this is only 29 out of 48. With regard to optical photometry the situation is even worse. Except for the well-known carbon star CW Leo none of the group IV and V stars seems to have been measured at optical wavelengths. There seems to be a misconception that infrared carbon stars (or in general infrared AGB stars) have no optical counterpart. However, several of these 'obscured' stars (usually AFGL sources) have been identified (e.g. Lebofsky and Kleinmann, 1976, Allen et al., 1977, Cohen and Kuhi, 1977).

To study the group IV and V stars in more detail we had several observing runs at La Silla in the beginning of 1991. Optical (V, R, I) photometry was obtained at the 1.5-m Danish telescope, NIR photometry at the 1.0-m and 2.2-m telescopes and CO data at the SEST.

One of the purposes of the observing runs was to confirm that some of our stars were indeed carbon stars. Many of the infrared carbon stars display the silicon carbide (SiC) feature in their LRS spectra, but some have an almost featureless LRS spectra (the group V objects) or are misclassified in the LRS atlas. Therefore, we obtained CVF spectra around 3 μm for a number of stars at

Table 1: *General parameters*

Name	l	b	S_{12}	S_{25}	S_{60}	S_{100}	C_{21}	C_{32}	LRS	VAR
08074–3615	253.5	– 1.8	156	100	26.6	6.1	–0.48	–1.44	22	9
11318–7256	297.3	–11.2	265	85.7	18.1	9.7	–1.22	–1.69	44	4
13477–6532	309.0	– 3.6	134	78.5	19.7	< 10.8	–0.58	–1.50	04	0

Table 2: *NIR photometry and spectrophotometry*

Name	J	H	K	L	M	Standard star	K-mag.
08074−3615	−	−	9.79 ± 0.02	4.51 ± 0.04	2.78 ± 0.05	HR 3842	3.39
	15.6:	13.7 ± 0.7	9.78 ± 0.05	4.57 ± 0.02	2.92 ± 0.04		
11318−7256	5.11 ± 0.04	3.12 ± 0.06	1.52 ± 0.06	−0.47 ± 0.05	−0.73 ± 0.05	HR 4523	3.32
	4.92 ± 0.02	3.00 ± 0.02	1.48 ± 0.01	−0.47 ± 0.02	−0.89 ± 0.03		
13477−6532	16.2:	10.39 ± 0.07	7.28 ± 0.03	2.91 ± 0.03	1.64 ± 0.03	HR 5459	−1.51

Note. If two entries are given, the top row refers to data from the 2.2-m telescope and the bottom row to the 1.0-m telescope. A colon indicates an uncertain value.

servations establish their carbon star nature. They have not been classified as optical carbon stars before. Their LRS classifications are 22 and 04, although visual inspection of the LRS spectrum revealed weak emission around 11 μm.

The SEST data were taken on March 24–26, 1991. We used two Schottky receivers with the wide-band AOS backend. The main beam efficiencies and HPBW (half power beam width) at 88.6 (HCN(1–0)), 115.3 (CO(1–0)) and 230.5 (CO(2–1)) GHz were 0.76 (56″), 0.71 (44″), 0.50 (23″), respectively. The velocity resolution at 115 GHz was 1.81 km/s. The CO(2–1) data were smoothened to give the same resolution. The pointing was found to be accurate within 10″. Calibration was done by a standard chopping wheel technique, switching between the sky and an ambient load. Linear baselines were subtracted. The spectra were obtained using dual beam switch mode with a throw of 11.5′. The spectra are displayed in Figure 3. The derived parameters are given in Table 3 where we list the rms noise temperature, the velocity with respect to the local standard of rest, the expansion velocity as measured as half the full width at zero intensity, the peak temperature and the integrated intensity under the line. The velocities are in km/s and the temperatures are in K expressed as main beam temperatures.

IRAS 08074−3615 was detected at CO(1–0) by Zuckerman and Dyck (1986). Their peak temperature of 0.20 K compares well to our value. They quote an expansion velocity of 17.3 km/s which is smaller than ours. They did not publish the spectrum so we cannot comment on the difference. The HCN (1–0) transition was detected by Lucas et al. (1988) with an intensity of 9.2 K km/s. Again, no spectrum was published. IRAS 11318−7256 was independently detected recently by Nyman et al. (1991) in CO(1–0) with a peak temperature (0.17 K) and intensity (7 K km/s) which are very similar to our values. Our measurements of CO(2–1) and HCN(1–0) in 11318−7256 and CO(1–0), CO(2–1) and HCN(1–0) in 13477−6532 are all new detections.
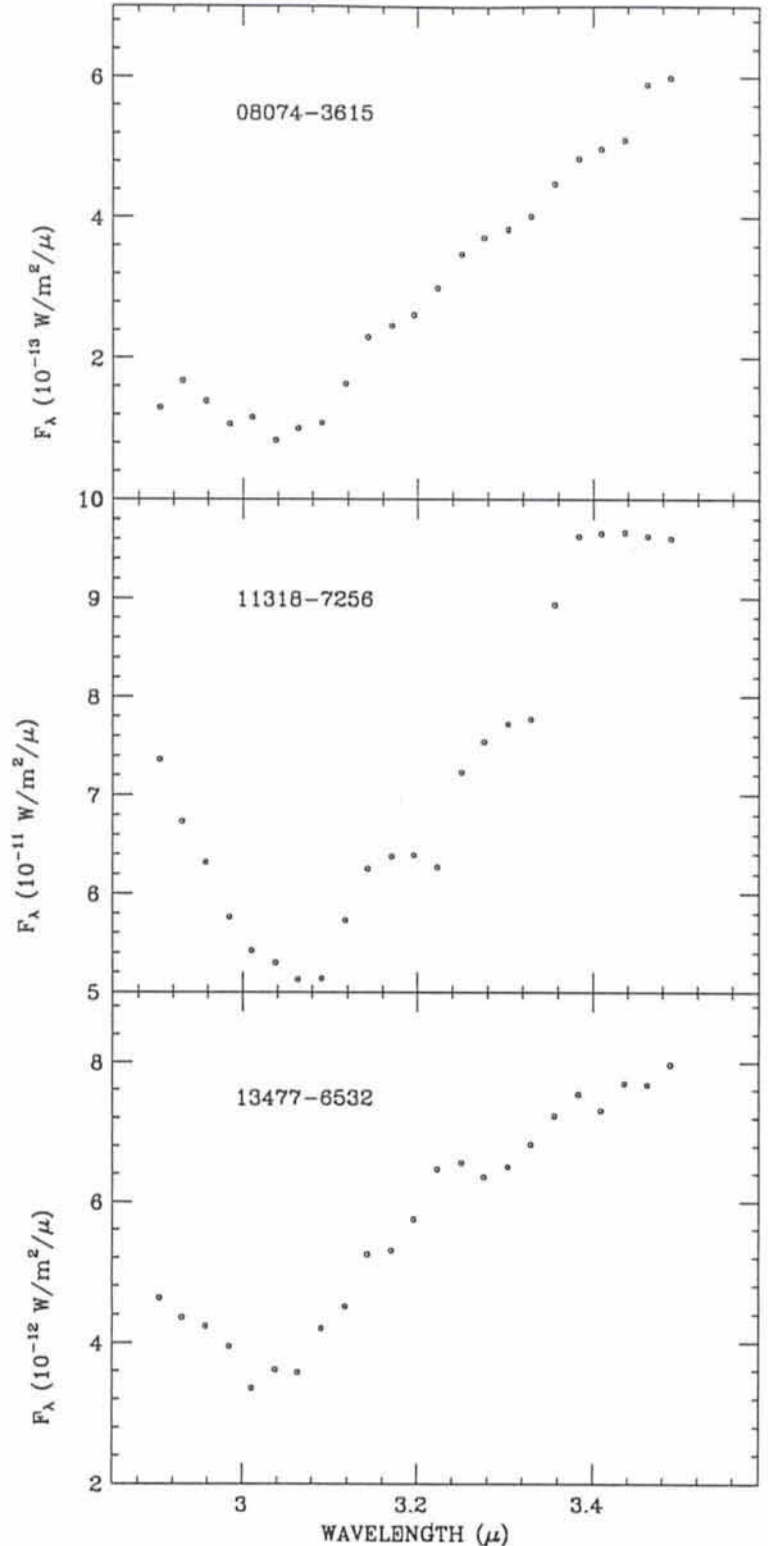

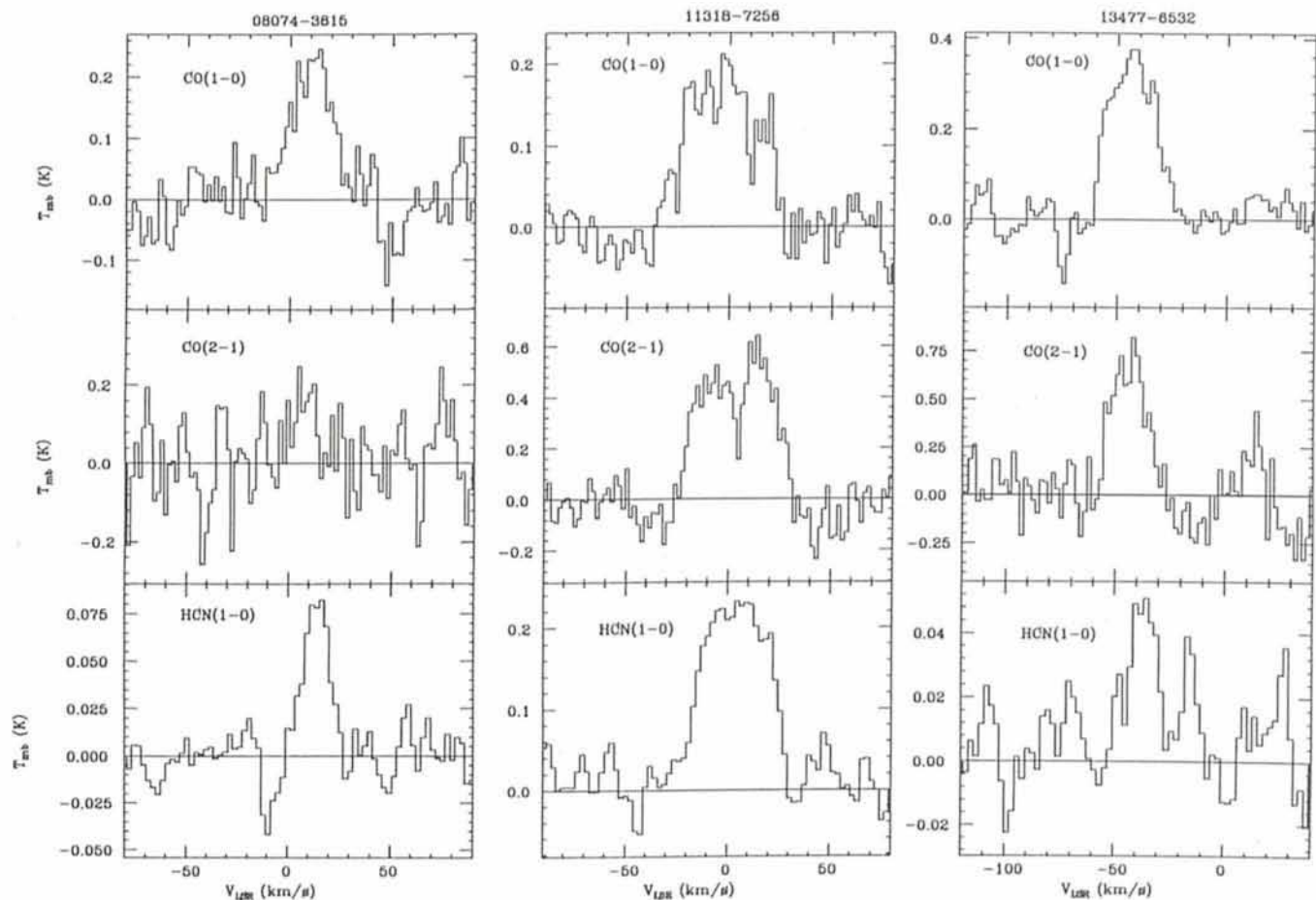Figure 2: *The 3-μm CVF spectra of the three stars discussed here.*

Figure 3: *The CO(1-0), CO(2-1) and HCN(1-0) data.*

3. The Analysis

The NIR and CO data are used to determine bolometric corrections and mass-loss rates in a way identical to Groenewegen et al. (1991) to which we refer for details.

Distances were determined from the observed bolometric flux using $M_{bol}=-4.9$ (L=7050 $L_\odot$), the mean value observed for carbon stars in the LMC (Frogel et al., 1980).

Near-infrared colour temperatures were derived by fitting a blackbody to the J, H, K, L, M magnitudes. Mass-loss rates were determined from the CO line profiles as discussed by Groenewegen et al. The results are displayed in Table 4 where we list near-infrared colour temperature, total observed flux at earth, bolometric corrections with respect to the colour-corrected IRAS 12 µm magnitude (BC_{12}), the distance in kpc and the mass-loss rate. These values supercede the data listed for these stars in Tables 2 and 5 of Groenewegen et al. Note however that due to the radiative transfer modelling discussed below and the numerical uncertainty in calculating the observed flux at earth, the final values for these quantities are different.

4. A Radiative Transfer Model

Combining the NIR data with the IRAS data, we have observations of the most important part of the spectral energy distribution (SED). Since these stars are fairly red, their energy output in the optical is insignificant. In this section we present the results of radiative transfer calculations attempted to fit the observed SED as well as the LRS spectrum.

We used the model of Groenewegen and de Jong (1992). This model allows for time-dependent mass-loss rates and radius-dependent velocity laws. In the calculations presented below we restrict ourselves to simple r^{-2} density laws unless otherwise mentioned. The programme simultaneously solves the radiative transfer equation and the thermal balance equation for the dust. The inner radius is determined by the model to equal the adopted dust temperature at the inner radius, which is an input parameter. The outer radius is determined from the condition that the dust temperature at the outer radius is 20 K. Other input parameters are the expansion velocity of the circumstellar shell and the mass-loss rate, both assumed for the moment to be constant, the absorption coefficient Q which is assumed to be a mix of AC amorphous carbon

Table 3: *CO and HCN data*

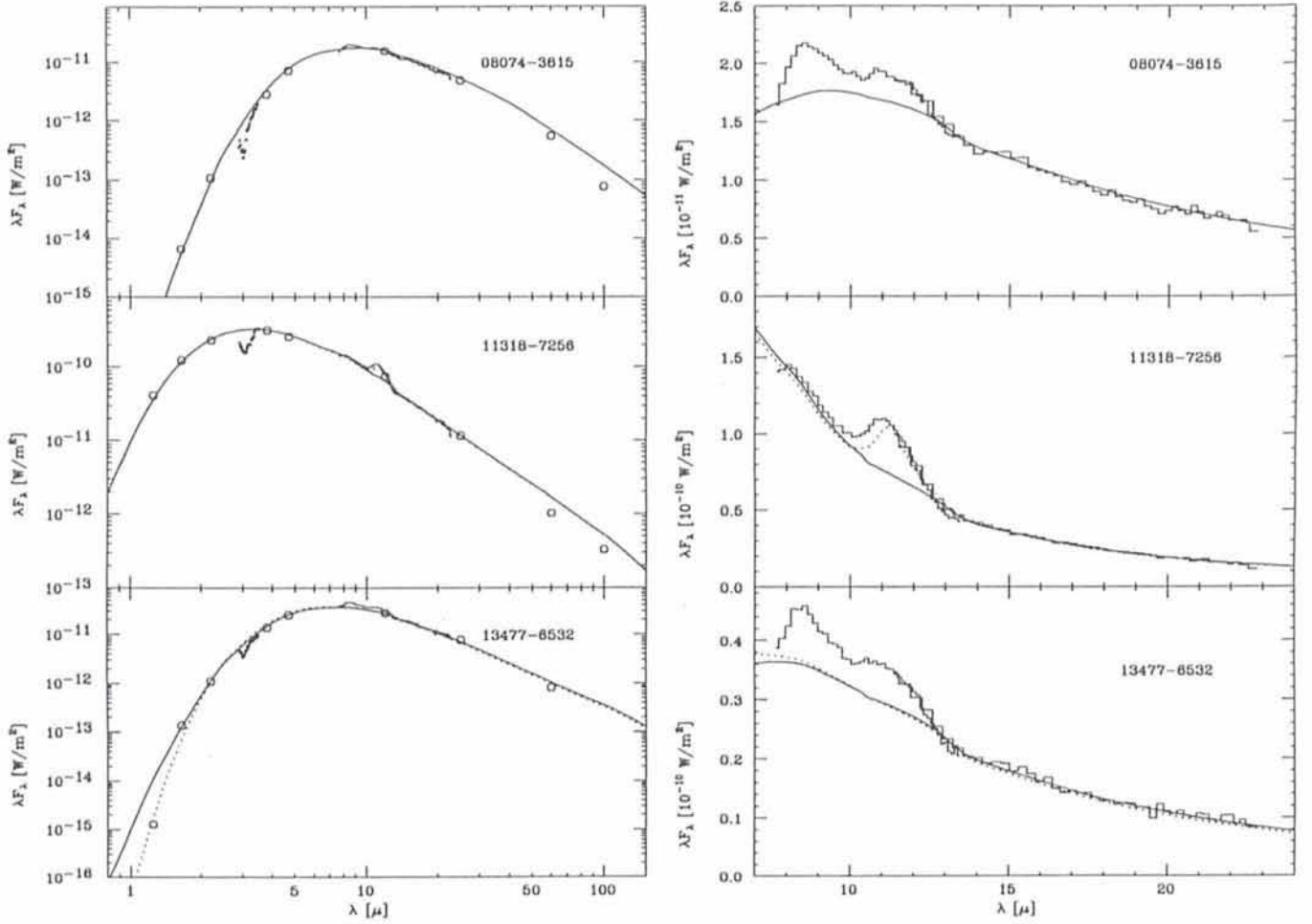| Name	Transition	T_{rms}	V_{LSR}	V_{exp}	T_{peak} (K)	I (K km/s)
08074-3615	CO(1-0)	0.042	10	21	0.24	5.6 ±0.2
	CO(2-1)	0.11	–	–	–	<4.8[a]
	HCN(1-0)	0.012	14	~18	0.080	1.26±0.03
11318-7256	CO(1-0)	0.028	– 6	32	0.18	7.2 ±0.7
	CO(2-1)	0.082	2	28	0.52	21 ±1.0
	HCN(1-0)	0.025	5	28	0.22	8.9 ±0.8
13477-6532	CO(1-0)	0.042	–43	19	0.36	9.9 ±0.3
	CO(2-1)	0.14	–44	15	0.70	14.6 ±1.0
	HCN(1-0)	0.012	~–40	–	0.048	0.9 ±0.1

Note. Derived from $V_{exp} T_{rms}$.

Figure 4: *Observed and predicted spectral energy distributions and LRS spectra. For details of the model parameters see text.*

(Bussoletti et al., 1987[1]) and SiC (Pegourie 1988) and the dust-to-gas ratio ψ which will be the main independent variable. Minor input parameters are the grain size a, assumed to be $0.03\,\mu$ and the grain density ϱ, assumed to be $3.3\ g/cm^3$. The shape of the spectrum, for a fixed temperature at the inner radius, is solely determined by the optical depth at some reference wavelength.

$$\tau \sim \frac{\dot{M}\ \Psi\ Q/a}{R_*\ r_{in}\ v_\infty\ \rho}$$

The temperature of the central star was assumed to be 2500 K. This choice is not critical as long as most of the radiation is reemitted in the infrared. The stellar radius was fixed at 447 $R_\odot$.

Because the IRAS sources are variable with unknown periods, the NIR and IRAS data cannot be expected to have been taken at the same phase. Therefore we proceeded in the following way. The optical depth τ was changed in such a way as to fit the NIR data. Then the 25-μm flux was scaled to fit the

model prediction. The same scale factor was applied to the other IRAS fluxes. This is justified because the predicted C_{21}, C_{32} and C_{43} colours hardly depend on the optical depth and their variation is much less than the error in the observed colours due to the uncertainty in the IRAS fluxes. The LRS spectrum was scaled in such a way that the long wavelength part $(\lambda > 18\,\mu)$ fitted the model. It proved necessary to correct the observed IRAS fluxes of 08074–3615, 11318–7256, 13477–6532 by –55 %, +13 % and –17 %, respectively. The largest correction is necessary for the IRAS source with the highest variability flag. Because a change in the IRAS fluxes changes the integrated flux at earth and therefore the distance (for a fixed luminosity) and mass-loss rate we recalculated both quantities. The final values are d=3.04 kpc, $\dot{M} = 5.6\ 10^{-5}\ M_\odot/yr$ (08074–3615);

d = 0.70, $\dot{M} = 4.90\ 10^{-6}$ (11318–7256) and d = 2.07, $\dot{M} = 3.3\ 10^{-5}$ (13477–6532).

The results of some radiative calculations are gathered in Figure 4 where in the left panel the observed NIR magnitudes, the 3 μm spectrum, the IRAS data and the LRS spectrum is plotted together with the model fits and in the right panel the observed LRS spectrum and the fits (the full lines) and it should be noted that we did not attempt to fit the 3-μm spectrum.

The parameters of the models are collected in Table 5, where the assumed mass percentage of SiC and the assumed temperature at the inner radius are listed. Derived parameters are the inner and outer radius (in stellar radii), the optical depth at 0.5 μm and the dust-to-gas ratio.

In the case of 11318–7256 we also calculated models with lower values of

Table 4: *Some derived parameters*

Name	T_{nir} (K)	F (10^{-10} W/m²)	BC_{12}	D (kpc)	$\dot{M}$ ($M_\odot$/year)
08074–3615	490	0.54	8.53	2.0	2.5 (-5)
11318–7256	1294	5.63	6.54	0.63	3.9 (-6)
13477–6532	566	0.66	8.14	1.85	1.6 (-5)

[1] Actually we multiplied the Q-values of Bussoletti et al. by a factor of 5 to let their results agree with those of Koike et al. 1980.
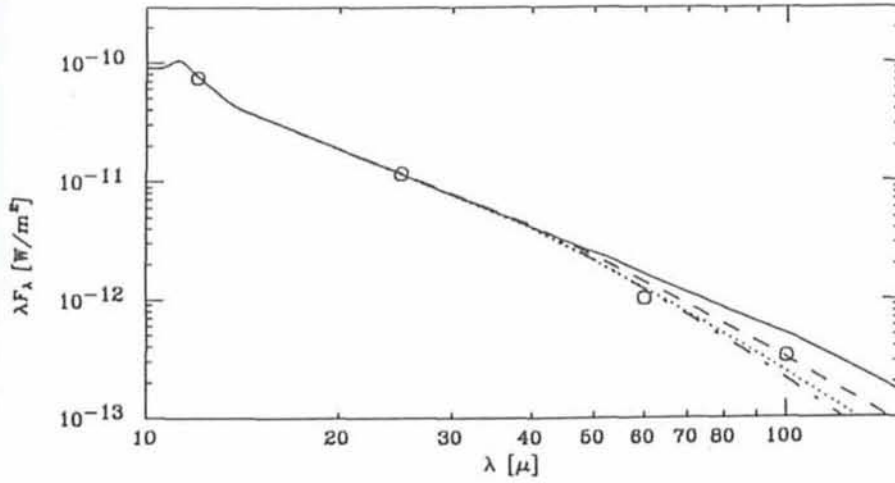
Figure 5: *The long-wavelength part of the spectrum of 11318-7256 for the standard model (solid line) and for models with reduced absorptivity (dashed line), variable mass loss (dotted line) and smaller outer radius (dot-dashed line).*

T_{inner}. Only values >1300 K give good fits. A mixture of 40 % SiC and 60 % amorphous carbon can explain the feature at 11.3 μm fairly well.

For 08074-3615 and 13477-6532 only pure amorphous carbon models are shown because we could not get a satisfactory fit of the broad feature between 10 and 12.5 μm with the SiC of Pegourie. Furthermore, there is evidence in both stars for emission between 7.5 and 10 μm.

5. Discussion

We presented NIR photometry, spectrophotometry and CO/HCN data for three carbon stars from the infrared-complete carbon star sample of Groenewegen et al. (1991). Assuming a mean luminosity of 7050 $L_{\odot}$ we derive distances and mass-loss rates. Using a radiative transfer model we derive dust-to-gas ratios of $\Psi \approx 0.0007$ ($\approx 1/1600$). The main uncertainty in this value is the absolute value of the absorptivity. When the mass-loss rates are calculated from CO data (i.e. $\dot{M} \sim D^2$) and for fixed effective temperatures, Ψ scales with $\sim D^{-1}$ or $\sim L^{0.5}$, so the assumed luminosity is not a major source of uncertainty. The dust-to-gas ratio we derive is a factor of 2 lower than usually quoted (0.0013 for our value of $\kappa(60\,\mu) = 520$ cm^2 g^{-1}, Jura 1986) but recently Sahai (1990), using a self-consistent CO model for U Cam finds $\Psi \leq 0.00015$. Analysis of other carbon stars also indicate low dust-to-gas ratios (Sahai, 1991).

With regard to the broad-band features in the LRS spectrum we showed that in the case of the optically visible group III star 11318-7256 a satisfactory fit could be obtained with a mixture of 40 % SiC and 60 % amorphous carbon. In the case of the two infrared carbon stars of group IV there

seem to be two broad features: one between 7.5 and 10 μm and the other between 10 and 12.5 μm. The latter feature seems to be too broad to be explained in terms of SiC.

The feature between 7.5 and 10 μm, peaking at 8.6 μm is most puzzling. Willems (1988) discovered an unidentified feature at 8.6 μm in the spectra of group II stars. He did not find it in group III stars (consistent with 11318-7256), which have thicker circumstellar shells. Now we find a feature at 8.6 μm in group IV stars, with even thicker shells. Is this feature (see also Baron et al., 1987) related to the feature in group II stars?

In all three cases our model predicts too much flux at 60 and 100 μm. We consider four possibilities: (1) the envelope is resolved by the IRAS beam, (2) the outer radius is smaller, (3) a steeper emissivity law and (4) a lower mass-loss rate in the past.

The 100-μm emission comes mainly from the region with dust temperatures ~30 K which is at about 21,000 stellar radii corresponding to 60″ diameter at a distance of 0.7 kpc. The IRAS beam at 100 μm was roughly 100″ so the shell is probably not resolved.

To investigate the other possibilities we calculated three additional models for 11318-7256 with (a) a smaller outer radius ($r_{outer} = 5000$ R∗; the dot-dashed line in Fig. 5), (b) an emissivity law Qλ $\sim \lambda^{-1.5}$ for λ >40 μm (dashed line) and (c) a mass-loss rate which increased by

a factor 2 over the past 3300 years (dotted line). One cannot distinguish between these three possibilities on the basis of the fits in Figure 5. It has been advocated that the detection of HCN emission is a sufficient criterium to identify optically invisible carbon stars. However, oxygen-rich stars have also been detected in HCN. From Lindqvist et al. (1988) we derive that the mean of the ratio I(HCN)/I(CO(1-0)) in their 10 oxygen-rich stars with detected HCN is 0.12 and the maximum value observed is 0.26. The same ratio in our stars is 0.23, 1.24 and 0.09 respectively. This means that solely on the basis of HCN emission, in 2 out of 3 cases the confirmation as carbon stars could not have been made. We suggest that the presence of the 3.1 μm feature is a more suitable carbon star identification mark than the HCN/CO ratio.

References

Allen D.A., Hyland A.R., Longmore A.J., Caswell J.L., Goss W.M., Haynes R.F., 1977 *Ap.J.* **217**, 108.

Baron Y., de Muizon M., Papoular P., Pegourié B., 1987, *Astron. Astrophys.*

Bouchet P., Manfroid J., Schmider F.-X., 1991, ESO preprint 748.

Bussoletti E., Colangeli L., Borghesi A., Orofini V., 1987, *Astron. Astrophys. Suppl.* **70**, 257.

Cohen M., Kuhi L.V., 1977, *PASP* **89**, 829.

Frogel J.A., Persson S.E., Cohen J.G., 1980, *Ap.J.* **239**, 495.

Groenewegen M.A.T., de Jong T., van der Bliek N.S., Slijkhuis S., Willems F.J., 1991, *Astron. Astrophys.* in press.

Groenewegen M.A.T., de Jong T., 1992, in preparation.

Jura M., 1986, *Ap.J.* **303**, 327.

Koike C., Hasegawa H., Manabe A., 1980, *Ap.&SS* **67**, 495.

Koornneef J., 1983, *Astron. Astrophys.* **128**, 84.

Lebofsky M.J., Kleinmann S.G., 1976, *A.J.* **81**, 534.

Lindqvist M., Nyman L.A., Olofsson H., Winnberg A., 1988, *Astron. Astrophys.* **205**, L15.

Table 5: *Radiative transfer model parameters*

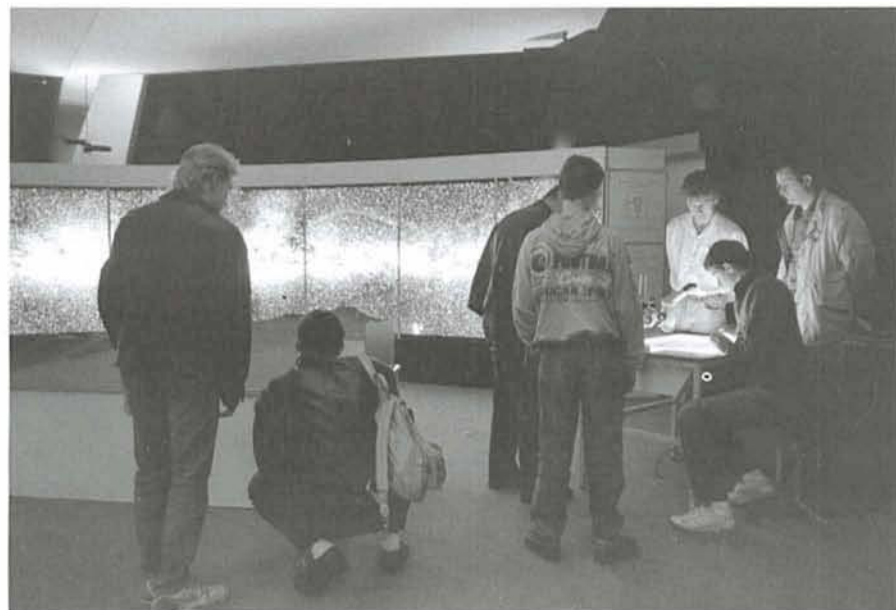| Name	In Figure 4	Percentage SiC	T_{inner} (K)	r_{inner} (R∗)	r_{outer} (R∗)	$\tau_{0.5}$	Ψ
08074-3615	solid line	0	900	9.67	53200	28.8	0.00086
11318-7256	solid line	0	1800	1.68	50400	7.62	0.00065
	dotted line	40	1800	1.68	55400	8.01	0.00104
13477-7256	solid line	0	1000	7.20	36000	20.7	0.00072
	dotted line	0	1300	4.42	35400	28.0	0.00060

Lucas R., Guilloteau S., Omont A., 1988, *Astron. Astrophys.* **194**, 230.

Nyman L.A., Booth R.S., Carlstrom U., Habing H.J., Heske A., Omont A., Sahai R., Stark R., van der Veen W.E.C.J., Winnberg A., 1991, *Astron. Astrophys. Suppl.* in press.

Pegourié B., 1988, *Astron. Astrophys.* **194**, 335.

Ridgway S.T., Carbon D.F., Hall D.N., 1978, *Ap.J.* **225**, 138.

Sahai R., 1990, *Ap.J.* **362**, 652.

Sahai R., 1991, in preparation.

Stephenson C.B., 1989, Pub. Warner and Swasey Obs., vol. 3, no. 2.

Van der Veen W.E.C.J., Olofsson H., 1990, *From Miras to Planetary Nebulae*, eds. M.O. Mennessier, A. Omont, Editions Frontières, Gif-sur-Yvette, p. 139.

Willems F.J., 1988, *Astron. Astrophys*, **203**, 51.

Willems F.J., de Jong T., 1988 *Astron. Astrophys.* **196**, 173.

Zuckerman B., Dyck H.M., 1986, *Ap.J.* **311**, 345.

Open House at ESO

On Saturday, October 12, 1991, ESO Headquarters in Garching again opened its doors to the public. More than 2000 persons took the opportunity to visit the organization and learn about science and technology at our organization; this corresponded to 1 person every 10 seconds. There was a lot of interest and curiosity, especially about the VLT and the Hubble Space Telescope, the latter being presented by the ESA/ESO Space Telescope European Coordinating Facility, installed at ESO HQ. Visitors of all ages could choose among various attractions; they saw some of the ESO video films, were introduced to the virtues of large CCDs, admired the rear-lighted Milky Way panorama and finally filled out the "Star-Quiz" to participate in the lottery with ESO books and posters as main prizes.

About 20 ESO staff members took part in the preparations for this event and were present during seven hectic hours to guide the many visitors. There was a continuous, very lively interaction and by the end of this long day, the good result lit quite a few smiles on otherwise worn-out faces.

Astronomy from Large Databases II

Strasbourg Observatory – 14–16 September 1992

A follow-up event to the 1987 conference on "Astronomy from Large Databases" (Eds. F. Murtagh and A. Heck, ESO Conf. and Workshop Proc. 28) is timely. The area has seen much progress. "Astronomy from large Databases II" will allow archival research results from various experiments to be reviewed.

Much has happened in the area of astronomical databases in recent years. HST is in full operation; some such as EXOSAT have stopped growing and now function for retrieval purposes only; NED has come into being; etc. Hundreds, or even thousands, of papers have been based on data retrieved from archives. Archived material from various sources is increasingly combined with data obtained through joint observational campaigns involving ground-based and space-borne experiments working in different wavelength ranges.

Technically databases have evolved. SIMBAD 3.0 is fully operational. User interfaces now include windows and point-and-click access mechanisms, hypertext and hypermedia. Commercial products have considerably improved. Distributed databases are now highly relevant, pointing to the important role of networks. CD-ROMs and other storage media are more and more widely used. The 1987 conference predates the births of ESIS and ADS, among many other developments.

Scientific Organizing Committee:

M.F. A'Hearn (University of Maryland, College Park); P. Benvenuti (ST-ECF, Garching); R. Bonnet (ESA, Paris); M. Crézé (Strasbourg Observatory) (Chairman); R. Giacconi (STScI, Baltimore); B. Hauck (Institut d'Astronomie, Lausanne) A. Heck (Strasbourg Observatory) (Proceedings Editor); G. Helou (IPAC, Pasadena); F. Murtagh (ST-ECF, Garching) (Proceedings Editor); S. Nishimura (NAOJ, Tokyo); G. Riegler (NASA, Washington); P. Giommi (ESRIN, Frascati); M. Strickman (NRL, Washington); P.A. Vanden Bout (NRAO, Charlottesville); H. van der Laan (ESO, Garching); and H.-U. Zimmermann (MPE, Garching).

The Proceedings will be published by the European Southern Observatory.

Contact addresses:

André Heck, Observatoire Astronomique, 11 Rue de l'Université, F-67000 Strasbourg, France. Tel.: + 33 88 35 82 22; Fax: + 33 88 25 01 60; E-mail: heck@frccsc21.bitnet, heck@ccsmvs.u-strasbg.fr; or
Fionn Murtagh, Space Telescope – European Coordinating Facility, European Southern Observatory. Tel.: + 49 89 32 00 62 98; Fax: + 49 89 32 00 64 80; E-mail: fmurtagh@eso.org, murtagh@scivax.stsci.edu.

Surface Imaging of W Ursae Majoris Contact Binaries

C. MACERONI[1], F. VAN 'T VEER[2], O. VILHU[3]

[1]Osservatorio Astronomico di Roma, Italy;
[2]Institut d'Astrophysique de Paris, CNRS, France;
[3]Observatory and Astrophysics Laboratory, University of Helsinki, Finland

1. Introduction

The W UMa type binaries are contact systems formed by two solar type components and are probably the most enigmatic group among close interacting binaries.

The eclipsing W UMa systems show a light curve with minima of about the same depth, therefore the effective temperatures of the two components should be almost the same, in spite of the fact that they always are dwarf stars of different mass. The difference $\Delta T_e = T_{e,1} - T_{e,2}$, the index 1 indicating the primary (i.e. the more massive) component, is not more than some hundred degrees, even for mass ratios of only some tenths, and it can even be negative, with a smaller component hotter than the more massive one (again by some hundred degrees). The physical explanation of these well-established small temperature differences is one of the challenges, until now without a completely satisfactory answer, of close binary astrophysics. Binnendijk was probably the first to realize this paradoxical situation and we may call this unexplained but well-known property the *Binnendijk paradox*.

This peculiar temperature difference, which is certainly related to the production and to the transfer of energy between the two components, is not the only enigma of W UMa binaries. Already in the forties Kuiper (1941) pointed out that contact binaries filling the inner Roche lobe should have a ratio of the volumes determined by the Roche geometry. This predicts, in a very large range of mass ratios, $V_2/V_1 = q^{1.35}$. On the other hand the ZAMS relation requires $V_2/V_1 = q^\alpha$ with $\alpha = 2.0 \pm 0.1$. The two relations can be simultaneously fulfilled only for $q = 1$, but all the known W UMa systems have mass ratios smaller than one. This is the so-called *Kuiper paradox*.

Both paradoxes teach us that the components of W UMa binaries have temperatures and radii that strongly deviate from the predictions for single stars evolving between ZAMS and TAMS, at least for one of the components.

The difficulties in formulating a consistent scenario are enormous: for instance the solution of the Binnendijk paradox requires the modelling of the energy transfer through a thin common envelope. This cannot be performed without taking into account strong Coriolis forces and unknown magnetic fields between tidally interacting components.

The problem deriving from the Roche lobe filling of the two components, which is confirmed by the light-curve solutions obtained by means of the Wilson-Devinney procedure (see next section), is also without clear solutions. The major difficulty is, in this case, to predict how the volumes of the two stars will react in the case of mass transfer. This mass transfer is a direct consequence of the angular momentum loss experienced by the system by virtue of magnetically trapped ionized stellar winds and controlled by the dynamo of the convective zone. The angular momentum loss mechanism, first formulated by Schatzman (1962) for solar-type single stars, is also a fundamental ingredient in the process leading to the formation of solar-type contact binaries from detached systems. By virtue of spin-orbit coupling, in fact, it will produce a shrinking of the orbit and finally transform the
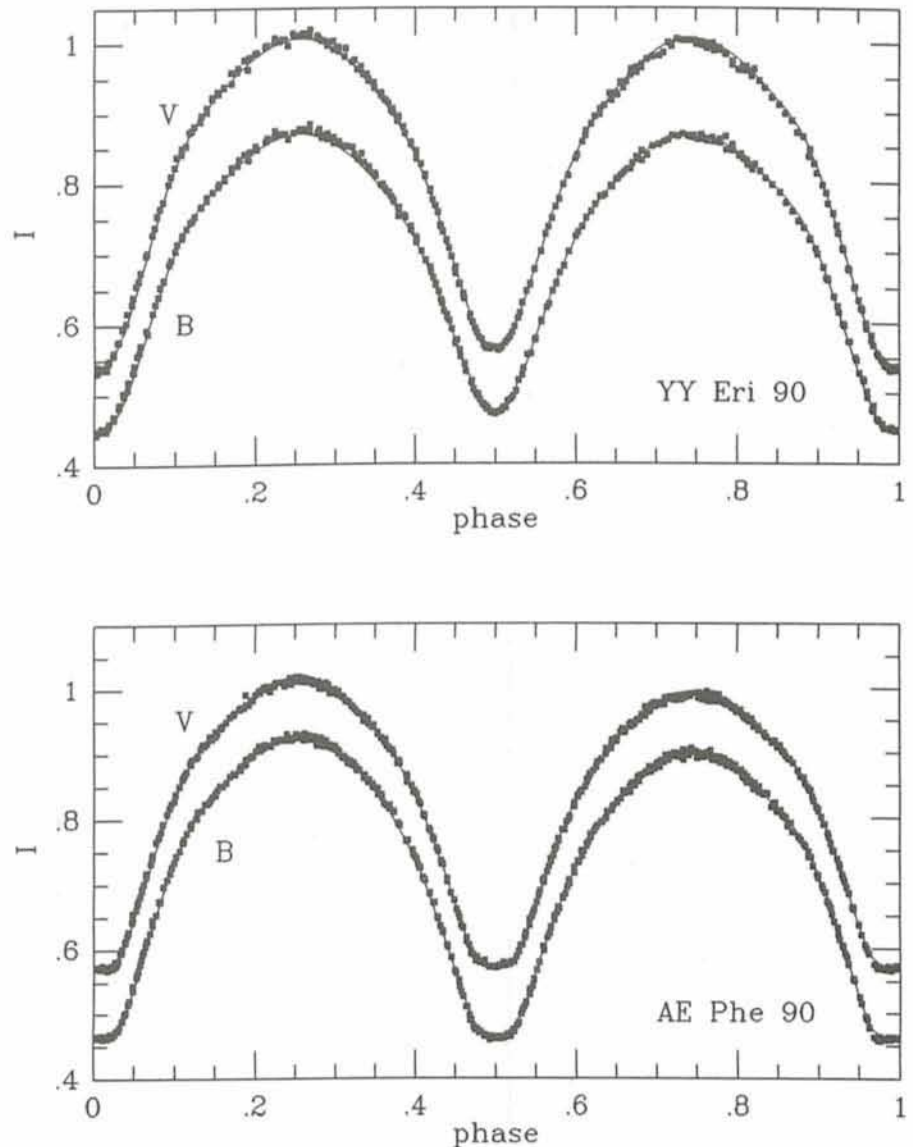

Figure 1: B and V light curves of YY Eri and AE Phe. The continuous lines (often hidden by the observed points) are the light-curve solutions.
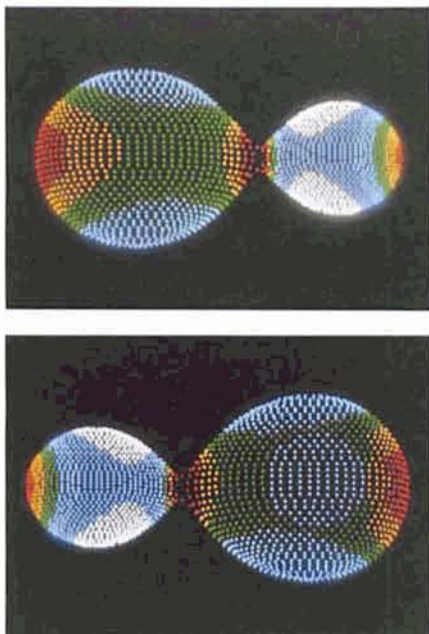
Figure 2(a): *Effective temperature distribution, from the light-curve solution, for the surface of AE Phe visible at phase 0.25. Effective temperature goes from 5020 to 6130 K. The colour scale is shown in Figure 3.* (b) *Effective temperature distribution of AE Phe at phase 0.75.*

Figure 3: *Effective temperature distribution from the light-curve solution of YY Eri at phase 0.25 (the same, in this case, as the distribution at phase 0.75). Effective temperature goes from 5050 to 5630 K. The colour scale goes from dark red to white with increasing T_e.*

and mass exchange producing hot spots) and those of magnetic activity. The best way to solve the problem is a Doppler Imaging analysis of high-dispersion spectra which yields a brightness surface map of the system. This is the reason why we proposed a programme of simultaneous spectroscopic and photometric observations of two suitable southern W UMa systems, AE Phe and YY Eri. The programme, the method of data analysis and the (provisional) results are described in the following sections.

2. The Observations

2.1 The photometry

We had six observing nights in November 1989 and seven more one year later. The stars were simultaneously observed with the CAT telescope, equipped with the CES spectrograph, short camera and CCD and with the ESO 50-cm telescope (with its single-channel photometer, the EMI 9789Q photomultiplier and the standard B, V filters). Unfortunately in the 1989 season three nights out of six were non-photometric, AE Phe was observed for two nights and YY Eri only for one. As a consequence we got only incomplete light curves. The 1990 season, however, was completely successful: we had 100% of photometric nights.

The first thing we found out was that the primary minima were in both cases delayed by about half an hour with respect to the ephemerides given by Gronbeck (1976, for AE Phe) and Breger (1981, for YY Eri). This means a phase shift of respectively 0.060 and 0.077. The fact is not surprising given the shortness of the periods (both around 0.3 days) and the long time passed since the last ephemerides.

From the individual observations, (Fig. 1) we derived the mean point light curves which were solved by means of the Wilson and Devinney code, in the last standard distributed version (Wilson, 1979) which includes a partial treatment of dark/hot spots.

The code uses a physical model of the contact binary based on the Roche lobe configuration. The surface brightness distribution of the common envelope deviates from a uniform distribution because of gravity darkening effect (von Zeipel, 1929; Lucy, 1968), which makes the poles brighter than the back and the equators of the components, and because of the mutual reflection of the irradiated light (brightening the facing hemispheres). The model is used to compute a theoretical light curve as function of a number of physical parameters: the wavelength, the mass ratio,
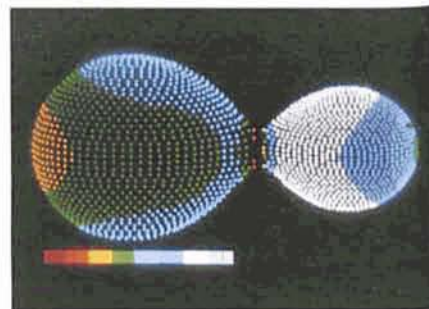
detached system into a contact binary (Van 't Veer, 1975; Vilhu, 1982).

There is no doubt about the presence of even strong magnetic fields in these stars: we have direct evidence from the light curve perturbations, which are attributed to dark or hot spots, and from indirect clues, i.e. the excited chromospheres and coronae.

In principle dark spots on the surface of the primary component can explain the inversion of the temperature difference, but this type of model would require the permanent presence of extended dark spots on the back hemisphere of the primary, a thesis difficult to support. However, we know that bright and/or dark spots with shorter lifetimes (say, ~ some years) are present from the perturbations of the light curves. All W UMa binaries that have been observed for some years show light-curve variations. These can cover every phase domain, but they are best visible during the maxima and minima and may consist of a change of height and depth of these extremes. It is also possible that the phase of one or more of these extremes is shifted.

Even if the signatures of surface inhomogeneities clearly appear in the light curves, the photometry alone cannot unambiguously determine the type of the perturbations (hot or dark), and their location, so that one cannot distinguish between the effects of the interaction between the two components (energy

the inclination, the filling factor (which express the degree of filling of the space between the internal and external Roche critical surfaces), the difference between the effective temperatures, the luminosity ratio and, finally, three coefficients taking into account the limb darkening, the gravity darkening and the reflection effect.

An elementary linearized least square algorithm, with derivatives computed by finite differences approximation, provides the differential corrections to a starting set of adjustable parameters. By means of an iterative procedure the method converges to the best set of parameters, i.e. what is commonly called the light-curve solution. This numerical procedure is often hindered by strong correlations among the adjustable parameters, which demands a decrease of their number, by using theoretical or estimated values (this is often the case for the values of the gravity darkening, the limb darkening and the reflection coefficients), and the use of the method of subsets (Wilson and Biermann, 1976).

The WD code is in general successful in finding morphologically excellent and physically meaningful solutions (one should perhaps mention that the most common difficulty with it is the non-unicity, at least with respect to some parameters, and not the lack of solutions). This is true at least as long as the curves do not show perturbations asymmetric with respect to the minima. In the last case it is still possible to model the common envelope introducing hot or dark spots, even if, for reasons connected to the determinacy of the solutions, the spot parameters are not adjusted. However, in spite of this constraint, the solution with spots is very often non unique: the photometry alone does not contain enough information to discriminate between a hot spot

of given location and size and a dark spot elsewhere (see for instance Maceroni, Van 't Veer and Van Hamme, 1990. Maceroni and Van 't Veer, 1990). A long continuous series of (multi-wavelength) observations of the same system can help to overcome the problem, but repeated homogeneous observations are not available for most of the known systems. This explains the importance of using simultaneously the photometry and the high-dispersion spectroscopy, which yields independent information about the location of the perturbed regions.

Figures 2 and 3 show the geometrical configuration corresponding to the simultaneous (in B and V) solutions of Figure 1, together with the spot location and the effective temperature distribution. Both systems show asymmetric perturbations of the light curves; the most evident feature of this effect is that the maximum following primary minimum (max I) is brighter than the other (max II).

In the case of AE Phe we modelled this feature by means of a hotter spotted region reaching maximum visibility at phase 0.25. This choice was suggested by the first indications from the spectroscopic data reduction, showing the presence of extra emission in H_α at max I.

With a similar procedure we have found the solution of YY Eri. In its case we find a region of enhanced brightness on the connecting neck.

2.2 The high-dispersion spectroscopy

The Doppler Imaging method is based on the fact that a dark starspot produces a bright bump in a rotationally broadened absorption line profile. This can be intuitively understood considering what happens to the line profile if we insert a completely dark (and small) spot on the surface of a rotating star. The effect will be the disappearance of the contribution of the now darkened region from the profile. This consists of a narrow absorption feature, displaced from the line centre by the roation, and of a contribution to the continuum at all the other wavelengths of the broadened line. The final algebra gives that at the wavelengths corresponding to the velocity shift of the spot the flux decreases less than at the others, thus producing the bright bump. During a stellar rotation the bump moves across the profile in a way connected to the position on the surface. It is therefore clear that one can, in principle, extract information on the surface brightness distribution from a set of Doppler-broadened profiles taken at different phases.
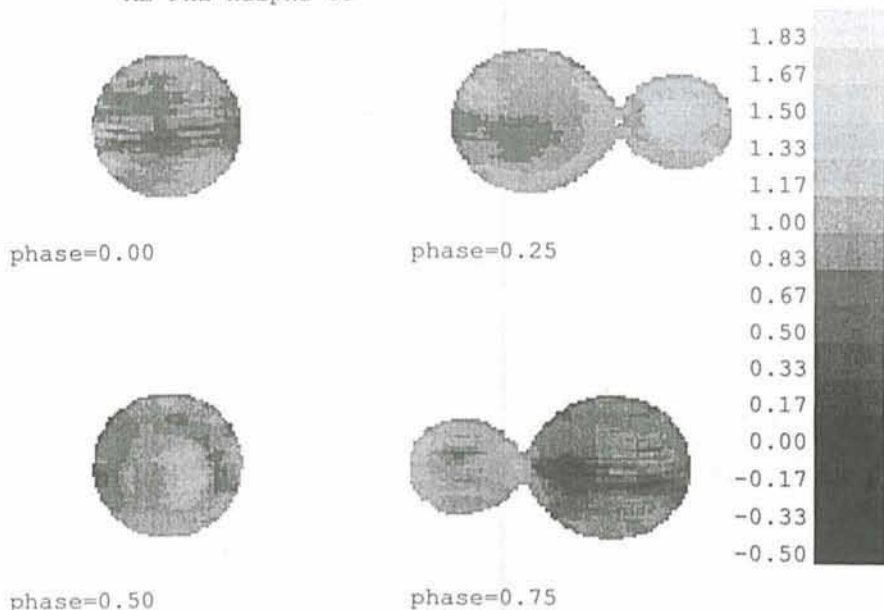
AE PHE Halpha 89

Figure 4: *Doppler images of AE Phe. The mapped quantity, S, is the scale factor of the solar H_α equivalent width (see text). S = 0 means that no line is present, S < 0 means emission line. Qualitatively the relation with the temperature is in the sense that dark areas correspond to lower T_e.*

In practice, however, the "inverse problem" of reconstructing a brightness surface map from the profiles is rather difficult, being an "ill-posed" problem. This means that one can find many spot distributions producing the same effect on the line profiles. As a consequence one has to apply further constraints (usually in the form of a regularizing function which chooses the simplest of all possible maps). A detailed description of the method can be found in Vogt and Penrod (1983) and in Piskunow, Tuominen and Vilhu (1990).

The application of the Doppler imaging technique to contact binaries is not at all straightforward. First of all, severe constraints limit the observable sample. The most serious difficulty arises from the short periods (and hence high rotational velocities) coupled to low luminosities of these systems. The exposure times should be a compromise between the need of high S/N ratio, necessary to resolve weak features in a heavily broadened profile, and that of covering no more than 0.05 in phase (which means exposures shorter than 20 minutes). With CAT telescope and CES spectrograph at a resolution of about 60,000 we were obliged to select relatively bright systems ($m_v \sim 8$) and strong lines: the Balmer H_α line at 6563 Å and the Sodium D1 and D2 at 5890/95 Å. The disadvantage of the strong lines, compared to the weak Fe lines commonly used in Doppler imaging, is that their interpretation is more difficult, because of contamination by the chromospheric layers. However,

they are also sensitive to photospheric spots and one should also say that enhanced chromospheres are probably connected with spots.

Additional difficulties are due to the fact the modelling of a contact system is much more difficult than that of a single star (or a detached binary): the unperturbed photosphere (i.e. without spots) is not uniformly bright and, moreover, one has to take into account the surface shape and the corresponding radial velocity distributions.

The surface images of Figures 4 and 5 are the preliminary results of the analysis of the H_α profiles. In the first step of the treatment we assumed that the H_α equivalent width, W, could be expressed as $W = S*W_\odot$, being $W_\odot$ the solar value and S only function of the position on the surface. Furthermore, we also assumed that the profile shape is the same as that of the sun, being again simply scaled by a factor S. This is only a first-order approximation, the next step will be the computation of the local line profile by means of model atmospheres.

The local profiles were broadened and weighted using the local radial velocities and outgoing fluxes in the observer direction computed by means of the WD code.

The maps of Figures 4 and 5 show with different grey tones the resulting S distribution. The transformation of the S scale into a temperature scale, directly comparable with Figures 2 and 3, requires the dependence of W on the effective temperature and gravity, and
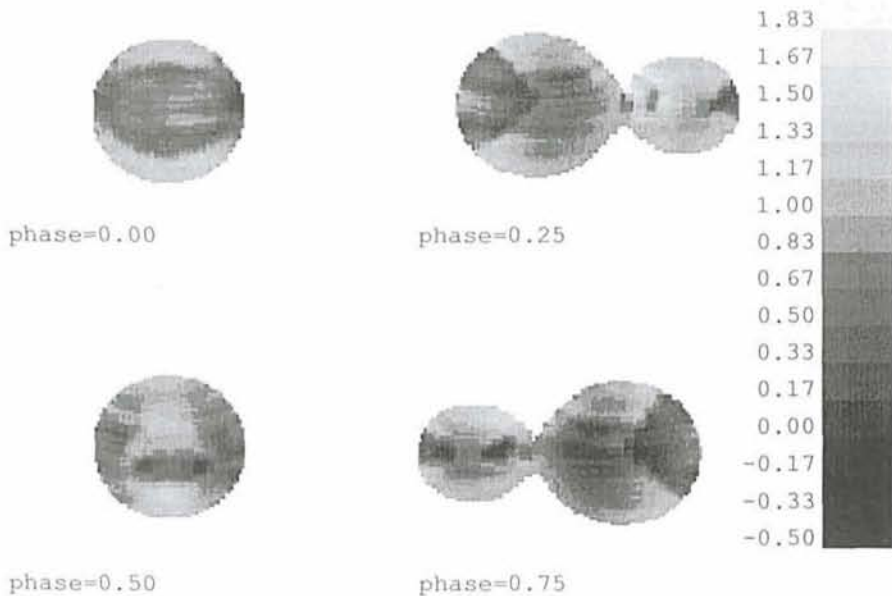
phase=0.00 phase=0.25

```
1.83
1.67
1.50
1.33
1.17
1.00
0.83
0.67
0.50
0.33
0.17
0.00
-0.17
-0.33
-0.50
```

phase=0.50 phase=0.75

Figure 5: *Doppler imaging surface maps of YY Eri.*

hence the use of the appropriate model atmospheres. However, on a more qualitative ground, we know that darker tones correspond to colder areas; from a first rough estimate S = 1.83 corresponds to 350 K above the mean and S = 0.5 to 400 K below.

The similarity between the photometric and spectroscopic maps is evident, at least with reference to the distribution on a large scale. In both cases the fitting of the data requires a smooth nonuniform temperature distribution with the stellar poles hotter than the backs and the equators. Therefore we can say that the models from photometry and spectroscopy are at this level fully consistent. On the other hand, the detailed analysis of the surface features requires a less simple treatment, that we are still developing. Even in absence of spots

we have a T distribution over the surface, which implies a variation of the line equivalent width and affects the reference values of S (i.e. the value corresponding to the unperturbed photosphere). To disentangle this effect from the actual brightness variation we are undertaking the computation of local profiles by means of model atmospheres.

3. Discussion and Conclusions

The Doppler imaging was already successfully applied to less rapidly rotating objects by other people, but as far as we know never to W UMa stars. With this experience we intended to examine if it is also possible to obtain new information about these capricious, rapidly rotating objects. The reason for

this approach was clear. From the measurements of visible light curve, UV and X we know that these binaries are seats of magnetic activity. Furthermore, it is generally believed that high AML is controlling the evolution of these binaries towards the single-star stage, involving mass transport from the secondary to the primary component. Nobody presently understands how this mass transport takes place and how it is interacting with magnetic, tidal and Coriolis forces. It can be hoped that from a better survey of the brightness inhomogeneities on the surface, a better insight in the origin of these inhomogeneities, and related large-scale motions, can be obtained.

Our first results are encouraging for a further development of the application of this method. However, we feel that the next step will most probably require the use of the 3.6-m telescope, to have the possibility of enlarging the observable sample and of analysing less strong (and simpler) spectral lines.

References

Binnendijk L. 1970, *Vistas in Astron.* **12**, 217.
Breger M. 1981, *PASP* **93**, 528.
Gronbeck, B. 1976, *Astron. Astrophys. Suppl.* **24**, 399.
Kuiper P.G. 1941, *Ap.J.* **93**, 133.
Lucy L.B. 1968, *Ap.J.* **151**, 1123.
Maceroni C., van Hamme W., Van 't Veer F. 1990, *Astron. Astrophys.* **234**, 177.
Maceroni C., Van 't Veer F. 1990 in *Active Close Binaries.* Ed. C. Ibanoglu, Kluwer Acad. Publ. Dordrecht, p. 309.
Piskunov N.E., Tuominen I., Vilhu O. 1990, *Astron. Astrophys.* **230**, 363.
Schatzman E. 1962, *Ann. Astrophys.* **25**, 18.
Van 't Veer F. 1975, *Astron. Astrophys.* **40**, 167.
Vilhu O. 1982, *Astron. Astrophys.* **109**, 17.
Vogt S.S., Penrod G.D. 1983, *PASP* **95**, 565.
Wilson R.E. 1979, *Ap.J.* **234**, 1054.
Wilson R.E., Biermann, P. 1976, *Astron. Astrophys.* **48**, 349.

Are the Nebulae Around R Coronae Borealis Stars Evolution or Ejection Related?

D. POLLACCO, Department of Physics and Astronomy, St. Andrews University, Scotland

The R Coronae Borealis (R CrB) stars are a rare group of cool hydrogen-deficient supergiants whose light variations are characterized by dramatic fading of up to visual mag. 9 and a slow recovery to maximum. Spectroscopically they appear to be extremely hydrogen-deficient and carbon rich. Their evolutionary history has been the source of much controversy. Mixing scenarios for single

AGB stars (Schönberner, 1986) have been unable to reconcile the observed photospheric abundances with model predictions. Recently two rather exotic scenarios have emerged that address this problem:

● *The last thermal pulse scenario* (Renzini, 1979, 1981 and Iben et al., 1983). Calculations have shown that if a white dwarf suffers a thermal

pulse it may be intense enough to reignite a helium-burning shell sending the star towards the AGB for a second time ('Born again' AGB star). The R CrB stars are suspected to be at this stage. This process is accompanied by large-scale mixing of the photosphere. Although the computational work is great it does appear that the time spent at the AGB is
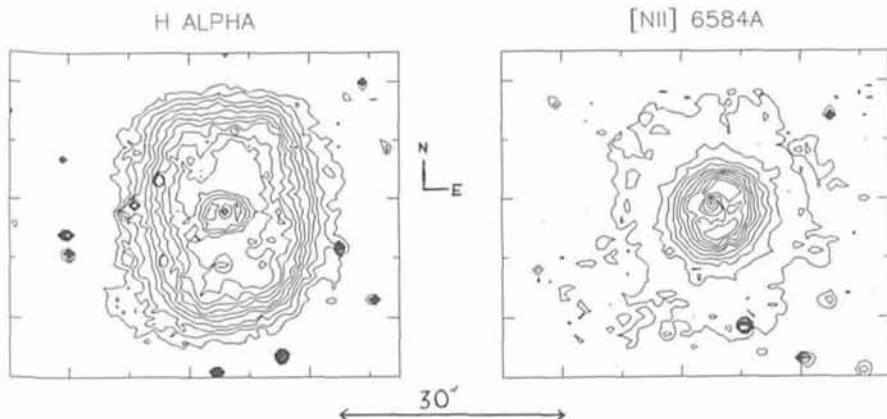
Figure 1a/b: *Narrow-band images of V 348 Sgr and its surrounding nebula taken with the ESO/ MPI 2.2-m telescope in 1987. In each case there are ten contours equally spaced between the sky level and the peak flux in the central nebula. These images are continuum subtracted – although differences in the PSF through the different filters and images show that some stellar residue remains.*

strongly mass dependent and even for the lowest mass objects may be too short to account for the suspected R CrB lifetimes. Subsequent evolution is via a Schönberner track to the white dwarf configuration.

● *The merged white dwarf scenario* (Webbink, 1984). It is thought possible that a double degenerate binary consisting of He and CO white dwarfs may lose sufficient angular momentum by gravitational radiation/material ejection to allow the system to merge within a Hubble time. In these circumstances it is expected that the lighter He dwarf will be smeared around the other producing the observed abundances.

The first clues to the evolutionary status of the R CrB stars may have been found by Herbig (1949, 1968) who while observing the proto-type R CrB in deep minima found possible evidence of [O II] λ3727/9Å emission. These lines only occur in low-temperature and density material and suggest that R CrB may be surrounded by a low-surface brightness nebula. IRAS observations of R CrB have revealed the presence of a huge fossil dust shell (Walker, 1986) some 8 pc in diameter. Gillett et al. (1986) tried to understand the heating of the shell but concluded that the stellar and interstellar radiation fields are far too feeble to account for the observed shell temperature.

The hot R CrB stars are thought to be similar to the R CrB stars but have much higher photospheric temperatures (Pollacco, 1989, Pollacco and Hill, 1991). The brightest member of this class, V 348 Sgr, is known to be surrounded by a faint nebula. Figure 1a/b shows the nebula's morphology as observed through Hα and [NII] λ6584Å narrow-band filters using the ESO/MPI 2.2-m telescope remotely from Garching.

These images are continuum subtracted and show an amazing morphology difference (normally images of PN in these ions display roughly similar structures). Spectroscopy obtained with the AAT (Fig. 2) shows the nebula to be of low excitation. An analysis of this indicated that helium is heavily overabundant, while simple and more complicated modelling failed to predict the observed nebular ionization and extent at the inferred surface temperature of the central star (~20,000 K: Schönberner and Heber, 1986). However, convergence was achieved using black-body models (the limiting case) if the stellar temperature was raised by some 10,000 K (Pollacco et al., 1990). UV spectra do not give any indications of another body in the system, so we are forced to accept that V 348 Sgr must have been hotter in the recent past (the recombination timescale of the nebula is 120–2300 yr). We conclude that V 348

Sgr is rapidly evolving towards the red supergiant region of the HR diagram – probably the R CrB region.

In order to test this scenario more thoroughly we (Pollacco et al., 1991) have used the NTT to search for faint nebulae around cool R CrB stars. Multiple images were obtained of UW Cen in very deep minima that clearly show the star to be surrounded by a faint (and small) nebula of unusual physical appearance (Fig. 3). The morphology consists of a fainter outer envelope of circular appearance while the central parts are dominated by a pair of reasonably collimated and diagonally opposed "jets" (I use this word lightly). Narrow-band imaging and spectra (Fig. 4) obtained with the NTT suggest that the nebular emission is dominated by a scattering component with no obvious signs of line emission (our detector had little efficiency at λ3720 Å). Despite the overwhelming excellence and hence enjoyment of using the NTT, this run was overshadowed by a certain student – who shall remain nameless – who found during a long slew that he was unable to control the contents of his stomach.

This structure is proving difficult to understand in the context of the evolutionary scenarios set out above. However, considering the ejection velocities implied by chromospheric lines (~200 km s⁻¹) observed during the decline to minimum, these structures could easily be produced within the theoretical age of the R CrB phase (Schönberner, 1977). Hence it is more likely that the jet structure is related to the process causing the minima. In line with this, Pollacco et al. (1991) suggest that in UW Cen and by implication all R CrB stars, there is also a jet in or close to the line of sight.
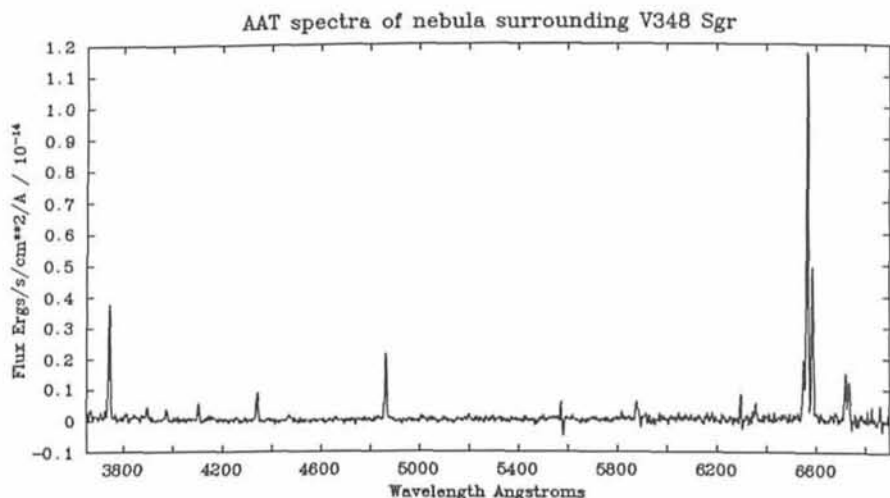

Figure 2: *Sum of 5 hr worth of IPCS spectra taken with the AAT in 1987. Note the relatively strong appearance of HeI λ5876Å which is not expected for a central source of this temperature (~20,000 K).*
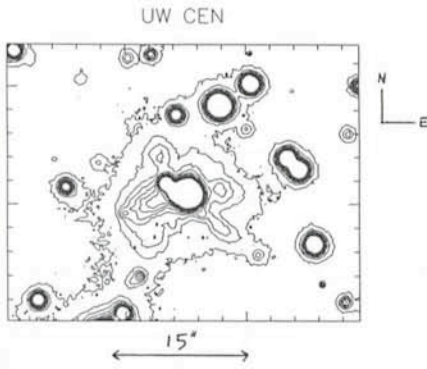
Figure 3: *NTT V band image of the classical R CrB star UW Cen obtained when the star was in a deep minimum. In this diagram there are ten contour levels equally spaced between the sky and 10 % of the peak stellar flux.*

Spectroscopic and photometric observations of R CrB stars at different points of their light curve suggest that the deep minima may be caused by an ejection of material in the line of sight with subsequent condensation producing an effect analogous to a solar eclipse ("the consortium of puffs model", Feast, 1986). As the dust clumps disperse, the star slowly returns to its former brightness. At maximum brightness many R CrB stars appear to vary with a ~40-day period and in the cases of RY Sgr and R CrB itself (the best studied objects) these oscillations are thought due to radial pulsations. R CrB stars are known to be surrounded by hot circumstellar shells (800 K) so that at IR wavelengths the shell flux becomes increasingly dominant until at L it is the outstanding contributor. Observations of RY Sgr show that the shell is powered by the stellar radiation field as it also displays the ~40-day variation and this continues despite the optical minima and with a similar magnitude. The shell

pulsation is superimposed on a much longer period variation (1000–3000 days). Feast (1990) has found that optical declines are often associated with rising of bright periods in L flux and suggested that ejected material gathers in the shell until at some critical density condensation occurs. Stellar radiation pressure then drives the clumps to great stellar distance where upon they disperse. The long-term variation in L corresponds to a "refilling" of the shell by ejected stellar material (quasi-periodic relaxation oscillations). An implication of Feast's model is that ejected material is randomly expelled but Stanford et al. (1988) have found polarimetric evidence in support of a preferred plane of ejection. Feast (1990) rejects this scenario due to geometric considerations (no R CrB-like stars are known that do not display deep minima[1] and interprets the polarimetric data as indications of a grain collimation direction. This latter criticism could also be levelled at the jet model but Pollacco et al. point out that with a sufficiently large jet opening angle (and this seems valid in the case of UW Cen) the statistical occurrence of R CrB-like stars not displaying minima would be small. Both Stanford et al.'s and Feast's models imply some collimation mechanism is at work – be it non-radial pulsation (Stanford et al.) or a magnetic field (Feast).

Future observations of other R CrB stars in deep minima will allow us to confirm or reject this model and may shed light on the jet collimation mechanism. While the detection of extended

line emission will lend strong support for Renzini's ideas.

This work is carried out in collaboration with C.N. Tadhunter (RGO), P.W. Hill (St. Andrews), L. Houziaux (Liège) and J. Manfroid (Liège).

References

Feast, M.W. 1986. in: IAU Coll. No. **87**, *Hydrogen-Deficient Stars and Related Objects*, p. 151, eds. Hunger, K., Schönberner D. and Rao, N. Kameswara (Reidel, Dordrecht).

Feast, M.W. 1990, in: *Confrontation Between Stellar Pulsation and Evolution*, Bologna, Italy, (A.S.P. Conference Series), in press.

Gillett, F.C., Backman, D.E., Beichmann, C. and Neugebauer, G., 1986. *Astrophys. J.*, **310**, 842.

Herbig, G. 1949. *Astrophys. J.*, **110**, 143.

Herbig, G. 1968. *Mem. Soc. R. Sci. Liège*, **17**, 353.

Iben, I. Jr., Kaler, J.B., Truran, J.W. and Renzini, A., 1983. *Astrophys. J.*, **264**, 605.

Pollacco, D.L., 1989. *The Evolutionary Status of the Hot R CrB Stars*, Ph.D. Thesis, St. Andrews University.

Pollacco, D.L. and Hill, P.W., 1991. *Mon. Not. R. Astr. Soc.*, **248**, 572.

Pollacco, D.L., Tadhunter, C.N. and Hill, P.W., 1990. *Mon. Not. R. Astr. Soc.*, **245**, 204.

Pollacco, D.L., Hill, P.W., Houziaux, L. and Manfroid, J., 1991. *Mon. Not. R. Astr. Soc.*, **248**, 1P.

Renzini, A., 1979. in: *Stars and Stellar Systems*, p.135, ed. Westerlund, B.E. (Reidel, Dordrecht).

Renzini, A., 1981. in: *IAU Coll. No. 59*, *Effects of Mass loss on Stellar Evolution*, p. 319, eds. Chiosi, C. and Stalio, R. (Reidel, Dordrecht).

Schönberner, D. 1977, *Astron. Astrophys.*, **57**, 437.

Schönberner, D. 1986. In: *IAU Coll. No. 87*, *Hydrogen-Deficient Stars and Related Objects*, p. 471, eds. Hunger, K., Schönberner, D. and Rao, N. Kameswara (Reidel, Dordrecht).

Schönberner, D. and Heber, U., 1986. in: *IAU Coll. No. 87*, *Hydrogen-Deficient Stars and Related Objects*, p. 217, eds. Hunger, K., Schönberner D. and Rao, N. Kameswara (Reidel, Dordrecht).

Stanford, S.A., Clayton, G.C., Meade, M.R., Nordsieck, K.H., Whitney, B.A., Murison, M.A., Nook, M.A. and Anderson, C.M., 1988. *Astrophys. J.*, **325**, L9.

Walker, H.J. 1986. In: *IAU Coll. No. 87*, *Hydrogen-Deficient Stars and Related Objects*, p. 407, eds. Hunger, K., Schönberner D. and Rao, N. Kameswara (Reidel, Dordrecht).

Webbink, R.F. 1984. *Astrophys. J.*, **277**, 355.

---

[1] This statement may not be correct as it is becoming increasingly apparent that a good number of R CrB stars suffer minima only rarely – sometimes only at discovery.
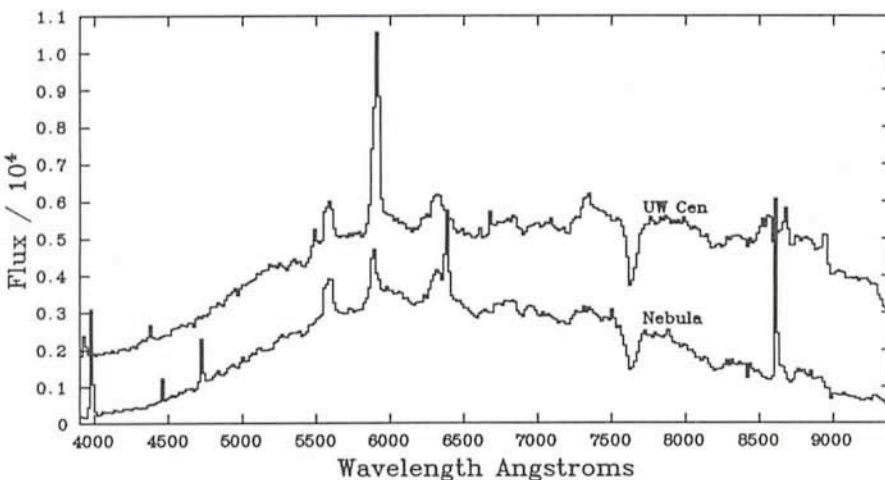
Figure 4: *EFOSC spectra obtained east-west through the central regions of Figure 3. The spectrum of the nebula is similar to that of the star but with a bluer energy distribution. This behaviour is indicative of a reflection nebula.*

Discovery of the First Eclipsing Binary Barium Star

A. JORISSEN[1], J. MANFROID[2] and C. STERKEN[3]

[1]*European Southern Observatory;* [2]*Institut d'Astrophysique, Université de Liège, Belgium;* [3]*Vrije Universiteit Brussel, Belgium*

1. Barium Stars

Barium stars are a family of peculiar red giant stars whose envelopes exhibit overabundances of carbon as well as of elements heavier than iron. First identified by Bidelman and Keenan (1951), they represent about 1% of all red giants of types G and K. Their kinematic behaviour appears to be similar to that of A or early F main-sequence stars; accordingly, barium stars should have an average mass of about 1.5 to 2 $M_\odot$ (Hakkila 1989a).

McClure (1983) found that a large fraction of barium stars belong to spectroscopic binaries. Jorissen and Mayor (1988) showed that virtually all known southern barium stars with large barium overabundances are spectroscopic binaries, and McClure and Woodsworth, (1990) obtained orbital periods in the range 80 d to more than 10 y. White dwarf (WD) companions are inferred from the mass function distribution, although very few of them can be detected directly from their UV radiation (Böhm-Vitense, 1980, Dominy and Lambert, 1983, Böhm-Vitense, Nemec and Proffitt, 1984).

The fact that all barium stars belong to binary systems clearly means that binarity must somehow be responsible for their chemical peculiarities. It was sometimes suggested that the presence of a companion could perhaps modify the outcome of the helium flash occurring in low-mass stars, possibly triggering the extra-mixing leading to the synthesis of heavy elements (e.g., McClure, 1984). However, some barium systems are quite wide (P > 10 y), and it is difficult to imagine that such a distant companion could have an effect on the internal structure of the barium star.

Mass transfer from the former primary towards the barium star, when the primary was a heavy-element rich S or carbon star on the asymptotic giant branch (AGB), seems more likely. The observation of a 10 μm (N band) excess in many barium stars (Hakkila, 1989b), which is not correlated with the other atmospheric peculiarities, may point towards the presence in the system of dust left over from a former mass-loss episode. Again, many barium systems appear to be too wide for mass transfer through Roche lobe overflow (RLOF) to occur (Tout and Eggleton, 1988). Moreover, post-RLOF systems general-

ly have circular orbits (e.g., Webbink, 1986), which is not the case for all barium stars. Boffin and Jorissen (1988) suggested instead that the accretion by the barium star of the wind from the former AGB primary may be efficient enough to account for the observed chemical peculiarities.

2. Interest of a Photometric Monitoring of Barium Stars

Since barium stars are single-lined spectroscopic binaries (SB1), only partial information can be obtained about their orbital parameters. The detection of possible photometric variations related to the binary nature of these stars could provide further insight in the characteristics of these systems. However, the relatively large orbital separation (estimated as several AU) and the low luminosity of the companion (dictated by the SB1 nature of the system) imply that photometric variations, if present, should be of rather small amplitude and have a long period.

Landolt (1983) was the first to look for photometric variability of barium stars. He obtained UBV photoelectric observations of several barium stars at KPNO and CTIO at irregular intervals over a time span of more than a decade. His photometry was basically non-differential, but included the measurements of a number of standard stars of similar brightness as the barium stars of his programme. Assuming the mean error of observations in V for standard stars to be about 0.007 magnitude, he concluded that 6 stars of the sample (which contained 17 barium stars) showed variations at or above the 3 σ level. All stars were however observed less than a dozen times under very different observing conditions and no lightcurve is provided. *Our more accurate photometric monitoring, described in Section 3, does not confirm these variations in all but one case.*

3. The Long-Term Photometry of Variables Programme at ESO

High accuracy and homogeneity over periods of *several years are required for* monitoring barium stars. Both requirements, together with the potential of extensive observing time (4 to 6 months/year), are offered by the Long-Term Photometry of Variables (LTPV) pro-

gramme operating at ESO since 1982 (Sterken, 1983).

The Strömgren uvby magnitudes of a sample of 19 barium stars have been monitored since July 1984 in a differential way: for each programme star, two comparison stars were selected among nearby G or K giants. The observation frequency is about 2/week during typical one-month observing runs. That frequency was increased to one measurement/night during three observing campaigns around the predicted time of eclipse of the companion of HD 46407 by the red giant (Section 4).

Observations were performed on the ESO 50-cm telescope or on the Danish 50-cm telescope (four-channel simultaneous photometer). The reduction to the standard uvby system is performed with the "multi-night" algorithm described by Manfroid (1985), taking into account the *total set of measurements* carried out at the ESO 50-cm or Danish 50-cm telescopes *since the beginning of the monitoring*. Offsets between observing runs are avoided in that way, since there is just one colour matrix for the whole set of measurements in a given system. Checks were of course made to control the stability of the system over the whole period considered.

The accuracy of the differential magnitudes can be estimated from the standard deviations of the differences between comparison stars. For both the Danish 50 and ESO 50 systems (referred to in the following as D50 and E50-6, respectively, according to the notation of Jorissen, Manfroid and Sterken, 1991; see also Manfroid et al., 1991), 50% of the considered comparison pairs have a standard deviation in the y channel smaller than 0.003 mag for observations spanning several years. The mean value of these r.m.s. deviations is somewhat smaller for the D50 system (0.007 mag) than for the E50-6 system (0.009 mag). Colour indices in the E50-6 system are however much less accurate than in the D50 system, mainly because the latter are obtained with a four-channel photometer. In what follows, we will therefore mainly make use of the more accurate D50 measurements. More details about the observing policy, the reduction method and the resulting accuracy can be found in Manfroid et al. (1991).

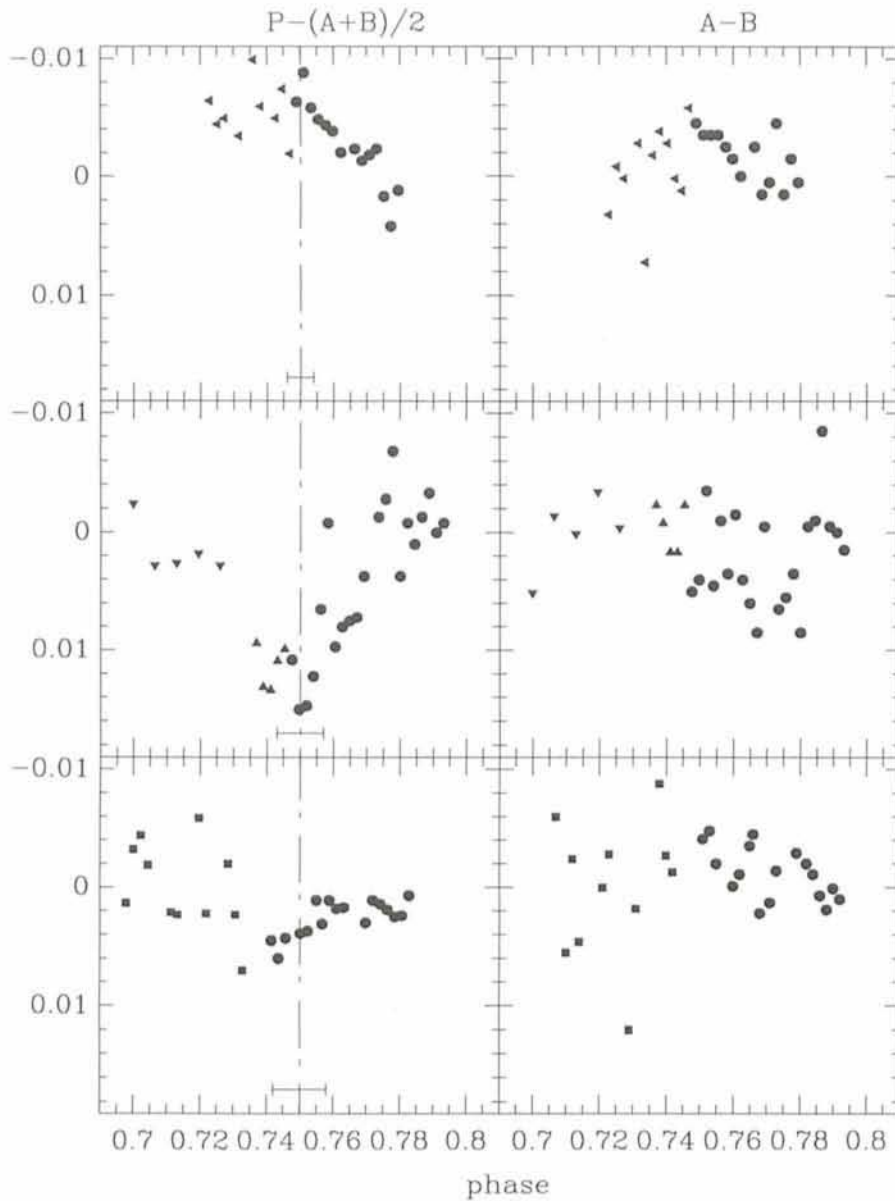A detailed discussion of the results of the photometric monitoring for the sam-

Figure 1: *Results of the three observing campaigns around the time of the predicted eclipses ($\varphi = 0.75$): February 1985 (upper panel; cycle 1), November 1988 (middle panel; cycle 4), February 1990 (lower panel; cycle 5). Phases are computed adopting the orbital elements of McClure and Woodsworth (1990). The uncertainty on the predicted time of total eclipse is displayed by the horizontal error bar around the value $\varphi = 0.75$. The left panels present the differential P-(A+B)/2 magnitude in the Strömgren y channel, whereas the right panels display the differential A-B y magnitude, where P stands for the barium star and A and B for the two comparison stars (respectively HR 2379 and HR 2367). The zero point of the magnitude scale is the mean value of the corresponding differential magnitude in a given system (● = D50 system; ◄ = E50-5 system; ▲ = E50-6 system; ▼ = ESO50-8 system; ● = E50-x system). The ordinate axis is oriented in such a way that a decrease in brightness corresponds to a dip in the curve.*

ple of 19 barium stars is presented in Jorissen, Manfroid and Sterken (1991). The main result of our monitoring is that the two barium stars with the shortest orbital periods in the sample, HD 121447 (~ 185 d, Jorissen and Mayor, in preparation) and HD 46407 (458.6 d; McClure and Woodsworth, 1990), are the only ones to present small, albeit significant, light variations. In the case of HD 121447, it is not yet clear, however, whether these variations at a level $\sigma_y = 0.020$ mag (to be compared with $\sigma_y = 0.009$ mag for the magnitude difference

between the corresponding comparison stars) are specifically related to the binary nature of the star, or whether HD 121447, which is also the coolest known barium star (K7 III, Lü et al., 1983), is simply a microvariable as any other very red star.

4. HD 46407: The First Eclipsing Binary Barium Star

HD 46407 (HR 2392, y = 6.27, b − y = 0.66, K0III Ba3) has the second shortest orbital period in our sample (P = 458.6 d,

McClure and Woodsworth, 1990). Its spectroscopic ephemeris was used in order to predict the times of a possible eclipse of the companion by the barium star. During the 7-year span of the monitoring, only three eclipses were predicted to occur at a time when the star was easily observable. HD 46407 was observed once a night for 20 to 40 nights during these periods (February 1985, November 1988 and February 1990).

A clear dip is seen in the lightcurve in November 1988 while the comparison pair remains stable (Fig. 1). Since this dip is exactly centred on the predicted time for the total eclipse, there is little doubt that an eclipse has actually been detected. Very accurate measurements were carried out during the February 1990 campaign at the Danish 50-cm telescope, and reveal that, if any, the eclipse was much shallower. The measurements of February 1985 are puzzling, since a statistically significant trend is indeed observed, but if it were to correspond to the eclipse ingress, there would be a > 0.03 phase lag with respect to the spectroscopic ephemeris.

Figure 2 presents the phase diagram for all D50 measurements, adopting P = 458.1 d and T = JD 2 445 296.0 (time of maximum velocity), which correspond to the lower bounds of McClure and Woodsworth's elements. The measurements of February 1985 are lagging in that phase diagram as well, so that the current uncertainty on the circular orbital elements (±0.5 d on P and ±1 d on T) cannot resolve the discrepancy. The superposition of the February 1985 eclipse ingress on the November 1988 data would require a 451.7 d period, not very different from McClure's spectroscopic period, although well outside its formal error bar.

The phase diagram of Figure 2, adopting McClure and Woodsworth's (1990) spectroscopic period, reveals that a very broad secondary eclipse may be present as well. A clear trend was in fact observed for $0.35 < \varphi < 0.5$ in cycle 2, and the drop in brightness around phase 0.35 was confirmed by the observations of cycle 6. Again, the large scatter in that phase range indicates that the spectroscopic period is probably not the best choice for constructing a photometric phase diagram. A careful period analysis of our data remains to be done.

In summary, the lightcurve of HD 46407 derived from the currently available photometric observations in the D50 system displays a sharp "primary" eclipse (companion behind the barium star) and a possible shallow "secondary" eclipse. In November 1988, the
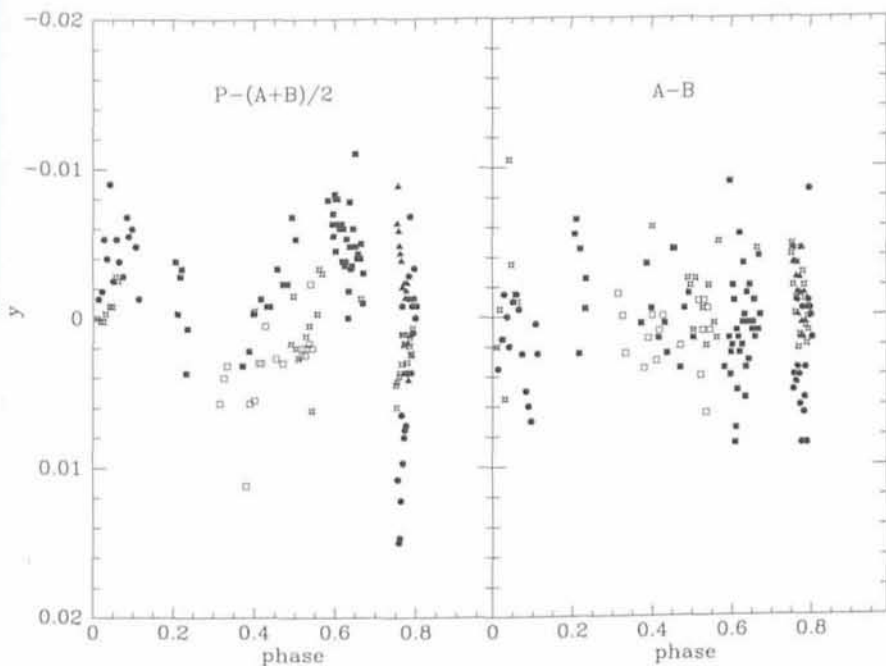
Figure 2: *Phase diagram for the whole set of y measurements in the D50 system (left panel: barium star relative to comparison pair; right panel: comparison pair), adopting the spectroscopic elements from McClure and Woodsworth (1990). The various symbols refer to the different cycles (starting from JD 2 445 296.6): ▲ = cycle 1, ■ = cycle 2, ● = cycle 4, ☆ = cycle 5, □ = cycle 6. Note the presence of a very wide secondary eclipse (transit of the companion in front of the barium star). Note that, because P-(A+B)/2 involves the average of the two differential measurements P-A and P-B, the uncertainty on P-(A+B)/2 is √2 times smaller than the one on A-B.*

primary eclipse had a depth of ∼ 0.02 mag in y and a full width of $\Delta\varphi \sim 0.05$ (i.e. about 20 d); the primary eclipse was much shallower in February 1990. The shallow secondary eclipse occurs when the companion is in front of the barium star. Its depth is at least 0.01 mag in the y band and it extends over about 50% of the orbital period. It might well be that the brightness of HD 46407 is slowly varying over the whole orbital period.

The b − y index is marginally variable, at variance with the v − b index which exhibits large variations. Quite interestingly, the variations of the v − b index and of the y magnitude appear to be roughly correlated: when the star is fainter, it is also redder, as shown by Figure 3. This behaviour is typical of light-scattering processes, so that we suggest that the eclipsed light is actually the light from the barium star itself which is backscattered by dust trapped (in a disk?) around the companion.

Dust must be present in a rather extended region around the companion, since the November 1988 eclipse was about three times longer than it would have been expected for the eclipse of a point-like source by a red giant of radius 15 $R_\odot$ (and a semi-major axis of 1.5 AU; total duration of 7 d or $\Delta\varphi = 0.015$). Moreover, there does not seem to be a flat bottom in the eclipse lightcurve, indicating that the eclipse is never total. The phase lag of February 1985 can also be accounted for by this explanation,

since dust ought not to be distributed in a spherically symmetric way around the companion.

Although this model seems to account qualitatively for the observed behaviour, it remains to be tested quan-

titatively: the depth of the eclipse will yield an estimate of the amount of dust required and the wavelength dependence of the scattering cross-section should be compatible with the relative variations of b − y and v − b. The following questions also remain to be answered: is such an explanation compatible with the absence of IR excess for HD 46407 (Hakkila and McNamara 1987, Hakkila 1989b)? And how can dust grains remain trapped around the companion for long periods of time (Poynting-Robertson effect)?

The photometric monitoring of HD 46407 is still going on; polarimetric measurements are also in progress. Finally, a similar photometric monitoring is being carried out for the two barium stars with the shortest known orbital periods (HD 77247 and HD 121447), and it will be interesting to know whether a behaviour similar to that of HD 46407 will be observed.

In conclusion, the behaviour of HD 46407 is a clear example of a phenomenon that can only be studied as part of a carefully planned long-term project relying on service observing: (i) continuous photometric monitoring should be carried out in order to get the general light curve; (ii) each eclipse needs more than one month of daily observing; (iii) they only occur every 1.3 years and one third of them are missed because of the proximity to the Sun. In addition, we must also emphasize that only a small telescope is needed. The LTPV project
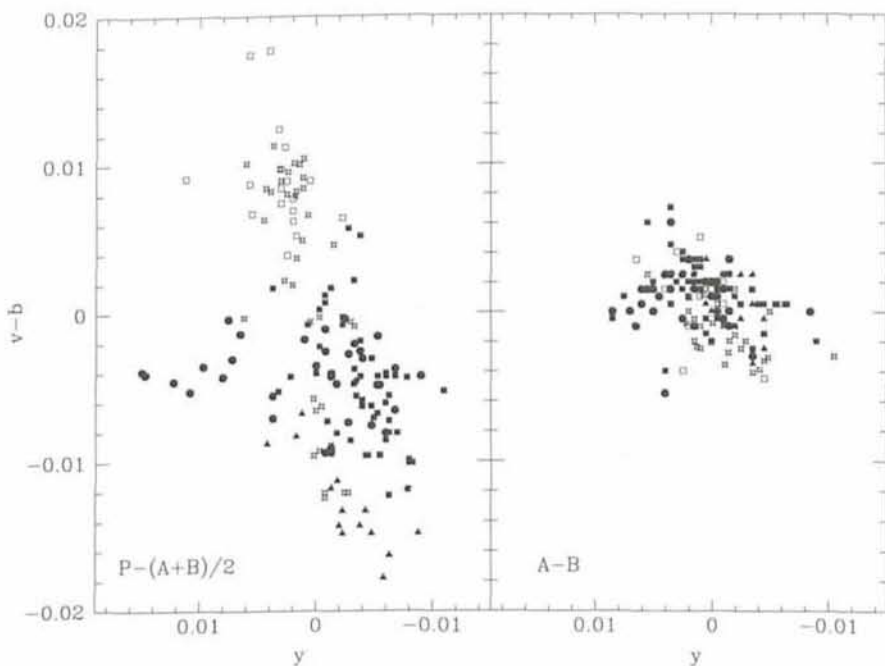

Figure 3: *The (y, v − b) diagram of the barium star (left panel) and the comparison pair (right panel) in the D50 system. Symbols and magnitude zero points are as in Figure 2. Note the triangles, which exhibit within a single observing run the general trend observed for the whole set of measurements. The filled circles standing to the left of that general trend correspond to the November 1988 eclipse.*

at ESO clearly represents the only available opportunity to address that kind of problem.

References

Bidelman, W.P., Keenan, P.C. 1951, *Ap.J.*, **114**, 473.
Boffin, H.M.J., Jorissen, A. 1988, *Astron. Astrophys,*, **205, 155**.
Böhm-Vitense, E. 1980, *Ap.J.*, **239**, L79.
Böhm-Vitense, E., Nemec, J., Proffitt, Ch. 1984, *Ap.J.*, **278**, 726.
Dominy, J.F., Lambert, D.L. 1983, *Ap.J.*, **270**, 180.
Hakkila, J. 1989a, *A.J.*, **98**, 699.
Hakkila, J. 1989b, *Astron. Astrophys.*, **213**, 204.
Hakkila, J., McNamara, B.J. 1987, *Astron. Astrophys.*, **186**, 255.
Jorissen, A., Mayor, M. 1988, *Astron. Astrophys.*, **198**, 187.
Jorissen, A., Manfroid, J., Sterken, C. 1991, *Astron. Astrophys.*, in press.
Landolt, A.U. 1983, *PASP*, **95**, 644.
Lü, P.K., Dawson, D.W., Upgren, A.R., Weis, E.W. 1983, *Ap.J.*, **52**, 169.
Manfroid, J. 1985, habilit. thesis, Univ. of Liège.
Manfroid, J., Sterken, C., Bruch, A., Burger, M., de Groot, M., Duerbeck, H., Duemmler, R., Figer, A., Hageman, T., Hensberg, H., Jorissen, A., Madejsky, R., Mandel, H., Ott, H., Reitermann, A., Schulte-Ladbeck, R., Stahl, O., Steenman, H., vander Linden D., Zickgraf, F.-J. 1991, *Astron. Astrophys. Suppl.*, **87**, 481.
McClure, R.D. 1983, *Ap.J.*, **268**, 264.
McClure, R.D. 1984, *PASP*, **96**, 117.
McClure, R.D., Woodsworth, A.W. 1990, *Ap.J.*, **352**, 709.
Sterken, C. 1983, *The Messenger*, **33**, 10.
Tout, C.A., Eggleton, P.P. 1988, *MNRAS*, **231**, 823.
Webbink, R.F. 1986, in: *Critical Observations vs Physical Models for Close Binary Systems*, eds. K.C. Leung and D.S. Zhai, New York, Gordon and Breach.

The Rise of SN 1987 A

It is now almost five years since SN 1987A exploded in the LMC. In the meantime, the visual brightness has decreased to about one millionth of what it was at the time of maximum. It is still being observed with large telescopes, also at La Silla, but the elusive pulsar has not yet been directly detected.

The four pictures were taken during amateur patrols in Australia at the time of the explosion by Robert H. McNaught (Plates 2, 3 and 7) and Frank B. Zoltowsky (Plate 5). They show the early rise in brightness of this famous object; the intensity and the angular scale have been rescaled to allow direct comparison. A recent, careful remeasurement of the magnitudes of SN 1987A on these plates has shown that earlier published estimates are too faint by 0.2–0.8 magnitude (McNaught and West, to appear in *Astronomy and Astrophysics*). The new values are in better agreement with the theoretical lightcurves, but they do not by themselves permit to decide which of the two neutrino events that were observed in the morning of February 23, 1987, was the actual time-zero.

SN 1987A

PLATE 2
FEB 22.468

PLATE 3
FEB 23.444

PLATE 5
FEB 23.622

PLATE 7
FEB 24.453
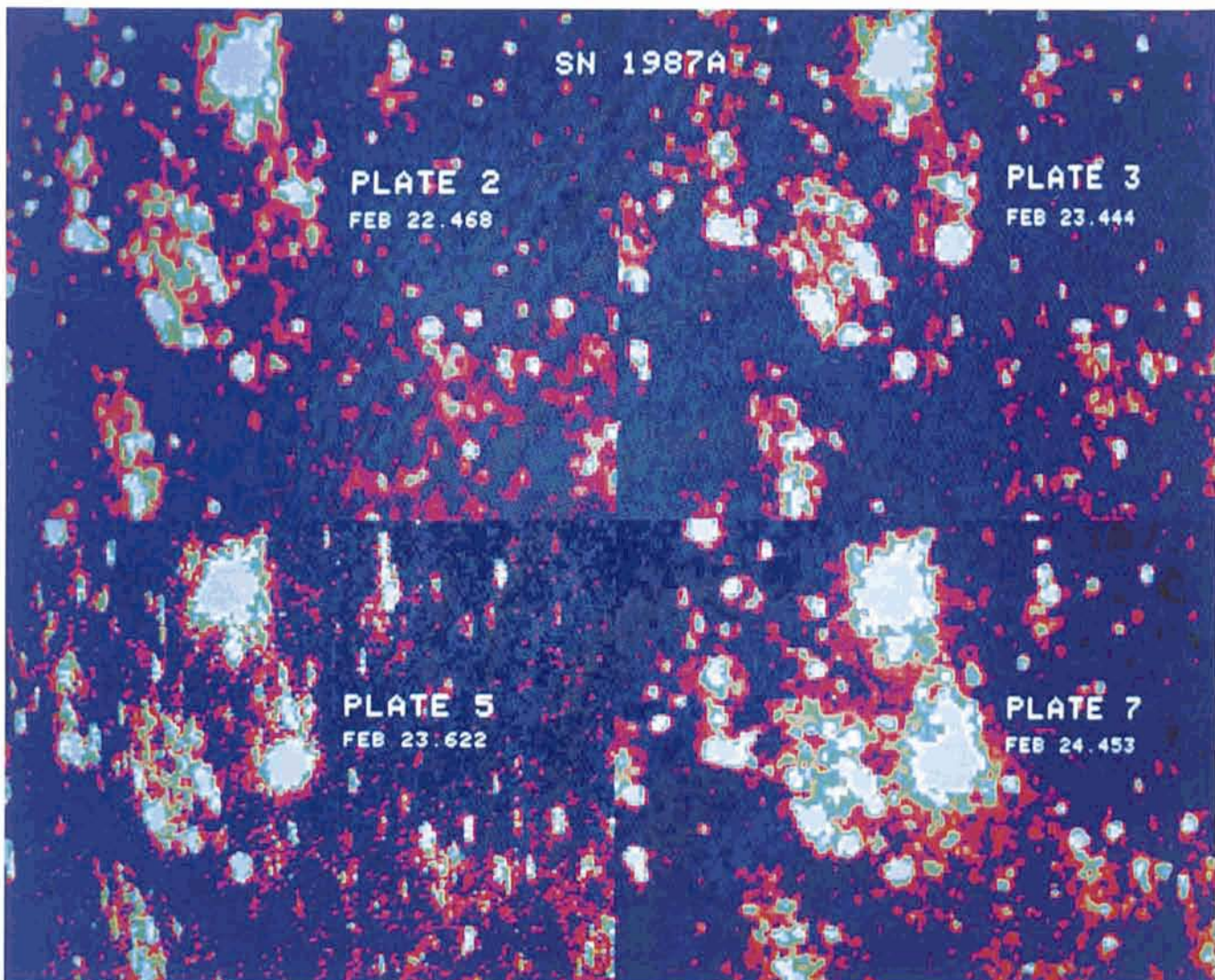
A New Large Arc Revealed by Early NTT Images

E. GIRAUD, ESO

The international effort devoted to the search for gravitational arcs has recently been reviewed by B. Fort (1991) in Hamburg. About 10 clusters with at least one "large" arc (length > 10") are reported.

The cluster presented here was detected as an X-ray source of $3.16 \cdot 10^{-13}$ ergs cm^{-2}s^{-1} by the Imaging Proportional Counter on board of *Einstein Observatory*, and was identified with a faint cluster of galaxies by Gioia et al. (1984, Second Medium Sensitivity Survey). Its optical position is RA=0302 44.6, Decl.=+1658 28.0. Images show a very rich cluster with two large galaxies, a morphology which is roughly similar to that of Abell 370. I reobserved this cluster between November 1989 and January 1990 with the NTT. Such a northern cluster was observed from La Silla because at that time the NTT field rotator was still under testing.

Eight images were obtained in V and R, with two different CCDs mounted on EFOSC 2 (Melnick et al., 1989): the RCA No. 5 which has pixels of 30 μm giving a scale of 0.26 arcsec/pixel and a Thomson low-noise CCD with pixels of 19 μm. Images were taken at various position angles. They were corrected for flat field using master flats built up with images taken during the same night, aligned, rescaled and coadded at fractional pixel value. The central part of the final image is shown in Figure 1. There is a faint halo, well visible in R, around the two brightest galaxies. Approximately at mid-distance from these objects is a faint filament. Perhaps the first idea when looking at this image is that of a shock surface between the halos of two large colliding galaxies. Another possible explanation is gravitational lensing of a faint (V > 24.5) background object. Simple gravitational models with two potentials predict well the orientation of a nearly straight arc at this location. If this is a genuine gravitational arc, the amplification would be of the order of 15, presenting a rather unique chance to obtain a spectrum of an otherwise ~25th magnitude galaxy.

Rich clusters are slowly starting to play a role of gravitational telescope for the investigation of the remote population of galaxies. They discriminate the gravitationally lensed arclets from other extragalactic faint objects, although any arclet may be an elongated cluster member. Assuming that the arclets are amplified objects, the exposure time for acquiring a spectrum is shorter than for the source object. Most of the arclets, however, are still beyond reach of present-day spectroscopy. Finding large arcs, i.e. with large amplification, is probably a unique way of shortening by a factor of 5 or more the exposure time needed for spectroscopy of these otherwise very faint objects.

Deep photometric surveys of galaxies have shown that the number-galaxy counts in I are close to non-evolution models (Tyson, 1988). Counts in B and U, however, have a much steeper slope that can only be accounted for with some form of evolution (Shanks et al., 1984, Metcalfe et al., 1987, Tyson, 1988, Majewsky, 1989). At faint magnitudes the difference in slope between number counts in B and I translates into an increasing fraction of blue objects. In the past three years, interest in this population has increased enormously, but the redshift distance of these objects and the nature of the blue population are still unknown. An open question is why this blue population seems to have disappeared today. Were they compact AGNs? Extended objects with nuclear or extranuclear star formation? Mergers? Did they disappear after an initial starburst (Cowie et al., 1991)? Did they merge to form the present-day giant galaxies (Guiderdoni and Rocca-Volmerange, 1991)?

Very good deep images, selected among the best taken during the commissioning period of the NTT, show that at magnitudes between V=22 and V=24, the very blue objects do not belong to a single population (Giraud, 1991); there is (a) a class of compact objects surrounded by a nebulosity, (b) a class of irregular objects with probable isophote distortions at the limit of reso-
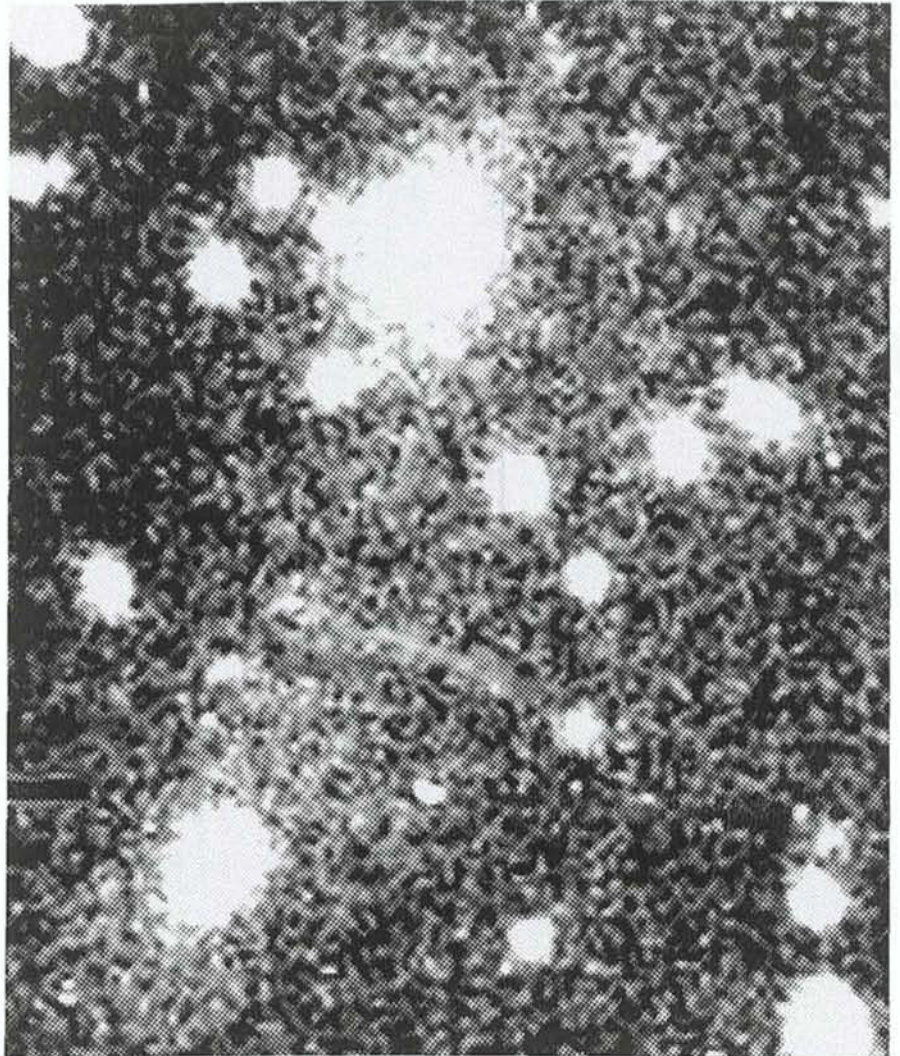

Figure 1: *The central region of the X-ray cluster CL0302+1658 at z=0.4 showing the two main galaxies, a weak halo, and a filament of 20" approximately, which might be either a gravitational arc or a feature related to the intracluster medium.*

lution and (c) double or multiple systems. It is for example possible that nuclear activity, chaotic star formation and merging are responsible for the blue colours in compact, irregular and multiple systems, respectively. Spectra of blue, low-surface-brightness arcs will provide us with the redshift distance of these objects and possibly with some indications of their physics.

Acknowledgements

I would like to thank the technical staff on La Silla for their efforts in making the NTT, instruments, and new detectors working at best during these nights of the commissioning period. I thank Jorge Melnick for the allocated time.

References

Cowie L.L., Gardner J.P., Waincoast R.J., Hodapp K.W., 1991, preprint.
Fort B., 1991, preprint.
Gioia I.M., et al., 1984, *Ap.J.*, **283**, 495.
Giraud E., 1991, ESO preprint.
Guiderdoni B., and Rocca-Volmerange B., 1991, preprint.
Lilly S.J., Cowie L.L., and Gardner J.P., 1990, *Ap.J.*, preprint.
Majewski S.R., 1989, in *The Epoch of Galaxy Formation*, Eds. Frenk et al., Kluwer Dordrecht, p. 85.
Melnick J., Dekker H., and D'Odorico, 1989, *ESO Operating Manual* No. **4**.
Metcalfe N., Fong R., Jones L.R., and Shanks T., 1987, in *High Redshift and Primeval Galaxies*, Eds. Bergeron et al., Edition Frontières, p. 37.
Shanks T., Sevenson P.R.F., Fong R., and McGillivray H.T., 1984, *Mon. Not. R. Astron. Soc.*, **206**, 767.
Tyson J.A., 1988, *Astron. J.*, **96**, 1.

Diffuse Bands and Peculiar Interstellar Clouds

P. BENVENUTI[1], I. PORCEDDU[2]

[1]*ST-ECF, ESO – Affiliated to Astrophysics Division, Space Science Department, ESA;*
[2]*Stazione Astronomica, Cagliari, Italy.*

1. Introduction

The Diffuse Interstellar Bands or DIBs, as they are usually called, are absorption features which are generated in the interstellar medium by a still unidentified set of carriers. The DIBs were firstly mentioned by Heger (1921), while their stationary character and their interstellar origin was confirmed by Merrill (1936). The most extensive survey has been published by Herbig in 1975, on the basis of photographic plate spectra: he reported 39 DIBs in the spectral range 4400–6700 Å, 24 of which were observed for the first time. By now six more DIBs have been discovered beyond 6700 Å.

During the past years the interest for the DIBs has grown considerably, particularly because the new observing techniques and the improved quality of the spectra allowed a deeper analysis of their profiles, highlighting more and more details on their behaviour and therefore making them an interesting candidate as markers of the physical and chemical status of the interstellar medium. However, in spite of the higher resolution and the excellent high S/N ratio which can be obtained from modern spectrographs coupled to CCD detectors, the nature of the carriers of the DIBs remains a mistery: their long lasting challenge may indeed be among the reasons for the continuing interest in them. Comprehensive reviews on the DIBs' topic, together with extensive bibliography, have been published by Bromage (1987) an Krelowski (1989).

In this short paper we discuss our approach to the study of these interstellar features and present some of the results we have obtained so far.

2. DIBs: What Do We Know?

The most recent high-quality (high resolving power as well as very high signal-to-noise ratio) observational data (Snell and Van de Bout 1981, Massa et al. 1983, Seab and Snow 1984, Krelowski and Walker 1987, Westerlund and Krelowski 1988, Benvenuti and Porceddu 1989, Crawford 1990, Le Bertre 1990, Porceddu et al. 1991), and the parallel theoretical studies (Douglas 1977, Van de Zwet and Allamandola 1985, Léger and d'Hendecourt 1985, Allamandola et al. 1989, Cossart-Magos and Leach 1990) allow us to define some constraints on the DIBs' problem:

● the presence of DIBs is *related* to the colour excess, in the sense that the lack of reddening implies the absence of the DIBs: but the DIBs' intensity along one line of sight is only loosely correlated to the value of the
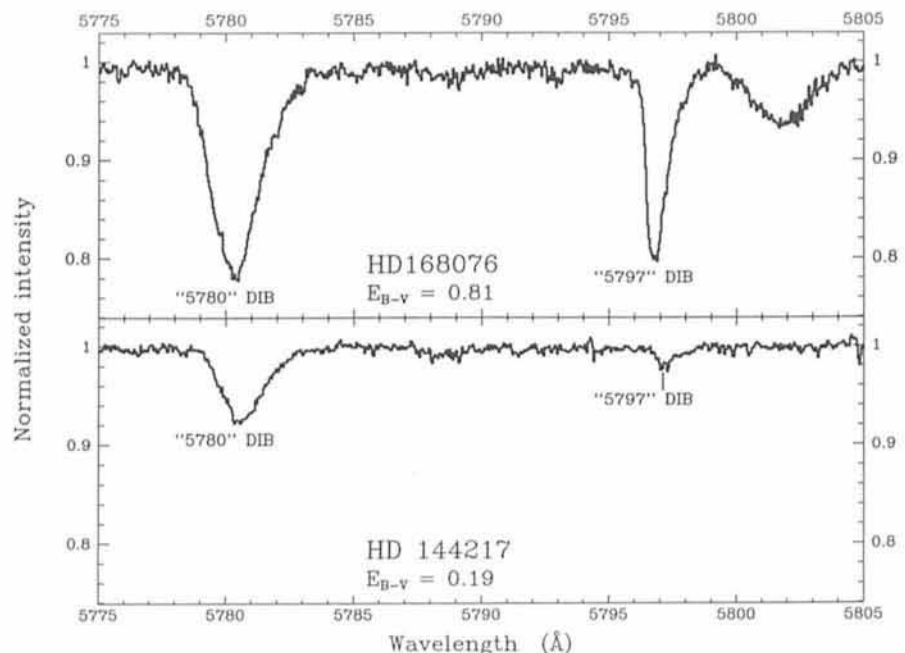
Figures 1 a and b: *The intensity ratio of the DIBs 5780 and 5797 and its variation along different lines of sight.*

reddening in that direction. This fact becomes particularly evident for low reddening values which implies obscuration by a single interstellar cloud. For higher values, the *averaging* effect over several clouds tends to flatten out the differences;

- similarly, the DIBs intensity is not strongly correlated with the 2200 Å extinction bump: dust and carriers of the DIBs, although coexisting in the interstellar medium, have an independent history;
- the line profile of the DIBs seem quite stable, both for the narrow and shallow features. With the exception of an intriguing case which is discussed below, the observed broadening of the profile can be explained in terms of Doppler shifts due to the different velocities of the intervening clouds;
- the DIBs seem to be generated not by a single agent but by several carriers: they can therefore be grouped into "families", the components of which show well-defined intensity ratios;
- the most recent theoretical works indicate the Polycyclic Aromatic Hydrocarbons (PAHs) as a strong candidate for a molecular carrier of the DIBs: but the laboratory results have still to be confirmed by the observations.

These facts have modified the previous hypothesis of an interstellar medium producing everywhere the same whole set of diffuse bands. Therefore, a good strategy for further investigation is to concentrate the observational effort on lines of sight along which some components of the Interstellar Medium (including the DIBs) deviate from the *average* behaviour.

3. Observational Material and Discussion

In 1986 we started a wide survey on the DIBs in the spectral range 5700–6700 Å. The whole data set comes from observations obtained with the ESO CAT/CES telescope equipped with the Short Camera and the RCA CCD #9. Given the relative brightness of our targets, the CAT/CES instrumentation is the most suited for such a survey, also because it offers the possibility of obtaining the necessary observing time. The quality of the data, as it can be seen from the figures, is excellent: some limitations arise from the limiting magnitude, which is about 8 for the Short Camera at a resolving power of 50,000.

Our current database includes about one hundred lines of sight in the direction of bright stars; for all of them we observed the DIBs at 5780, 5797, 6196,
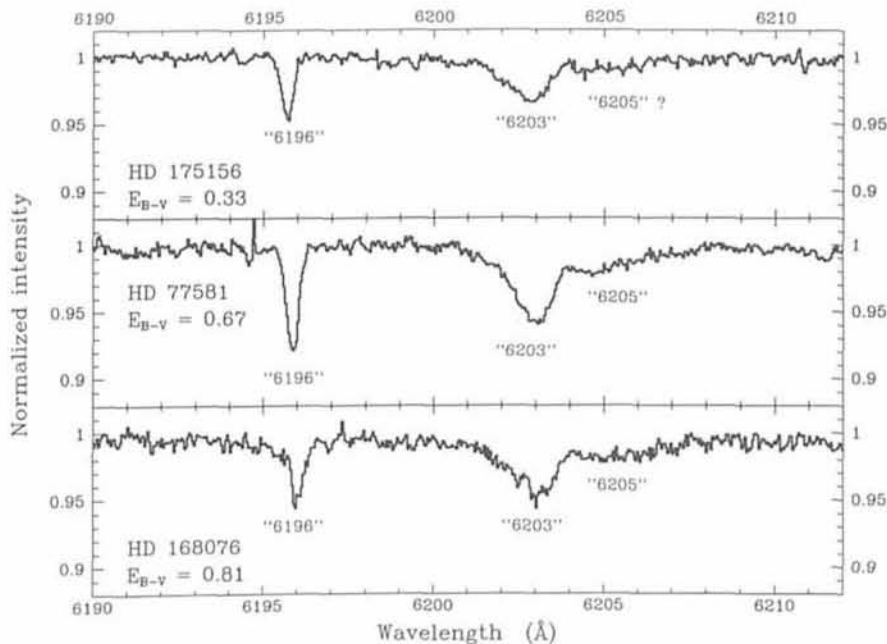
Figures 2 a–c: *The intensity ratio and its variation for the DIBs around 6200 Å. The two overlapping components at 6203 and 6205 Å are clearly seen.*

6203, 6269 and 6284 Å, while for a subset of the targets we observed also the DIBs at 5705, 5850 and 6614 Å.

Some of the observations have been done by remote control from Garching. The experience with this new observing style has been generally positive, although we sometimes felt the need for a closer and more extended checking of the instrumental set-up (. . . as well as a longing for the midnight snack!).

In the following, we describe some of the most peculiar situations we found in our data, in particular: the varying intensity ratios between features belonging to different families, the lack of some of the diffuse bands along peculiar lines of sight, and the apparent absence of DIBs when the reddening is mainly due to circumstellar matter.

3.1. The varying intensity ratios I: 5780 vs. 5797

The 5780 band is a relatively strong and narrow feature, showing an asymmetric profile, while the band at 5797 is very narrow and weaker than the 5780 one. Only recently has it been shown that these two diffuse bands do not share the same carrier (Chlewicki et al. 1986, Krelowski and Walker 1987, Benvenuti and Porceddu 1989); all these papers also report that the variation of relative intensity of the two diffuse features is not usually accompanied by any profile change. Moreover, their intrinsic profiles, i.e. the ones which originate in a single cloud, were found to be the same also in clouds producing different extinction curves

(Westerlund and Krelowski 1988, Porceddu et al. 1991 a).

Figures 1 a and 1 b show the varying behaviour of the two features in two selected cases. Their belonging to different "families" is evident from the independent intensity variation.

3.2. The varying intensity ratios II: the DIBs around 6200 Å

The group of diffuse features around 6200 Å (at 6196, 6203 and 6205 Å), is slightly different from the previous case. The spectra and related conclusions which have been presented by several authors (Chlewicki et al. 1987, Krelowski and Walker 1987, Benvenuti and Porceddu 1989) do not allow us to assign in a definite way these features to a single DIB's family. Our observational data (Benvenuti and Porceddu 1989, and Porceddu et al. 1991) show that the broad, asymmetric DIB absorption at 6203 Å can be resolved into two overlapping features, the second one being centred at about 6205 Å. As it can be seen from Figures 2 a–c the intensity ratio between the two components at 6203 and 6205 Å is not constant. Analysis of the complete data set indicates that the 6196 and 6203 Å DIBs may share the same family of the 5780 feature, but the 6205, if present, does not.

3.3. Missing DIBs and profile broadening

As it has been seen from the previous examples, the relative intensity ratios of the DIBs which are members of different
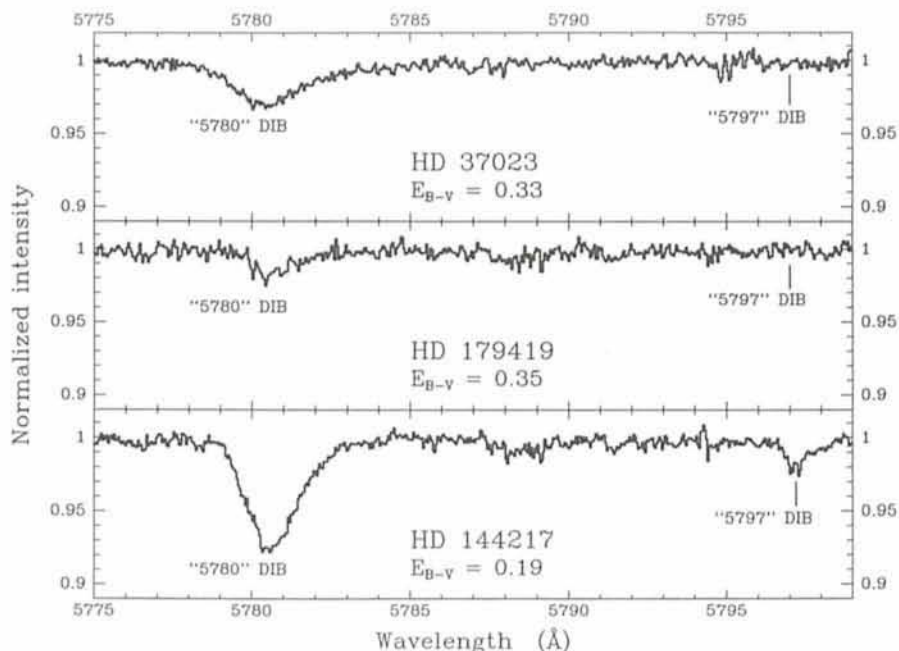
Figures 3 a–c: *Missing DIBs: the 5797 feature disappears and the 5780 intensity is strongly reduced along "peculiar" lines of sight.*

families are strongly variable: we can think of the lacking of one or more diffuse bands as the extreme case of such a variability. We found cases in which the 5797 Å DIB is strongly reduced or completely absent: for instance, the star β Sco (HD 144217, Fig. 1 b and 3 c), presents a strong reduction of the 5797 feature in comparison to the 5780 one. But probably the most representative case of lacking of the 5797 DIB is the Trapezium star HD 37023 (θ^1 Ori D), Figure 3 a. Indeed, all the Trapezium stars share this peculiarity, as they are evidently embedded in and seen through the same cloud, whose nature should also be responsible for the weakness of the 5780 Å DIB in relation to the value of E(B-V) = 0.33. The same behaviour is shared by a few more stars, as, for example, by HD 179419 (E(B-V) = 0.35) which is shown in Figure 3 b: in this case, despite the relatively high value of the reddening, the 5780 feature is extremely weak and the 5797 is not seen at all.

The medium in the direction of the Orion Trapezium stars is interesting for another reason, i.e. the observed unusually large broadening of the 5780 band. The observations of interstellar sodium lines by Hobbs (1978) indicate that several components are present toward the line of sight of the Trapezium stars. These components have recently been confirmed by our high-resolution (R = 100,000) spectra (Porceddu 1991, in preparation) and from them the velocity of the clouds can be accurately measured. However, a Doppler broadening of a "single-cloud" 5780 DIB profile, obtained by using the velocity information

from the sodium spectra, is not large enough to justify the observed width in the case of the profile of HD 37023, supporting the hypothesis that the broadening is intrinsic (Porceddu et al. 1991 b). If this fact is confirmed, and, more important, observed in other well-defined interstellar clouds, it may be used in further constraining the nature of the absorbing carrier of the 5780 DIB.

3.4. Where the DIBs seem not to live: the case of the Be stars

The last interesting example we have included in our gallery of peculiar cases is that of the spectrum of a Be star, in

which the observed reddening is mainly due to circumstellar matter. As it can be seen from Figure 4 b, the 5780 and 5797 DIBs are completely absent, despite the relatively high value of the reddening (compare the spectrum of the "normal" star HD 44458 in Figure 4 a). This absence may indicate that these DIBs cannot be generated or survive in an environment such as the circumstellar shell of a Be star. Indeed, other studies, e.g. on the behaviour of the 2200 Å feature, indicate that the circumstellar material may be quite different from the diffuse medium, particularly in the dust grain composition. It seems therefore promising to further investigate how this "environmental" differences, including the irradiation by the central star, affect the various "families" of DIBs.

A more detailed analysis, based on a wider sample of Be southern stars from which we picked the above example, is in preparation. In this case, a well-known problem in the interpretation of the data is the difficulty of disentangling the circumstellar from the diffuse medium contribution in the total reddening. We could overcome this problem by observing an open cluster in which normal B and Be coexist and for which the diffuse medium reddening is obviously the same: if we get the necessary observing time!

References

Benvenuti, P., Porceddu, I., *Astron. Astrophys.*, **223**, 329, 1989.

Chlewicki, G., van der Zwet, G.P., van Ijzendorn, L.J., Greenberg, J.M., *Astrophys. J.*, **305**, 455, 1986.

Cossart-Magos, C., Leach, S., *Astron. Astrophys.*, **233**, 559, 1990.

Heger, M.L., *Lick Obs. Bull.*, **10**, 146, 1922.
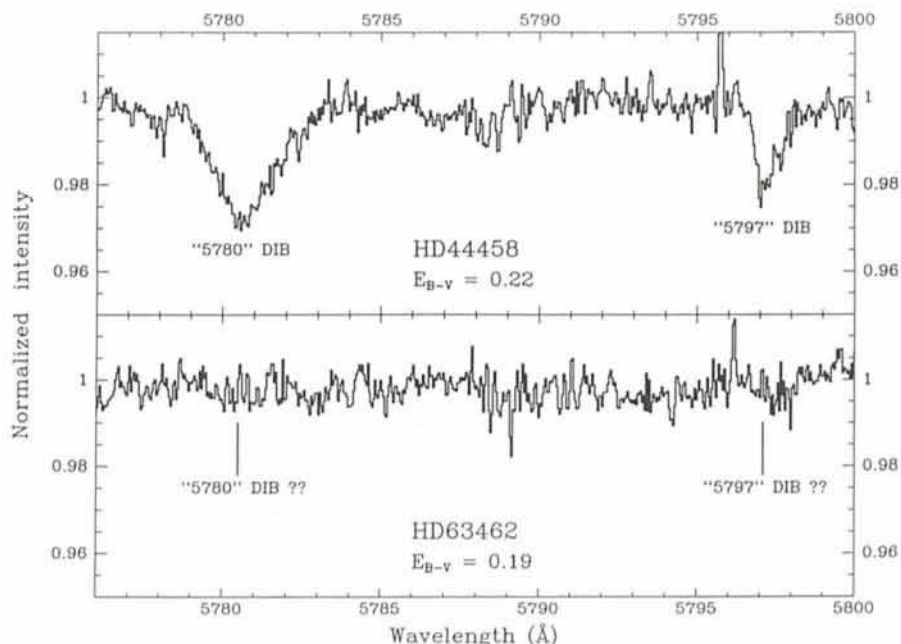
Figures 4 a–b: *The missing DIBs in Be stars.*

Hobbs, L.M., *Astrophys. J. Suppl. Ser.*, **38**, 129, 1978.

Krelowski, J., Walker, G.A.H., *Astrophys. J.*, **312**, 860, 1987.

Krelowski, J., in *Interstellar Dust*, L.J. Allamandola and A.G.G.M. Tielens (eds.), IAU Symp. 135, Kluwer Acad. Publ. p. 67, 1989.

Krelowski, J., Westerlund B., *Astron. Astrophys.*, **190**, 339, 1988.

Porceddu, I., Benvenuti, P., Krelowski, J., *Astron. Astrophys.*, in press, 1991 a.

Porceddu, I., Benvenuti, P., Krelowski, J., *Astron. Astrophys.*, submitted, 1991 b.

Westerlund, B.E., Krelowski, J., *Astron. Astrophys.*, **203**, 134, 1988.

Westerlund, B.E., Krelowski, J., *Astron. Astrophys.*, **218**, 216, 1989.

Exhibition in Berlin

The ESO exhibition opened at the Zeiss Großplanetarium in (East-) Berlin on November 1, 1991. The City of Berlin was represented by Mr. Arndt, Staatssekretär für Schule, Berufsbildung und Sport and the Mayor of Berlin-Prenzlauer Berg, Dr. Dennert.

This planetarium is one of the world's largest and was inaugurated in 1987 on the occasion of the 750th anniversary of Berlin.

It has the latest Zeiss projector with all possible technical finesses.

Already on the opening day there were lots of visitors and many more are expected during the 3 months' duration of the exhibition.

ESO is particularly pleased to make its exhibition available at an institution which only recently was incorporated into the Federal Republic, at the time of the German re-unification. There is little doubt that it will be of particular interest to the inhabitants of the parts of Berlin surrounding the Planetarium.

Mr. Arndt, Undersecretary of State for Education, Vocational Training and Sports, opens the ESO Exhibition in Berlin.

Looking for Optical Emission from Gamma-Ray Bursters

M. BOER, C. MOTCH, *Max-Planck-Institut für Extraterrestrische Physik, Garching bei München, Germany*

H. PEDERSEN, *Copenhagen University Observatory, Denmark*

S. BRANDT, A.J. CASTRO TIRADO, N. LUND, *Danish Space Research Institute, Lyngby, Denmark*

A. SMETTE, *ESO, La Silla*

1. Gamma-Ray Bursts: a 20-Year-Old Mystery

Discovered some 20 years ago [1] gamma-ray bursts (hereafter GRB) remain mysterious: these transient sources emit only during times ranging from a few milliseconds to several minutes, and they are observed only in the X-ray/Gamma-ray range, from 1 keV to more than 100 MeV. They have no obvious counterparts, either transient or quiescent, in other spectral regions, e.g. optical [2] or in soft X-rays [3] [4]. Further-

more, their light curves, and their energy spectra are extremely diverse: there is no "typical" gamma-ray burst and among the 600 bursts observed until now, not even a general classification has been established. With 3 notable exceptions, none has been observed to repeat. The exceptions are the soft repeaters SGR 1806-20 [5] [6], SGR 1900+14 [7] and the GBS 0526-66 [8] March 5b, 1979 GRB, which is located in the direction of the LMC).

Until recently, there was a general

agreement on the galactic neutron star origin of these sources, based on the characteristic time scales of the events (sometimes less than a millisecond) and on the presence of strong magnetic field signatures in their energy spectra. In that case, with more than 600 detections to date (and an actual detection rate of 1 per day), GRBs would have been the most common manifestation of neutron stars in our galaxy. However, recently the situation became quite confused with the announcement by the

BATSE team [9] that the distribution of gamma-ray burst sources is apparently quite isotropic and (from the analysis of their detection rate in a way similar to the logN – logS test) that their experiment sees almost all GRB occurrences. Taken together, these observations exclude a galactic origin and favour a cosmological origin for GRBs although a very local or an extended galactic halo origin seem not to be excluded, and there is some debate on the possible instrumental biases. However, none of these suggestions fit all the observations and this shows the need to obtain independent data on these sources.

2. Localizing the Sources

There are two ways to localize GRB sources. The first one is the so-called triangulation (or time of arrival) method. Using the time delay between the detection of the same event by several instruments, widely separated in space, one can derive the direction of the source. In order to obtain accurate positions, the triangulation method needs at least 2 detectors on interplanetary spacecraft. The current interplanetary network uses the GRB detectors aboard the Pioneer Venus Orbiter (PVO) and the Ulysses mission (which will leave the ecliptic in February 1992) in addition to the instruments on near-Earth platforms (Granat, Ginga, Solar A, Compton GRO, DMSP). This method may reach very good accuracies, 0.25 arcmin^2 for GRB 790305b (Gamma-ray bursts are usually designed by the letter GRB followed by the event date, here March 5, 1979, and eventually a letter indicating the order of the event in the day), but for a very small number of strong bursts with a well-defined time structure.

The other approach uses the anisotrophy of the detector response to the signal direction of incidence, with several detectors (8 for the Burst and Transient Experiment – hereafter BATSE – onboard the Compton Gamma-ray Observatory – CGRO) localized symmetrically on the same spacecraft. In this "response anisotrophy" method, the accuracy reached is not as good, 1 to 5 degrees for BATSE on CGRO, but almost all bursts detected may be localized (about 150 during the first 6 months of the CGRO mission). The WATCH experiment, onboard the Granat satellite, uses a third method, with a rotating collimator grid, and provides localizations with an intermediate accuracy, typically 0.3 deg. for strong events. Except for a handful of error boxes which were well enough localized with the triangulation method, the error boxes are far too large to search for quiescent counterparts at any wavelength.
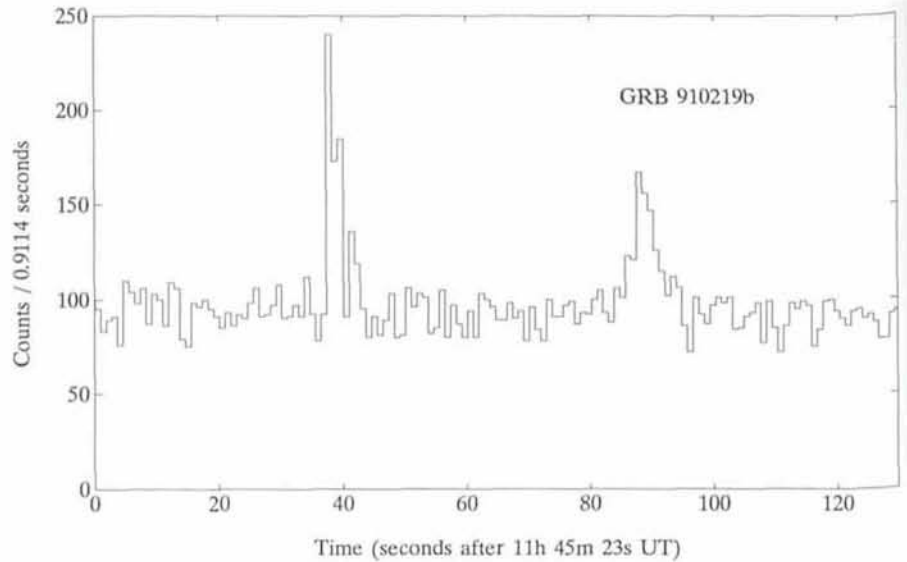
Figure 1: *Light curve of GRB 910219b as seen by the WATCH instrument in the 15 – 180 keV energy range with a time resolution of 0.9114 second.*

3. Do GRB Emit Visible Light?

Based on work on archival plates [10] [11] [12] there were claims that optical transients were observed in or near some gamma-ray burst error boxes. The reality of these events is not yet established and is the subject of a very hot debate [13] [14] [15]. However, GRB sources may well appear to be emitters at optical wavelengths, either as the result of the reprocessing of the gamma rays in an accretion disk or in the photosphere of a binary companion, or because of the thermal decay of the neutron star surface after the burst, which depends on the amount and on the depth of the energy release.

The goal of our project is to find this emission, or to set constraints on it. The WATCH, BATSE, and COMPTEL teams may provide rough localization within 12 to 14 hours after the burst. Shortly after, we expose a plate at the ESO Schmidt telescope. This plate may then be compared with the ESO, Palomar or UK sky surveys. If a new object is found, then follow-up studies may be triggered at larger telescopes. Later, when a more precise localization is eventually derived using the triangulation method, a more careful study of the GRB area may be done.

The discovery of an optical transient GRB counterpart may answer several questions about these elusive objects, such as their distance (galactic vs. cosmological), their membership to a binary system, the energy process. . . . A detection would provide us also with a localization suitable for a real deep search for a quiescent counterpart, and may result in a breakthrough in our understanding of these enigmatic sources. Even repeated non-detection

would set stringent constraints on the amount of energy emitted at optical wavelengths during and after the burst, on the thermal decay time of the source and on its nature. This would also be an important point in the debate on the reality of optical flashes, their astrophysical origin, and their association with the GRB phenomenon. Whatever is the outcome of our project, we hope that it will improve significantly the knowledge of gamma-ray burst sources.

References

[1] Klebesadel R.W., Strong I.B., Olson R.A.: 1973, *Astrophys. J. Letters*, **182**, 85.

[2] Motch, C. et al.: 1985 *Astron. Astrophys.*, **145**, 201.

[3] Boer M. et al.: 1988, *Astron. Astrophys.*, **202**, 117.

[4] Boer M. et al.: 1991, *Astron. Astrophys.*, **249**, 118.

[5] Atteia et al.: 1987, *Astrophys. J. Letters*, **320**, 105.

[6] Fenimore et al., 1987, *Astrophys. J. Letters*, **320**, 111.

[7] Mazets, E.S. et al.: 1979, *Sov. Astron. Letters*, **5**, 343.

[8] Golenetskii, S., Ilyinski V., Mazets E.: 1984, *Nature*, **307**, 41.

[9] Meegan C.A. et al.: 1991, IAU Circular 5358.

[10] Schaefer, B.E. et al.: 1981, *Nature*, **294**, 722.

[11] Hudec, R. Peresty, R., Motch C.: 1989, *Astron. Astrophys.*, **285**, 174.

[12] Greiner, J., Naumann, C., Wenzel W.: 1991, *Astron. Astrophys.*, **242**, 425.

[13] Zytkow, A.N.: 1990, *Astrophys. J.*, **359**, 138.

[14] Greiner, J.: 1991, *Astron. Astrophys.*, **234**, 251.

[15] Schaefer B.E., 1991, *Astrophys. J.*, **364**, 590.

Long-Slit Spectroscopy at La Silla: an Annotated Menu

W.W. ZEILINGER, ESO

1. Introduction

Spectroscopy of extended objects finds application both in Galactic (e.g. gas kinematics in planetary nebulae) and extragalactic fields. For many years measuring the kinematics in galaxies was restricted to the analysis of emission lines which can be traced relatively easily out to great distances from the nucleus. By contrast, absorption lines in galaxies are much more difficult to measure, because they are broadened by the velocity dispersion of the stellar component and since the intensity of the continuum decreases quite rapidly away from the centre. Only with improved detectors and improved data analysis techniques was it possible to access also this piece of information on the kinematics of extended objects. Also in the case of analysing spectra of faint point sources, long-slit spectroscopy allows an efficient sky subtraction.

The last years have seen a quite rapid evolution on the sector of the instrumentation. Until the mid-eighties most of the data were still obtained with image tube spectrographs (e.g. a Boller & Chivens spectrograph equipped with an EMI image tube as it was available at ESO) on photographic plates. The plates needed then to be digitized in order to be processed further. The subsequent step was the replacement of photographic plates with linear detectors. The first generation of linear detectors at La Silla was the Image Dissector Scanner (IDS) in combination with the Boller & Chivens spectrograph at the 3.6-m telescope. This detector allowed a very limited spatial resolution. There were two channels of which one usually was used for measuring the background. Only with CCDs was it then possible to obtain a similar field as with photographic plates. The spectral and spatial resolution, however, depended mainly on the pixel size, which for the first CCDs was quite large (30 μm^2) and somewhat constrained the observing programmes. There, the situation improved considerably with the arrival of the high-resolution CCDs. The latest upgrade now introduced multi-purpose instruments like EFOSC and EMMI. This generation of instruments not only allows a convenient change of wavelength ranges, dispersions and slit widths in the course of a night but give the observer also flexibility in selecting direct imaging or spectroscopic mode.

In the following chapters a brief guide to the instruments at La Silla with long-slit spectroscopy capability is presented. Since there is a variety of instrumentation available, this article is intended as a help for the potential user in selecting the most adapted instrument for his purpose. For the basic description of each instrument one may refer to the respective operating manuals of the instruments.

2. The Instrumentation Available at ESO

In Table 1 an overview is given over the specific instrumentation presently available at La Silla. For comparison also the Boller & Chivens spectrographs at the 3.6-m and 2.2-m are included although they are not offered any more. The setup of the instruments depends of course very much on the specific observing programme. In the following discussion more emphasis will be given to aspects of kinematic observations (i.e. obtaining radial velocities and velocity dispersions) because they require high spectral and spatial resolution on the one hand, and on the other hand a relatively large wavelength range needs to be covered in order to analyse as many lines as possible. The major applications of long-slit spectroscopy, particularly in extragalactic astronomy, are centred upon a few "traditional" wavelength regions of interest:

- for *emission lines*: the region around Hα (λ6563 Å) including the [N II] lines (λ6548 Å, λ6583 Å) for analysing the gas kinematics;
- for *absorption lines*: $\lambda\lambda$3700 – 4400 Å (including the Ca II K and H lines and the G band) and $\lambda\lambda$4900 – 5900 Å (including Fe I λ4921 Å, Mg I λ5175 Å, E band and the Na blend λ5893 Å) for deriving the kinematics of the stellar component. Limited information about the gas kinematics may also be obtained in these wavelength regions by measuring the [O II] doublet ($\lambda\lambda$3727-29 Å) and the [O III] line (λ5007 Å) respectively.

At the same time the observer wants to obtain as much spectral resolution as possible in these wavelength regions. In the case of kinematic observations, for example, a sampling better then 1 Å pixel^{-1} is desirable. Because of the higher red sensitivity of CCDs most part of the observational work is now done in the region >4900 Å. The physical size of the detector, then, determines the wavelength interval covered. Nowadays CCDs usually have 1024 pixels (or more) in the direction of the dispersion, so that each of the relevant wavelength regions can be observed with one grating setting only. For each instrument the optimal grating (or grism) has been selected in order to cover a wavelength region of about 1000 Å centred at $\lambda \approx$ 5200 Å (except for the EMMI Blue Channel configuration which refers to $\lambda\lambda$3700 – 4400 Å). The resulting sampling and spectral resolutions are compiled in Table 1. The entrance slit widths ω and spectral resolution σ_{inst} listed in Table 1 for each instrument are calculated for the maximum spectral resolution satisfying the Nyquist sampling theorem.

2.1 The Boller & Chivens Spectrographs

Originally the Boller & Chivens spectrographs were available at the 3.6-m, 2.2-m and 1.52-m telescopes. But presently only the one at the 1.52-m telescope is offered. This type of spectrograph turned out to be a very stable instrument optimized for long-slit spectroscopy of extended sources. In particular, the optimized collimator/camera focal length ratio allows small instrumental dispersions to be considered with relatively large slit widths. A wide range of gratings is available which allow to cover more or less the full optical wavelength band in various dispersions. A detailed list of the gratings together with their relative efficiency curves may be found in ESO Operating Manual No. 2. The dispersions typically used are of the order 58 Å mm^{-1} yielding a resolution of about 0.9 Å pixel^{-1}.

The change in the instrument orientation with respect to gravity as the telescope tracks the object in the sky is the principal cause for instrumental flexure, with the amount depending mainly on the zenith distance and the slit orientation. For the Boller & Chivens spectrographs the maximum shift measured in consecutive comparison line spectra was <0.5 pixel in an interval of 3 hours.

2.2 EFOSC1 and EFOSC2

The *ESO Faint Object Spectrograph and Camera* is available at the 3.6-m (EFOSC1) and its twin is available at the 2.2-m telescope (EFOSC2). This type of instruments uses grisms for spectroscopy which have a fixed wavelength range. Grisms have in general a higher efficiency than gratings. At EFOSC1 the highest dispersion available is about 120 Å mm^{-1} covering the wavelength

region between 3600 Å to 8600 Å (grisms B150, O150 and R150) in intervals of about 2000 Å, yielding a maximum resolution of about $\sigma = 1.7$ Å pixel^{-1}. Only EFOSC2 contains a set of grisms (#7, #8, #9 and #10) which is really useful for kinematic work ($\sigma = 1.3$ Å pixel^{-1}). But, as is evident from Table 1, in order to exploit the full resolution of EFOSC, a very narrow entrance slit is required (about 0.7 arcsec). At the level of a comparable instrumental setup EFOSC (and also EMMI) may be considered about three times more efficient than the Boller & Chivens spectrographs. No significant instrumental flexure has been measured.

Regarding the operation of EFOSC, one has to remember that there is no slit viewer. The positioning of the object on the slit has to be done via direct imaging and calculating the offsets with IHAP batches. Depending on the accuracy of the positioning, this may be a time-consuming task, especially if the instrument is rotated.

2.3 EMMI

The *ESO Multi Mode Instrument* at the NTT has a similar concept as EFOSC. In addition to grisms also gratings are available where the observer may change remotely the central wavelength in the course of the night. A dichroid allows simultaneous observations in the Blue and Red Channel. As for EFOSC, also EMMI needs a rather narrow slit in order to exploit the full spectral resolution.

The difference between EMMI and EFOSC becomes important mainly in terms of spectral resolution: with an integration time of 1 hour spectral information down to a surface brightness level of about $\mu_B \approx 21$ mag arcsec^{-2} was reached, with both the 3.6-m and the NTT, but in the case of EFOSC the instrumental dispersion was $\sigma_{inst} \approx 150$ km s^{-1} while with EMMI $\sigma_{inst} \approx 20$ km s^{-1} was obtained. For a similar surface brightness level, two hours of integration time at the 1.52-m telescope were needed ($\sigma_{inst} \approx 45$ km s^{-1}) using an RCA CCD as detector. This demonstrates that the Boller & Chivens at the 1.52-m telescope is for many applications a serious alternative to other instruments, particularly to EFOSC2 at the 2.2-m. The strong points of EFOSC and EMMI are their high spatial resolution and their efficiency in reaching faint surface brightness levels.

Since at the NTT the instrument adapter follows the field rotation, the amount of instrumental flexure present in the spectra depends on the length of the exposure time and of the position of the object on the sky. After a 2.5-hour inte-

Table 1: *Instrument configurations for long-slit spectroscopy*

telescope (1)	instrument (2)	scale slit length (3)	detector dimensions (4)	grating dispersion (5)	sampling [Å pixel^{-1}] (6)	ω (7)	σ_{inst} (8)
3.6-m	B & C[a]	36.67 174	RCA #8 640 × 1024 (15 μm) pixel	#26 59.5	0.89	1.6	44
	CASPEC[b]	24.07 114	TEK #26 512 × 512 (27 μm) pixel	6.5[e]	0.18	2.1	7
	EFOSC	22.47 180	RCA #8[d] 640 × 1024 (15 μm) pixel	O150[e] 130	2.0	0.7	85
NTT	EMMI Blue	15.05 360	TEK #28 1024 × 1024 (24 μm) pixel	#12[f] 38	0.91	0.8	58
	EMMI Red	23.15 360	Th #18[g] 1024 × 1024 (19 μm) pixel	#6 28	0.53	0.9	25
2.2-m	B & C[a]	59.33 294	RCA #11 640 × 1024 (15 μm) pixel	#26 59.5	0.89	2.6	44
	EFOSC2	17.47 300	Th #17 1024 × 1024 (19 μm) pixel	#8[h] 68	1.3	0.7	52
1.52-m	B & C	45.33 252	FA #27 2048 × 2048 (15 μm) pixel	#26 67.2	1.00	2.0	49

[a] ... no longer offered
[b] ... long-slit mode with short camera (f/1.6) and 31.6 groves mm^{-1} echelle grating
[c] ... dispersion at Hα region
[d] ... expected to be replaced by a Tek 512 × 512 (27 μm) pixel CCD (#26) during Period 49
[e] ... EFOSC O150 grism with fixed wavelength range λλ5000–7000 Å
[f] ... wavelength region λλ3700–4400 Å
[g] ... expected to be replaced by a coated FA 2048 × 2048 (15 μm) pixel CCD (#24) during Period 49
[h] ... EFOSC2 #8 grism with fixed wavelength range λλ4640–5950 Å

Notes to the columns:
(3) line 1: scale on the detector [arcsec mm^{-1}]
   line 2: maximum slit length [arcsec] which can be used in the unvignetted field
(4) with the exception of EMMI the direction of dispersion is always aligned with the columns of the CCD
(5) line 1: grating allowing a central wavelength around 5200 Å
   line 2: dispersion [Å mm^{-1}]
(7) minimum entrance slit width [arcsec] which satisfies the Nyquist theorem
(8) instrumental profile [km s^{-1}] using the slit width given in col. (7) calculated at $\lambda = 5200$ Å

gration a shift of about 0.4 pixels was measured. This amount of shift can, however, be easily corrected by taking arc spectra before and after the object spectrum.

2.4 CASPEC

An interesting alternative for high-resolution long-slit spectroscopy to the above cited instruments is the *ESO Cassegrain Echelle Spectrograph* at the 3.6-m telescope. A description of the latest upgrade is given by Pasquini and Gilliotte (1991). By replacing the cross disperser with a flat mirror in combination with an interference filter an about 50 Å wide region can be isolated allowing a spatial coverage of about 2.4 arcmin. In the present configuration several interference filters are available for the Hα, [O III] (λ5007 Å) and [O II] (λλ3727-29 Å) regions at various redshifts.

In principle one can use CASPEC also in its standard configuration if the interorder spacing (ranging from 5 to 19 arcsec as a function of wavelength) is sufficient for the required spatial extension. However, regarding throughput, the cross disperser is certainly less efficient than the flat mirror in the long-slit mode.

One may consider CASPEC about a factor 2.5 less efficient than the Boller & Chivens with an optimal 600 groves mm^{-1} grating in a comparable wavelength region and with comparable detectors.

3. Detectors

The detector is one of the decisive factors in determining not only the spectral and spatial resolution and coverage but also the total efficiency of the instrument. A certain limitation of the overall performance were the RCA CCDs with

their rather high read-out noise (typically between 40 and 60 e⁻) and often bad cosmetics. This forced the user to maximize the integration time which on the other hand produced an excessive number of cosmic-ray hits on the CCD. The removal of cosmic rays without modifying the underlying spectrum is not always an easy task, especially in the area of the object image. The safest approach consists in splitting the total exposure time in several shorter exposures. Then, one can rather easily remove cosmic-ray events by comparing intensities on a pixel-to-pixel basis. Here the change to the low read-out noise CCDs (like e.g. the Ford/Aerospace, Thomson and Tektronix CCDs which are available now at La Silla) improves the situation.

But one has to pay attention that in particular the FA and Th CCDs have a much lower relative quantum efficiency than the RCA and Tek CCDs. An RCA CCD has typically a peak RQE of about 75% while the FA and Th CCD have only about 45% relative quantum efficiency. The difference becomes dramatic especially in the wavelength region $\lambda\lambda 4000 - 5000$ Å where it goes up to $\Delta RQE \approx 50\%$. Therefore, in order to use a given instrument/detector combination at its maximum efficiency, one should compute beforehand whether the observations are going to be sky or noise limited.

The fact that the CCDs become progressively larger has on the one hand the obvious advantages in terms of larger wavelength coverage and gain in spectral resolution, which may improve also the efficiency of spending observing time. But on the other hand one has to realize that in the present configuration of the data-acquisition systems at La Silla a certain limit of data-processing capability has been reached or even exceeded. The HP-based computers are e.g. not capable to handle the full 2048 × 2048 pixel array data of the FA CCD. It has also to be taken in consideration that the read-out of a 1700 × 1700 pixel window, which is the maximum possible, takes about 3 minutes. Therefore the observer is well advised to select a read-out window as small as possible for his purpose in order not to lose too much time in read-out and handling of the images.

4. Concluding Remarks

In the previous sections, emphasis was given on instrumentational aspects for obtaining science data. But there are several additional points which, already at the moment of the observation, influence the quality of the results obtainable from the data reduction.

4.1 Sky subtraction

The subtraction of the night sky from spectra of extended sources is very crucial, in particular for absorption-line measurements. Ideally one would record the sky "on-line" together with the object spectrum on the same exposure, provided that the slit length is sufficient to have a region where the contribution of the object light is negligible. Due to the relatively small field at the 3.6-m telescope (about 3 arcmin), problems with the sky subtraction may arise very easily, especially if the angular extent of the object exceeds 60 arcsec and deep spectra want to be obtained. A rather reliable solution to this problem proved to be bracketing the object exposure by two exposures of a blank sky region having a comparable exposure time.

4.2 Comparison spectra

Good arc spectra are also an important factor in obtaining high-quality data. In the case of the Boller & Chivens spectrographs traditionally He/Ar lamps are used, which provide an arc spectrum with satisfactory S/N ratio even with short exposures (typically ≤120 seconds). At EFOSC and EMMI the situation is somewhat different: in particular in the case of EFOSC1 where the light of the calibration lamps is projected at a large distance from the lamps, the resulting arc spectrum is quite faint. At EFOSC2 and EMMI the results are better, but compared to the Boller & Chivens generally longer integration times are needed (up to 500 seconds) in order to arrive at an adequate intensity level. There is also the problem that in the wavelength region $\lambda\lambda 5000 - 6000$ Å there are only few Ar lines which, furthermore, are also faint, whereas the He lines easily saturate even with a 1-second exposure. In the case of EMMI the Th lamp proved to be more useful in this wavelength region. In addition the arc spectra are often contaminated by internal reflections ("ghosts"). But in general an accurate solution for the wavelength calibration up to about 0.1 pixel could always be achieved. In the context of the accuracy of the wavelength calibration also the instrumental flexure is an important factor as discussed before.

4.3 Selecting the "right" instrument

Apart from the purely instrumental questions, another important criterion for selecting a certain telescope/instrument combination is the operating efficiency of a given system. Depending on the configuration there may be a considerable time overhead in preparing and processing the exposures. There are no major differences in the operation of the different telescopes. All the four telescopes in question have a sufficiently accurate pointing that the object will be found in the central region of the field. Apart from the 1.52-m telescope, there are also similar procedures to determine and control the telescope focus. In many applications of long-slit spectroscopy it is necessary to rotate the instrument. A remote control of the rotator is available only at the 3.6-m telescope and the NTT. At the 2.2-m and 1.52-m telescopes the rotation of the instrument requires a manual action at the telescope which can be carried out in most cases only if the telescope has been put to the zenith. The 1.52-m telescope has no autoguider unit which may be a certain disadvantage for long exposure times although the tracking is generally very good.

The Boller & Chivens, CASPEC and EMMI have a slit viewer allowing a direct positioning of the object on the slit. In the case of EFOSC the positioning has to be done via offsets calculated from direct images.

Regarding the instrument control and data-acquisition system, the operation of EMMI is certainly the most time-consuming one. One needs on the average about 5 minutes to handle an exposure which compares to about 2 minutes with other instruments.

For most "standard" observations the Boller & Chivens spectrograph at the 1.52-m telescope may turn out to be all in all the more efficient instrument, since, altogether, there is much less time overhead due to positioning the object on the slit, instrument rotation, obtaining the arc spectra, read-out time of the CCD, etc. This becomes particularly important when the science exposure times are short (typically <1 hour). In addition, the newly available FA CCD at the 1.52-m telescope allows to cover a wavelength range of up to 2048 Å with a sampling of 1 Å pixel⁻¹. For high-resolution work at faint surface brightness levels, on the contrary, EMMI is clearly the most adapted instrument.

References

ESO CCD Manual, 3ʳᵈ edition (La Silla, May 1991).
ESO Operating Manual, No. 2: The Boller & Chivens spectrographs (1989). No. 4: EFOSC (1989). No. 9: CASPEC (1989). No. 14: EMMI (draft 1991).
Melnick, J., EFOSC2: Notes for observers (La Silla, April 1991). EMMI: Notes for observers (La Silla, Sept. 1991).
Pasquini, L. and Gilliotte, A., The Messenger, **65**, 50 (1991).

Near-Earth Object Observed at ESO

The strange object 1991 VG was observed at ESO with the Danish 1.54-m telescope during the night of December 1–2, 1991.

This object in the solar system was first seen as a small, moving point of light with the Spacewatch camera by astronomers in the USA in mid-November.

After some days, it became possible to compute its orbit and, most unusually, it was found to move in an orbit that is very similar to that of the Earth. It was also calculated that it would pass very close to the Earth in early December, possibly at a distance of about 450000 km, that is just outside the orbit of the Moon.

The observations at ESO indicate that this object may not be a natural object (a celestial boulder), but is perhaps artificial. It may for instance be an old rocket which was used to launch a spacecraft into interplanetary space many years ago.

The observations were carried out by ESO astronomers Richard M. West and Olivier Hainaut in the early morning of December 2, when this object, now known under the designation 1991 VG, was less than 600,000 km from the Earth. It was moving rapidly over the sky (about 12°/day) and could just barely be followed by the telescope. They measured the brightness to V = 17.7, which transforms into a size of about 10 metres, and found that it
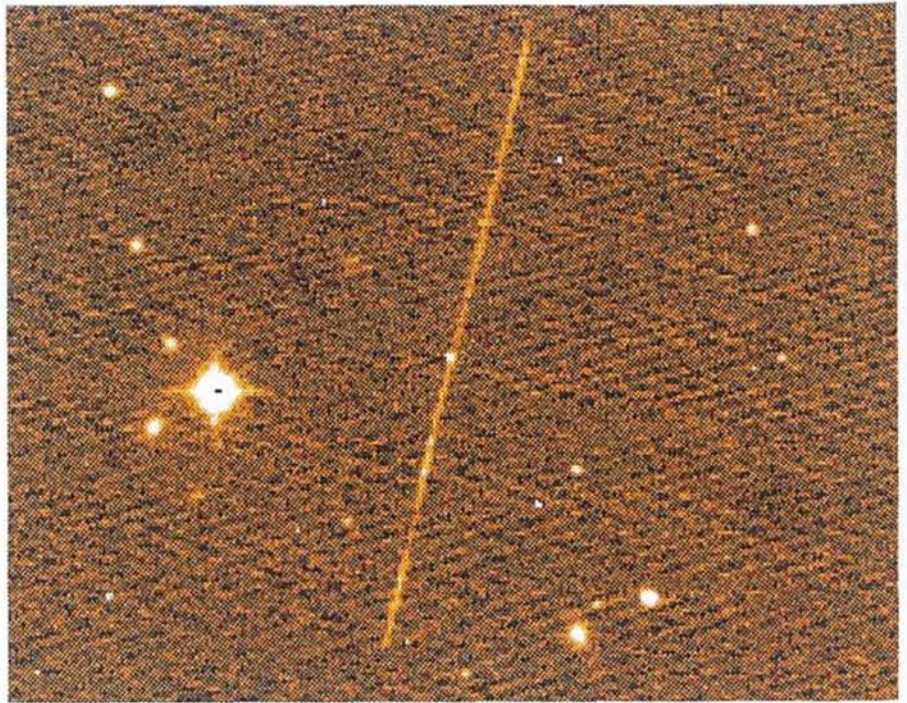
The figure shows the raw CCD image with the very long trail of 1991 VG, as obtained on December 2.15 UT, when it was moving at a rate of nearly 12°/day. The exposure lasted 4 minutes. The variable brightness along the trail is caused by the tumbling motion of the object.

rotates rapidly, several times each minute; it is probably tumbling during its flight.

The ESO astronomers also obtained accurate positions of 1991 VG, which will now help the Arecibo radio observa-

tory to direct radar beams towards 1991 VG, when it comes within the reach of these instruments later in December. The radar studies may finally settle the question about the nature of this mysterious object.
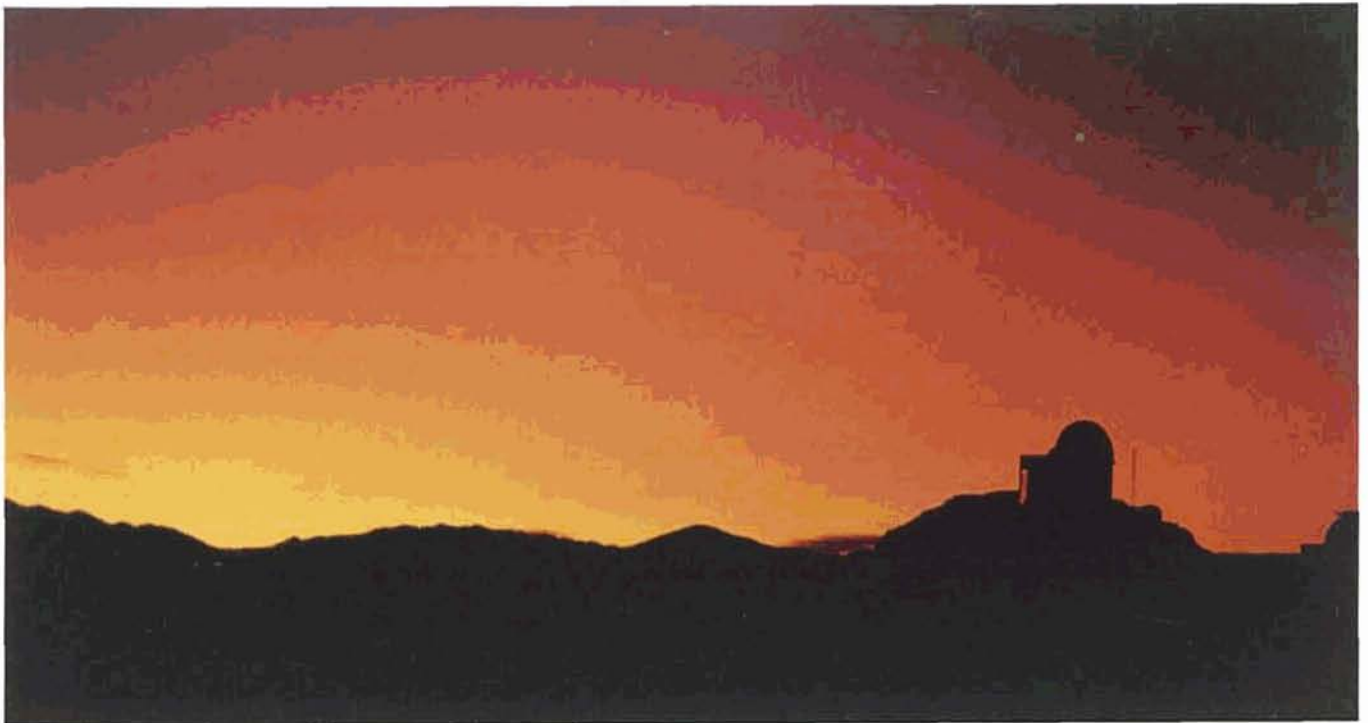
Sunrise over La Silla, behind the 3.6-m dome, as photographed by ESO astronomer Alain Smette at the end of October 1991. The sky is coloured red by the dust ejected into the stratosphere by the eruption earlier this year of the Pinatubo volcano on the Philippines.

MIDAS Memo

ESO Image Processing Group

1. Application Developments

The test and validation of all basic MIDAS commands have now been completed with the help of the Astronomy Group in ESO. This has led to the correction of many bugs and significant improvement of the documentation. Most of these upgrades are available in the 91NOV release of MIDAS.

In the Echelle spectroscopy package (context Echelle) new routines have been implemented which perform order definition and optimal extraction and provide an improved user interface.

A package for preparation of OP-TOPUS observations was implemented by A. Gemmo. It enables users to create the command files for drilling the star-plates directly from an object list in a MIDAS table file.

2. Problem Report Data Base

All user reports of Midas bugs and questions as of October 1991 are now being kept in a Midas-Problems database, as they are submitted to the ESO IPG. All related information (e.g. regarding the local environment, installation, etc.) is included in the DB and is available to both Midas users as well as to the person assigned to the bug fix. Once a solution to the problem has been found, whether or not it actually leads to a real code modification, a brief summary is included in the associated solution data base and a reference to a 'patch-file' containing more details (e.g. code modification) is given.

This facility has been developed in conjunction with the ESO Archive and is available to both internal users and external Midas sites through Starcat. In order to access it, internal users just invoke *starcat ESO midas* from any of the organization's main computers. External users need to connect to ESO first and log in under the *starcat* account (no password required), within starcat type *ESO midas* to access the DB.

3. MIDAS Releases

It has become the general impression of MIDAS site managers and MIDAS users that a rapid cycle of official releases (i.e. each half year) is no longer needed as the MIDAS system has stabilized. Therefore, the MIDAS Group has decided to decrease the rate of official MIDAS releases to once per year after the 91NOV version. This will also reduce the internal overheads and enables us to put more efforts in the development of application programmes.

It is foreseen to offer new MIDAS application packages and patches through an anonymous *ftp* account to avoid unnecessary delays for external sites. This will ensure that users will have both a stable core system, and access to new applications developed between the releases. MIDAS sites managers will be informed when this facility has become available.

4. MIDAS Hot-Line Service

The following MIDAS support services can be used to obtain help quickly when problems arise:

- EARN: MIDAS@DGAESO51.bitnet
- SPAN: ESO::MIDAS
- Eunet: midas@eso.uucp
- Internet: midas@eso.org
- FAX.: +49-89-3202362, attn.: MIDAS HOT-LINE
- Tlx.: 528 282 22 eso d, attn.: MIDAS HOT-LINE
- Tel.: +49-89-32006-456

Users are also invited to send us any suggestions or comments. Although we do provide a telephone service we ask users to use it in urgent cases only. To make it easier for us to process the requests properly we ask you, when possible, to submit requests in written form either through electronic networks, telefax or telex.

More information about MIDAS can be found in the ESO-MIDAS Courier which is the biannual newsletter on MIDAS related matters issued by the Image Processing Group and edited by Rein Warmels.

IRAC TEST RUN REPORT No. 2:
Performance of IRAC with the New Pupil Stop

When originally installed on the telescope in 1988, IRAC-1 had a 2.8-mm diameter pupil stop. Following the initial tests, a very low instrumental efficiency was measured, and it was thought at one point that the pupil stop was too small and was reducing the number of detected photons. The pupil stop was then drilled out by J.-L. Lizon to 3.7 mm, but no improvement of source signal was measured, and it was deduced that the low efficiency was due to the intrinsically low DQE of the Philips array and not to anything having to do with the camera. The latter was corroborated by laboratory measurements of the pixel fill-factor which was found to be only ~15 %, much lower than expected from the data detector sheet.

Following several observing and test runs, it was realized that the sky background was significantly higher than nominal (see Moneti et al., 1991, *The Messenger* No. **64**, 66). This was not a serious problem with the 32×32 engineering arrays that were used until December 1990: these arrays had a 2.3-μm cut-off wavelength and were not sensitive in the thermal infrared, i.e. at L, where the sky (and telescope) background is very high. At that time, the limiting sensitivities were clearly imposed by poor detector quality and not by the extra noise produced by the high sky background. With the arrival of the 64×64 array we began using the camera at L and the extra high background began to impose important limitations on the integration times (DIT) that could be used with the L filter.

In early October 1991 an insert was designed and built which could be placed inside the current pupil stop and which effectively reduces the pupil to 2.6 mm. This insert was installed and tested in November 1991 and a reduction in sky background was measured, while the instrumental zero points (i.e. the source signals) were unaffected. The new sky backgrounds are summarized in Table 1, and they are generally com-

parable to those measured with the standard photometers.

Table 1: *Sky* background with IRAC/2.2*

Filter	Background	
	ADUs/sec/pix*	mag/arcsec^2
J	1.5	14.5
H	2.8	13.8
K	6.2	13.7
L	19000	2.6

*With the 0.5"/pix scale.

With the new pupil stop the camera can be used efficiently at L with the 0.8"/pix scale using DITs of 0.8–1.0 sec depending on the actual outside temperature. At present the limiting sensitivity is still determined mostly by the poor quality of the Philips array, but the lowering of the background should be considered a first step toward the upgrade of IRAC-1 with a better array which is expected to occur in April–May 1992.

A. MONETI and H. GEMPERLEIN,
ESO, La Silla

Contents